Predictive model of BEC dark matter halos with a solitonic core and an isothermal atmosphere

Pierre-Henri Chavanis*

Laboratoire de Physique Théorique, Université de Toulouse, CNRS, UPS 31062, France

(Received 24 October 2018; published 31 October 2019)

We develop a model of Bose-Einstein condensate dark matter halos with a solitonic core and an isothermal atmosphere based on a generalized Gross-Pitaevskii equation [P. H. Chavanis, Eur. Phys. J. Plus **132**, 248 (2017)]. This equation provides a heuristic coarse-grained parametrization of the ordinary Gross-Pitaevskii equation accounting for violent relaxation and gravitational cooling. It involves a cubic nonlinearity taking into account the self-interaction of the bosons, a logarithmic nonlinearity associated with an effective temperature, and a source of dissipation. It leads to superfluid dark matter halos with a core-halo structure. The quantum potential or the self-interaction of the bosons generates a solitonic core that solves the cusp problem of the cold dark matter model. The logarithmic nonlinearity generates an isothermal atmosphere accounting for the flat rotation curves of the galaxies. The dissipation ensures that the system relaxes towards an equilibrium configuration. In the Thomas-Fermi approximation, a dark matter halo is equivalent to a barotropic gas with an equation of state $P = 2\pi a_s\hbar^2\rho^2/m^3 + \rho k_B T/m$, where a_s is the scattering length of the bosons and m is their individual mass. We numerically solve the equation of hydrostatic equilibrium and determine the density profiles and rotation curves of dark matter halos. We impose that the surface density of the halos has the universal value $\Sigma_0 = \rho_0 r_h = 141\ M_\odot/\mathrm{pc}^2$ obtained from the observations. For a boson with ratio $a_s/m^3 = 3.28\times 10^3\ \mathrm{fm}/(\mathrm{eV}/\mathrm{c}^2)^3$, we find a minimum halo mass $(M_h)_{\min} = 1.86\times 10^8\ M_\odot$ and a minimum halo radius $(r_h)_{\min} = 788$ pc. This ultracompact halo corresponds to a pure soliton which is the ground state of the Gross-Pitaevskii-Poisson equation. For $(M_h)_{\min} < M_h < (M_h)_* = 3.30\times 10^9\ M_\odot$ the soliton is surrounded by a tenuous isothermal atmosphere. For $M_h > (M_h)_*$ we find two branches of solutions corresponding to (i) purely isothermal halos without soliton and (ii) isothermal halos harboring a central soliton. The purely isothermal halos (gaseous phase) are stable. For $M_h > (M_h)_c = 6.86\times 10^{10}\ M_\odot$, they are indistinguishable from the observational Burkert profile. For $(M_h)_* < M_h < (M_h)_c$, the deviation from the isothermal law (most probable state) may be explained by incomplete violent relaxation, tidal effects, or stochastic forcing. The isothermal halos harboring a central soliton (core-halo phase) are canonically unstable (having a negative specific heat) but they are microcanonically stable so they are long-lived. By extremizing the free energy with respect to the core mass, we find that the core mass scales as $M_c/(M_h)_{\min} = 0.626(M_h/(M_h)_{\min})^{1/2}\ln(M_h/(M_h)_{\min})$. For a halo of mass $M_h = 10^{12}\ M_\odot$, similar to the mass of the dark matter halo that surrounds our Galaxy, the solitonic core has a mass $M_c = 6.39\times 10^{10}\ M_\odot$ and a radius $R_c = 1$ kpc. The solitonic core cannot mimic by itself a supermassive black hole at the center of the Galaxy but it may represent a large bulge which is either present now or may have, in the past, triggered the collapse of the surrounding gas, leading to a supermassive black hole and a quasar. On the other hand, we argue that large halos with a mass $M_h > 10^{12}\ M_\odot$ may undergo a gravothermal catastrophe leading ultimately to the formation of a supermassive black hole (for smaller halos, the gravothermal catastrophe is inhibited by quantum effects). We relate the bifurcation point and the point above which supermassive black holes may form to the canonical and microcanonical critical points $(M_h)_{\mathrm{CCP}} = 3.27\times 10^9\ M_\odot$ and $(M_h)_{\mathrm{MCP}} \sim 2\times 10^{12}\ M_\odot$ of the "thermal" self-gravitating bosonic gas. Our model has no free parameter so it is completely predictive. Extension of this model to noninteracting bosons and fermions will be presented in forthcoming papers.

DOI: 10.1103/PhysRevD.100.083022

I. INTRODUCTION

The nature of dark matter (DM) is still unknown and remains one of the greatest mysteries of modern cosmology. In the standard cold dark matter (CDM) model, DM is

*chavanis@irsamc.ups-tlse.fr

assumed to be made of weakly interacting massive particles (WIMPs) with a mass in the GeV to TeV range. They may correspond to supersymmetric (SUSY) particles [1]. These particles freeze out from thermal equilibrium in the early Universe and, as a consequence of this decoupling, cool off rapidly as the Universe expands. As a result, DM can be represented by a pressureless gas at zero thermodynamical temperature ($T_{\rm th}=0$) described by the Euler-Poisson equations or as a collisionless system of particles described by the Vlasov-Poisson equations [2]. The CDM model works remarkably well at large (cosmological) scales and is consistent with ever improving measurements of the cosmic microwave background from WMAP and Planck missions [3,4]. However, it encounters serious problems at small (galactic) scales. In particular, classical collisionless N-body simulations suggest that DM halos should be cuspy [5], with a density diverging as r^{-1} for $r\to 0$, while observations tend to favor a flat core density [6]. On the other hand, the CDM model predicts an overabundance of small-scale structures (subhalos/satellites), much more than what is observed around the Milky Way [7]. These problems are referred to as the "cusp problem" and "missing satellite problem." The expression "small-scale crisis of CDM" has been coined.

The small-scale problems of the CDM model are somehow related to the assumption that DM is pressureless. In order to remedy this difficulty, some authors have proposed to take into account the quantum nature of the DM particle.[1]

If the DM particle is a fermion, like a massive neutrino, as originally suggested in [11–13], gravitational collapse is prevented by the Pauli exclusion principle. Fermionic DM halos are described by the Fermi-Dirac distribution [14–44]. They generically have a core-halo structure consisting in a completely degenerate core (fermion ball) with a polytropic equation of state $P=(1/20)(3/\pi)^{2/3}h^2\rho^{5/3}/m^{8/3}$ and an isothermal atmosphere with an equation of state $P=\rho k_B T/m$. The core is stabilized by quantum mechanics and solves the cusp problem of the CDM model.[2] On the other hand, the density decreases as r^{-2} in the isothermal halo, yielding flat rotation curves in agreement with the observations [45]. This core-halo structure has been studied in detail in [14–44]. The mass of the fermions must be of the order of $m=170\ {\rm eV}/{\rm c}^2$ (see Appendix D of [46]) to account for the size of ultracompact DM halos like Fornax ($R\sim 1$ kpc and $M\sim 10^8\ M_\odot$) interpreted as the ground state ($T=0$) of the self-gravitating Fermi gas.

In this paper, we shall assume that the DM particle is a boson, like an ultralight axion (ULA) [47]. At very low temperatures, bosons form self-gravitating Bose-Einstein condensates (BECs). In that case, DM halos can be viewed as gigantic bosonic atoms at $T_{\rm th}=0$ where the bosonic particles are condensed in a single macroscopic quantum state. They are described by a scalar field (SF) that can be interpreted as the wave function $\psi(\mathbf{r},t)$ of the condensate. The bosons may be noninteracting or self-interacting. The wave properties of the SF are negligible at large (cosmological) scales where the SF behaves as CDM, but they become relevant at small (galactic) scales and can prevent gravitational collapse. However, for quantum mechanics to manifest itself at the scale of DM halos, the mass of the DM particle must be extremely small, of the order of $m=2.92\times 10^{-22}\ {\rm eV}/c^2$ (see Appendix D of [46]). These ultralight particles are not excluded by particle physics. This model is referred to as wave DM, fuzzy DM (FDM), BECDM, ψDM, SFDM [46–129] (see the introduction of [78] for a short history of this model). In this model, gravitational collapse is prevented by the quantum pressure arising from the Heisenberg uncertainty principle or from the scattering of the bosons. This leads to DM halos presenting a central core instead of a cusp. Since the quantum Jeans scale is finite [78], this suppresses the formation of small-scale structures even at $T_{\rm th}=0$. Therefore, quantum mechanics may be a way to solve the small-scale problems of the CDM model such as the cusp problem and the missing satellite problem. The viability of this model has been recently demonstrated by the high resolution simulations of Schive *et al.* [96,97] and the comprehensive paper of Hui *et al.* [122].

At the scale of DM halos, Newtonian gravity can be used so the evolution of the wave function of the BEC is governed by the Gross-Pitaevskii-Poisson (GPP) equations [78]:

$$i\hbar\frac{\partial\psi}{\partial t}=-\frac{\hbar^2}{2m}\Delta\psi+m\Phi\psi+\frac{4\pi a_s\hbar^2}{m^2}|\psi|^2\psi, \qquad (1)$$

$$\Delta\Phi=4\pi G|\psi|^2, \qquad (2)$$

where Φ is the gravitational potential, m is the mass of the bosons, and a_s is their scattering length. The interaction between the bosons is repulsive when $a_s>0$ and attractive when $a_s<0$. The mass density of a BECDM halo is $\rho=|\psi|^2$. Its total mass is $M=\int\rho d\mathbf{r}$.

A serious DM particle candidate is the QCD axion [130] which has been proposed as a solution of the

[1]Other possibilities to solve the CDM crisis invoke (i) self-interacting CDM with a large scattering cross section but negligible annihilation or dissipation [8], (ii) warm dark matter (WDM) where the dispersion of the particles is responsible for a pressure force that can halt gravitational collapse and prevent the formation of cusps [9], (iii) the feedback of baryons that can transform cusps into cores [10].

[2]In the case of large DM halos, quantum mechanics may be negligible and the core may be stabilized by thermal effects (see Appendix A).

charge parity problem of quantum chromodynamics (QCD) [131]. The QCD axion is a spin-0 boson with a mass $m = 10^{-4}$ eV$/c^2$ and an attractive self-interaction $a_s = -5.8 \times 10^{-53}$ m. Since the self-interaction is attractive, self-gravitating axions can form stable clusters only below a maximum mass $M_{\rm max} = 1.012\hbar/\sqrt{Gm|a_s|}$ and above a minimum radius $R_{99} \geq 5.5(|a_s|\hbar^2/Gm^3)^{1/2}$ evidenced in Refs. [78,79]. The equilibrium states result from the balance between the repulsive pressure arising from the Heisenberg uncertainty principle, the attractive self-interaction of the bosons, and the gravitational attraction. For QCD axions the maximum mass of axion stars is very small, of the order of $M_{\rm max} = 6.5 \times 10^{-14}\ M_\odot$ (corresponding to a radius $R_{99} = 3.3 \times 10^{-4}\ R_\odot = 230$ km) [119]. Obviously, QCD axions cannot form DM halos (i.e., DM halos are not self-gravitating BECs of QCD axions). QCD axions may form mini axion stars of the asteroid size (axteroids). These mini axion stars could be the constituents of DM halos in the form of mini-MACHOS. However, since they behave essentially as CDM, they cannot solve the CDM small-scale crisis.

Other kinds of axions may exist with a much smaller mass [47]. These ULAs could form DM halos similar to gigantic boson stars (see Appendix D of [46]). If the axions have a mass $m = 2.19 \times 10^{-22}$ eV$/$c^2 and an attractive self-interaction $a_s = -1.11 \times 10^{-62}$ fm, the maximum mass $M_{\rm max}$ and the minimum radius R_{99} of axionic clusters become comparable to the size of ultracompact DM halos like Fornax ($R \sim 1$ kpc and $M \sim 10^8\ M_\odot$). If the axions are noninteracting they must have a mass of the order of $m = 2.92 \times 10^{-22}$ eV$/c^2$ to account for the size of ultracompact DM halos. In that case, the equilibrium state results from the balance between the repulsive pressure arising from the Heisenberg principle and the gravitational attraction. Finally, if the axions have a repulsive self-interaction $a_s > 0$, they can account for the size of ultracompact DM halos with a larger mass m because, in the Thomas-Fermi (TF) limit, only the ratio $a_s/m^3 = 3.28 \times 10^3$ fm$/$(eV$/$c^2)^3 is constrained. In that case, the equilibrium state results from the balance between the repulsive pressure arising from the self-interaction of the bosons and the gravitational attraction. Cosmological considerations suggest that the bosonic DM particle has a repulsive self-interaction [46,98]. A repulsive self-interaction may also solve some tensions encountered in the noninteracting model (see the Remark at the end of Appendix D. 4 of [46]).

Although the GPP equations are simple to write down, they actually have a very complicated dynamics. A self-gravitating BEC at $T_{\rm th} = 0$ that is not initially in a steady state undergoes gravitational collapse (Jeans instability or free fall), displays damped oscillations, and finally settles down on a quasistationary state (virialization) by radiating part of the scalar field [132–134]. This is the process of gravitational cooling initially introduced by Seidel and Suen [132] in the context of boson stars. As a result of gravitational cooling, the system reaches an equilibrium configuration with a core-halo structure. The condensed core (soliton/BEC) is stabilized by quantum mechanics and has a smooth density profile. This is a stable stationary solution of the GPP equations at $T_{\rm th} = 0$ (ground state). Gravitational collapse is prevented by the quantum potential arising from the Heisenberg principle or by the pressure $P = 2\pi a_s\hbar^2\rho^2/m^3$ arising from the self-interaction of the bosons. This solitonic core (ground state) is surrounded by a halo of scalar radiation corresponding to the quantum interferences of excited states. As shown by Schive *et al.* [96,97], these interferences produce time-dependent small-scale density granules (of the size of the solitonic core) that counter self-gravity and create an effective thermal pressure. These noninteracting excited states are analogous to collisionless particles in classical mechanics. As a result, the halo behaves essentially as CDM and is approximately isothermal with an equation of state $P = \rho k_B T/m$ involving an effective temperature T (not to be confused with the thermodynamic temperature $T_{\rm th}$ which is equal to zero). The solitonic core solves the cusp problem of the CDM model (see also footnote 2) and the isothermal halo where the density decreases as r^{-2} yields flat rotation curves in agreement with the observations.[3] This core-halo structure (and the presence of granules) has been clearly evidenced in the numerical simulations of Schive *et al.* [96,97].

Gravitational cooling is a dissipationless relaxation mechanism similar in some respect to the concept of violent relaxation introduced by Lynden-Bell [136] in the context of collisionless self-gravitating systems described by the Vlasov-Poisson equations. A collisionless self-gravitating system that is not initially in a dynamically stable steady state undergoes gravitational collapse (Jeans instability or free fall), displays damped oscillations, and finally settles down on a quasistationary state (virialization) by sending some of the particles at large distances. This process is related to phase mixing and nonlinear Landau damping. Lynden-Bell [136] developed

[3]The halo cannot be exactly isothermal otherwise it would have an infinite mass [135]. In reality, the density in the halo decreases as r^{-3}, similarly to the Navarro-Frenk-White (NFW) [5] and Burkert [6] profiles, instead of r^{-2} corresponding to the isothermal sphere [135]. This extra confinement may be due to incomplete relaxation, tidal effects, and stochastic perturbations (see Sec. VI F and Appendix B for a more detailed discussion).

a statistical mechanics of this process and obtained, at the coarse-grained scale, an equilibrium distribution similar to the Fermi-Dirac distribution.[4] The Lynden-Bell distribution function takes into account a sort of exclusion principle implied by the Vlasov equation, similar to the Pauli exclusion principle for fermions, but of a nonquantum origin. In Lynden-Bell's theory, the quasistationary state has a core-halo structure with a completely degenerate core (effective fermion ball) and an isothermal atmosphere with an effective temperature, like in the fermionic model. The equation of state in the core is $P = (1/5)[3/(4\pi\eta_0)]^{2/3}\rho^{5/3}$ and the equation of state in the halo is $P = \rho T_{\rm LB}/\eta_0$. In the analogy between the gravitational cooling of self-gravitating BECs and the violent relaxation of collisionless self-gravitating systems, the bosonic core (BEC/soliton) corresponds to the fermion ball and the halo made of scalar radiation corresponds to the isothermal halo predicted by Lynden-Bell. Actually, since a collisionless system of bosons is described by the Vlasov-Poisson equations at large scales (where quantum effects become negligible), it is very likely that both processes (gravitational cooling and violent relaxation) are at work in self-gravitating BECs and may even correspond to the same phenomenon. As a result, self-gravitating BECs should have a core that is partly bosonic (soliton) and partly fermionic (in the sense of Lynden-Bell), surrounded by an effective isothermal halo. In conclusion, gravitational cooling and violent relaxation explain how collisionless self-gravitating systems can rapidly thermalize and acquire a large effective temperature T even if $T_{\rm th} = 0$ fundamentally. Gravitational cooling and violent relaxation may be at work during hierarchical clustering, a process by which small DM halos merge and form larger halos in a bottom-up structure formation scenario. It is believed that DM halos acquire an approximately isothermal profile, or more realistically a NFW or Burkert profile (see footnote 3), as a result of successive mergings.

In view of these remarks, it is important to obtain a parametrization of the processes of violent relaxation and gravitational cooling on a coarse-grained scale.

A classical collisionless stellar system is basically described by the Vlasov-Poisson equations. However, these equations generate a complicated dynamics associated with the concepts of phase mixing, violent relaxation, and nonlinear Landau damping. While the fine-grained distribution function $f(\mathbf{r}, \mathbf{v}, t)$ develops intermingled filaments and does not relax towards a steady state, the coarse-grained distribution function $\bar{f}(\mathbf{r}, \mathbf{v}, t)$, which averages over these filaments, does relax towards a steady state. However, the coarse-grained distribution function $\bar{f}(\mathbf{r}, \mathbf{v}, t)$ does *not* satisfy the Vlasov-Poisson equations. It satisfies a more complex kinetic equation. We have introduced in [137–139] a heuristic parametrization of violent relaxation in the form of a fermionic Fokker-Planck (or Landau) equation involving a diffusion term and a friction term. This equation respects the Lynden-Bell exclusion principle. The diffusion term accounts for effective thermal effects (fluctuations) and the friction term accounts for collisionless dissipation (nonlinear Landau damping). The competition between these two terms establishes, at statistical equilibrium, the Lynden-Bell distribution[5] in a process reminiscent of the fluctuation-dissipation theorem.

Analogously, in [140,141] we have introduced a heuristic parametrization of gravitational cooling and violent relaxation for self-gravitating BECs described by the GPP equations. We proposed to model these complicated processes on a coarse-grained scale by the generalized GPP equations [140,141][6]:

$$i\hbar\frac{\partial\psi}{\partial t} = -\frac{\hbar^2}{2m}\Delta\psi + m(\Phi + \Phi_{\rm ext})\psi + \frac{K\gamma m}{\gamma - 1}|\psi|^{2(\gamma-1)}\psi + \frac{m}{2}\left(\frac{3}{4\pi\eta_0}\right)^{2/3}|\psi|^{4/3}\psi + 2k_B T\ln|\psi|\psi - i\frac{\hbar}{2}\xi\left[\ln\left(\frac{\psi}{\psi^*}\right) - \left\langle\ln\left(\frac{\psi}{\psi^*}\right)\right\rangle\right]\psi, \quad (3)$$

$$\Delta\Phi = 4\pi G|\psi|^2, \quad (4)$$

[4]The theory of Lynden-Bell [136] applies to collisionless classical particles like stars as well as to collisionless quantum particles like fermions or bosons. Actually, in the fermionic DM model mentioned at the beginning of this Introduction, the Fermi-Dirac distribution is justified by the theory of violent relaxation (see the discussion in [26,39,40]), not by standard quantum mechanics. Indeed, the relaxation time towards the true Fermi-Dirac distribution with a temperature $T_{\rm th} \neq 0$ is larger than the age of the Universe by many orders of magnitude. Therefore, the DM halos cannot thermalize by a "collisional" process and one must rather invoke a process of violent collisionless relaxation [136]. As a result, the temperature T appearing in the Fermi-Dirac distribution is an effective temperature (the true thermodynamic temperature $T_{\rm th}$ is very small and can be taken equal to zero). It can be shown that the maximum value of the distribution function η_0 appearing in the Lynden-Bell distribution is of the same order as the bound m^4/h^3 set by the Pauli exclusion principle (see footnote 34 of [40]). This makes the analogy between the Lynden-Bell distribution and the Fermi-Dirac distribution even closer.

[5]When coupled to the Poisson equation, the Lynden-Bell (or Fermi-Dirac) distribution generates a halo with an infinite mass like the classical isothermal sphere [136]. This is because the Lynden-Bell distribution does not take into account the escape of high energy particles. However, it is possible to derive from the kinetic theory a truncated Lynden-Bell distribution taking into account the escape of high energy particles [138]. This model, which can be viewed as a sort of fermionic King model [39,40], has a finite mass.

[6]A detailed derivation of these equations will be given in a forthcoming paper [142].

where $\langle X\rangle = \frac{1}{M}\int \rho X d\mathbf{r}$ denotes a spatial average over the halo. The terms on the first line of Eq. (3) correspond to the ordinary GP equation (1). For the sake of generality, we have introduced an external potential $\Phi_{\rm ext}$ that could take into account the presence of a central black hole[7] or model other effects of astrophysical interest. In the following, for illustration, we shall consider the harmonic potential

$$\Phi_{\rm ext} = \frac{1}{2}\omega_0^2 r^2. \tag{5}$$

When $\omega_0^2 > 0$, it can mimic the tidal interactions arising from neighboring galaxies. When $\omega_0^2 < 0$, it can mimic a solid-body rotation of the system or the effect of dark energy (cosmological constant). The last term on the first line of Eq. (3) takes into account the self-interaction of the bosons. For the sake of generality, we have considered an arbitrary power-law nonlinearity [140,141] instead of the cubic nonlinearity present in the ordinary GP equation [144–147]. In the theoretical part of this paper, we shall give results valid for arbitrary values of γ and K. They can be useful in more general situations. However, in the applications, we shall specifically consider the standard BEC model corresponding to

$$K = \frac{2\pi a_s \hbar^2}{m^3} \quad \text{and} \quad \gamma = 2. \tag{6}$$

The terms on the second and third lines of Eq. (3) correspond to our heuristic parametrization of gravitational cooling and violent relaxation. The first term on the second line of Eq. (3) accounts for an effective fermionic core and the second term on the second line of Eq. (3) accounts for an isothermal halo, with an effective temperature T, surrounding the core. This fermionic core and this isothermal halo are justified by Lynden-Bell's theory of violent relaxation (the isothermal halo is also expected from the process of gravitational cooling).[8] These two terms could be combined into a single nonlinearity expressed as an enthalpic function $h_{\rm LB}(|\psi|^2)$ associated with the equation of state arising from the Lynden-Bell ($\sim$ Fermi-Dirac) distribution or from the fermionic King model (see [140,141] for a general formalism). In the present paper, we shall assume that the system is nondegenerate in the sense of Lynden-Bell and we shall accordingly neglect the contribution of the fermionic core.[9] As a result, we just consider the contribution of the isothermal halo and formally take $\eta_0 \to +\infty$. Finally, the term on the third line of Eq. (3) is a damping term that ensures that the system relaxes towards an equilibrium state. This is guaranteed by an H-theorem for a generalized free energy functional [140,141]. It is natural to have a friction term and a temperature term in the phenomenology of violent relaxation and gravitational cooling. This manifests a sort of fluctuation-dissipation theorem.[10] It can be shown [141,142] that the hydrodynamic representation of the generalized GPP equations (3) and (4) is consistent with the hydrodynamic moments of the fermionic Fokker-Planck equation introduced in [137] to parametrize the classical process of violent relaxation. In the case of BECs, quantum mechanics introduces additional terms which are the quantum potential and the pressure associated with the self-interaction of the bosons. When these terms become negligible at large scales one recovers the hydrodynamic equations of [137]. This consistency suggests that the parametrization of the GPP equations provided by Eqs. (3) and (4) is physically relevant.

This paper is organized as follows. In Sec. II we review the main properties of the generalized GPP equations (3) and (4) introduced in [140]. In Secs. III and IV we show that the equilibrium states of these equations determine a DM halo with a core-halo structure made of a solitonic core and an isothermal atmosphere. In Sec. V we provide a semianalytical description of this core-halo structure. We mention the analogy with the core-halo structure of fermionic DM halos studied in the past. In Sec. VI, we introduce a first model of BECDM halos (model I) in which the density profile does not present a plateau between the core and the halo. This model describes ultracompact DM halos that are purely solitonic (quantum ground state), small DM halos with a solitonic core and a tenuous isothermal atmosphere (quantum phase), and large DM halos which are purely isothermal without a solitonic core (gaseous phase). In Sec. VII, we introduce a second model of BECDM halos (model II) in which the density profile may present a plateau between the core and the halo. This model describes large halos that are purely isothermal without a solitonic core (gaseous phase) as in model I and large halos with a solitonic core and a massive isothermal atmosphere (core-halo phase). We argue that the solitonic core may represent a bulge but that it cannot mimic a supermassive black hole (SMBH). In Sec. VIII, we show that the previous solutions (quantum, gaseous, core-halo) can be recovered by studying the phase transitions of a thermal self-gravitating boson gas in a box. We discuss the stability of these solutions and determine the solitonic core mass as a function of the halo mass from thermodynamical considerations. We argue that, above a critical DM halo

[7]The case of an external potential $\Phi_{\rm BH} = -GM_{\rm BH}/r$ created by a central black hole is treated specifically in Ref. [143].

[8]The effective temperature appearing in Eq. (3) is related to the Lynden-Bell temperature by $k_B T/m = T_{\rm LB}/\eta_0$. Since the mass m of the particles does not intervene in collisionless systems, only the ratio $k_B T/m$ makes sense in our model. In other words, the temperature is proportional to mass [136].

[9]This term will be considered in a forthcoming paper [142].

[10]We show in Appendix C that these two terms emerge from a unified framework related to Nottale's theory of scale relativity [148].

mass, the quantum core (bulge) becomes unstable and is replaced by a SMBH. In Sec. IX, we consider astrophysical applications of our model. In particular, we connect the bifurcation between the gaseous phase (with a positive specific heat) and the core-halo phase (with a negative specific heat) to the canonical critical point $(M_h)_{\rm CCP} = 3.27\times 10^9\ M_\odot$ of the thermodynamical model and we connect the possible formation of SMBHs at the centers of galaxies to the microcanonical critical point $(M_h)_{\rm MCP}\sim 2\times 10^{12}\ M_\odot$.

II. PROPERTIES OF THE GENERALIZED GPP EQUATIONS

We propose to heuristically model the process of gravitational cooling and violent relaxation of self-gravitating BECs at $T_{\rm th}=0$ by the generalized GPP equations (3) and (4) which include a logarithmic nonlinearity and a source of dissipation (damping). These equations provide an effective description of the system's dynamics on a coarse-grained scale. In other words, they provide a coarse-grained parametrization of the fined-grained GPP equations (1) and (2). In this paper we assume that the system is nondegenerate (in the sense of Lynden-Bell) and ignore the contribution of the effective fermionic core ($\eta_0\to+\infty$).

A. Madelung transformation

In order to enlighten the physical meaning of the generalized GPP equations (3) and (4), we can write them in the form of hydrodynamic equations by using the Madelung [149] transformation. We write the wave function as

$$\psi(\mathbf{r},t)=\sqrt{\rho(\mathbf{r},t)}e^{iS(\mathbf{r},t)/\hbar}, \tag{7}$$

where $\rho=|\psi|^2$ is the density and $S(\mathbf{r},t)=-i(\hbar/2)\times\ln(\psi/\psi^*)$ is the action. We note that the effective temperature term in the generalized GP equation (3) can be written as $k_BT\ln\rho\psi$ and the dissipative term as $\xi(S-\langle S\rangle)\psi$. Following Madelung, we introduce the velocity field $\mathbf{u}=\nabla S/m$. Since the velocity is potential, the flow is irrotational: $\nabla\times\mathbf{u}=\mathbf{0}$. Substituting Eq. (7) into Eq. (3) and separating the real and imaginary parts, we find that the generalized GPP equations (3) and (4) are equivalent to the hydrodynamic equations [140]

$$\frac{\partial\rho}{\partial t}+\nabla\cdot(\rho\mathbf{u})=0, \tag{8}$$

$$\frac{\partial\mathbf{u}}{\partial t}+(\mathbf{u}\cdot\nabla)\mathbf{u}=-\frac{1}{\rho}\nabla P-\nabla\Phi-\nabla\Phi_{\rm ext}-\frac{1}{m}\nabla Q-\xi\mathbf{u}, \tag{9}$$

$$\Delta\Phi=4\pi G\rho, \tag{10}$$

where

$$Q=-\frac{\hbar^2}{2m}\frac{\Delta\sqrt{\rho}}{\sqrt{\rho}} \tag{11}$$

is the quantum potential and

$$P=K\rho^\gamma+\rho\frac{k_BT}{m}\quad(\gamma=1+1/n) \tag{12}$$

is the total pressure. The equation of state (12) is the sum of a polytropic equation of state due to the power-law nonlinearity in the generalized GP equation (3) and an isothermal (linear) equation of state due to the logarithmic term in the generalized GP equation (3). For the standard BEC model of Eq. (6), the polytropic equation of state writes

$$P=\frac{2\pi a_s\hbar^2}{m^3}\rho^2, \tag{13}$$

corresponding to a polytropic index $\gamma=2$ ($n=1$). It takes into account the self-interaction of the bosons. In that case, the total equation of state (12) becomes

$$P=\frac{2\pi a_s\hbar^2}{m^3}\rho^2+\rho\frac{k_BT}{m}. \tag{14}$$

On the other hand, Eq. (8) is the continuity equation, Eq. (9) is the momentum equation, and Eq. (10) is the Poisson equation. We note that the momentum equation involves a damping term, proportional and opposite to the velocity, corresponding to the last term in the generalized GP equation (3). Using the continuity equation (8), the momentum equation (9) can be rewritten as

$$\frac{\partial}{\partial t}(\rho\mathbf{u})+\nabla(\rho\mathbf{u}\otimes\mathbf{u})=-\nabla P-\rho\nabla\Phi-\rho\nabla\Phi_{\rm ext}-\frac{\rho}{m}\nabla Q-\xi\rho\mathbf{u}. \tag{15}$$

Equations (8)–(15) form the quantum damped barotropic Euler equations. When the quantum potential is neglected (TF approximation), we recover the classical damped barotropic Euler equations. These equations do not involve viscous terms since they are equivalent to the generalized GPP equations (3) and (4). As a result, they describe a superfluid. For dissipationless systems ($\xi=0$), we recover the quantum and classical barotropic Euler equations.

B. Connection with the equations of Brownian theory

In the overdamped limit $\xi\to+\infty$, we can formally neglect the inertial term in Eq. (9) so that

$$\xi\mathbf{u}\simeq-\frac{1}{\rho}\nabla P-\nabla\Phi-\nabla\Phi_{\rm ext}-\frac{1}{m}\nabla Q. \tag{16}$$

Substituting this relation into the continuity equation (8), we obtain the quantum barotropic Smoluchowski equation [150]:

$$\xi\frac{\partial\rho}{\partial t}=\nabla\cdot\left(\nabla P+\rho\nabla\Phi+\rho\nabla\Phi_{\rm ext}+\frac{\rho}{m}\nabla Q\right). \quad (17)$$

When the quantum potential is neglected (TF approximation), we obtain the classical barotropic Smoluchowski equation which arises in the context of nonlinear Fokker-Planck equations and generalized thermodynamics [151,152]. The isothermal equation of state $P=\rho k_BT/m$ yields an ordinary diffusion term with a diffusion coefficient given by the Einstein formula $D=k_BT/\xi m$. The polytropic equation of state $P=K\rho^\gamma$ leads to anomalous diffusion. If we neglect the advection term $\nabla(\rho\mathbf{u}\otimes\mathbf{u})$ in Eq. (15), but retain the term $\partial(\rho\mathbf{u})/\partial t$, and combine the resulting equation with the continuity equation (8), we obtain the quantum telegraph equation

$$\frac{\partial^2\rho}{\partial t^2}+\xi\frac{\partial\rho}{\partial t}=\nabla\cdot\left(\nabla P+\rho\nabla\Phi+\rho\nabla\Phi_{\rm ext}+\frac{\rho}{m}\nabla Q\right), \quad (18)$$

which can be seen as a generalization of the quantum barotropic Smoluchowski equation (17) taking inertial (or memory) effects into account. When the quantum potential is neglected, we recover the classical telegraph equation.

It is interesting to recover the equations of Brownian theory from the generalized GP equation (3) in the strong friction limit $\xi\to+\infty$. In this sense, the generalized GP equation (3) makes the connection between quantum mechanics ($\xi=0$) and Brownian theory ($\xi\to+\infty$). However, the analogy with Brownian theory is essentially effective as discussed in more detail in [140,141]. The Smoluchowski-Poisson equations describing self-gravitating Brownian particles in the strong friction limit have been studied in [153] and subsequent papers. If the strong friction limit is relevant,[11] these equations may find a new application (with a different interpretation) in the context of DM halos.

C. Generalization of the CDM model

The hydrodynamic equations associated with the CDM model correspond to Eqs. (8)–(10) with $P=Q=\xi=0$. Therefore, the fluid equations (8)–(10) associated with the GPP equations (3) and (4) generalize the hydrodynamic equations of the CDM model in different respects. First, the Euler equation (9) includes a quantum force $\mathbf{F}_Q=-(1/m)\nabla Q$ that takes into account the Heisenberg uncertainty principle. This force is equivalent to an anisotropic pressure force of the form $(F_Q)_i=-(1/\rho)\partial_jP_{ij}$, where $P_{ij}=-(\hbar^2/4m^2)\rho\partial_i\partial_j\ln\rho$ is the quantum pressure tensor. The Euler equation (9) also includes an isotropic pressure force with a polytropic equation of state $P=K\rho^\gamma$ due to the power-law nonlinearity in the generalized GP equation (3). For the standard BEC model (6), this pressure force takes into account the self-interaction of the bosons. These two terms (quantum force and self-interaction) are already present in the hydrodynamic equations associated with the standard GPP equations (1) and (2) [78]. The hydrodynamic equations (8)–(10) associated with the generalized GPP equations (3) and (4) involve, in addition, a pressure force with an isothermal equation of state $P=\rho k_BT/m$ due to the logarithmic nonlinearity present in the generalized GP equation (3). As a result, the complete equation of state is given by Eq. (12). Finally, the Euler equation (9) includes a damping term $-\xi\mathbf{u}$. The damping term ensures that the system relaxes towards an equilibrium state. This result is guaranteed by the existence of an H-theorem as discussed in the next section.

D. H-theorem

The free energy associated with the generalized GPP equations can be written in the usual form $F=E_0-TS_B$, where E_0 is the total energy, T the effective temperature, and $S_B=-k_B\int(\rho/m)(\ln\rho-1)d\mathbf{r}$ the Boltzmann entropy. The total energy $E_0=\Theta_c+\Theta_Q+W+W_{\rm ext}+U$ is the sum of the classical kinetic energy $\Theta_c=(1/2)\int\rho\mathbf{u}^2d\mathbf{r}$, the quantum kinetic energy $\Theta_Q=(1/m)\int\rho Qd\mathbf{r}$, the gravitational potential energy $W=(1/2)\int\rho\Phi d\mathbf{r}$, the external potential energy $W_{\rm ext}=\int\rho\Phi_{\rm ext}d\mathbf{r}=(1/2)\omega_0^2I$ (where $I=\int\rho r^2d\mathbf{r}$ is the moment of inertia) and the internal energy $U=[K/(\gamma-1)]\int\rho^\gamma d\mathbf{r}$ arising from the self-interaction of the bosons.[12] The generalized GPP equations satisfy an H-theorem [140]:

$$\dot F=-\xi\int\rho\mathbf{u}^2d\mathbf{r}\le 0. \quad (19)$$

When $\xi=0$, the generalized GPP equations (3) and (4) conserve the free energy ($\dot F=0$). When $\xi>0$, the free energy decreases monotonically ($\dot F\le 0$). We note that $\dot F=0$ if, and only if, $\mathbf{u}=\mathbf{0}$. Therefore, the dissipative term ensures that the system relaxes towards an equilibrium state for $t\to+\infty$.[13] In this sense, the generalized GPP

[11] Some arguments in favor of the strong friction limit are given in [141].

[12] The free energy can also be written as $F=E_*-TS_B-KS_\gamma$, where $E_*=\Theta_c+\Theta_Q+W+W_{\rm ext}$ is the ideal energy (without the self-interaction term), $S_\gamma=-[1/(\gamma-1)]\int(\rho^\gamma-\rho)d\mathbf{r}$ is the Tsallis entropy of index γ (the standard BEC model corresponds to a quadratic entropy with $\gamma=2$), and K is the polytropic temperature. We can introduce a mixed entropy combining the Boltzmann and Tsallis entropies as discussed in [140].

[13] This result assumes that F is bounded from below. For isothermal self-gravitating systems this is not the case. There is no minimum of free energy at fixed mass because the system can always lose free energy by evaporating. However, evaporation is a slow process. In practice, the system relaxes towards a quasiequilibrium state which occupies a finite region of space. When necessary, we shall artificially confine the system within a box, where the size of the box represents the typical size of the system [33,154].

equations can account, at least heuristically, for the complicated processes of violent relaxation and gravitational cooling.

Remark: The generalized GPP equations (3) and (4) are associated with the canonical ensemble (fixed temperature T). However, they can be extended to the microcanonical ensemble (fixed energy E) as discussed in Appendix I of [140].

E. Equilibrium state

Using Lyapunov's direct method, we can deduce from Eq. (19) that a stable equilibrium state of the generalized GPP equations is a minimum of free energy F at fixed mass M. Therefore, it satisfies the variational principle $\delta F-(\mu/m)\delta M=0$, where μ is a Lagrange multiplier (chemical potential) taking into account the conservation of mass. This gives the relation [140]

$$Q+m\Phi+\frac{1}{2}m\omega_0^2r^2+k_BT\ln\rho+\frac{K\gamma m}{\gamma-1}\rho^{\gamma-1}=\mu \quad (20)$$

that coincides with a static state $\psi(\mathbf{r},t)=\phi(\mathbf{r})e^{-iEt/\hbar}$ of the generalized GPP equations (3) and (4) provided that we make the identification between the eigenenergy and the chemical potential: $E=\mu$ [140]. Equation (20) can be rewritten as

$$\rho=\left\{\frac{k_BT}{|K|\gamma m}W\left[\frac{|K|\gamma m}{k_BT}e^{-\frac{\gamma-1}{k_BT}(m\Phi+Q+\frac{1}{2}m\omega_0^2r^2-\mu)}\right]\right\}^{\frac{1}{\gamma-1}}, \quad (21)$$

where $W(z)$ is a (generalized) Lambert function defined implicitly by the equation $We^W=z$ when $K>0$ and $We^{-W}=z$ when $K<0$. This equation determines the relation between the density ρ and the gravitational potential Φ at equilibrium.[14] When $K=0$ ($W=z$), we obtain the quantum Boltzmann distribution

$$\rho=e^{-\frac{1}{k_BT}(m\Phi+Q+\frac{1}{2}m\omega_0^2r^2-\mu)} \quad (22)$$

associated with the isothermal equation of state. When $T=0$ ($W=\ln z$), we obtain the quantum Tsallis distribution

$$\rho=\left[-\frac{\gamma-1}{K\gamma m}(m\Phi+Q+\frac{1}{2}m\omega_0^2r^2-\mu)\right]^{\frac{1}{\gamma-1}} \quad (23)$$

associated with the polytropic equation of state. For the standard BEC model, corresponding to $\gamma=2$, the relationship between ρ and Φ is linear (in the TF approximation). Combining Eq. (21) with the Poisson equation (10), we obtain a differential equation that determines Φ and ρ. When $K=0$, it reduces to the quantum Boltzmann-Poisson equation and when $T=0$ it reduces to the quantum Tsallis-Poisson equation.

F. Virial theorem

In order to understand qualitatively how the system relaxes towards equilibrium, it may be useful to consider the virial theorem. From the damped quantum barotropic Euler-Poisson equations (8)–(15), we can derive the time-dependent scalar virial theorem [140]:

$$\frac{1}{2}\ddot{I}+\frac{1}{2}\xi\dot{I}+\omega_0^2I=2(\Theta_c+\Theta_Q)+3\int P d\mathbf{r}+W. \quad (24)$$

This equation, together with the H-theorem (19), shows that the system generically converges towards an equilibrium state (or a quasiequilibrium state) by exhibiting damped oscillations. These damped oscillations are consistent with the phenomenology of gravitational cooling [132–134] and violent relaxation [136].

G. Gaussian ansatz

In order to determine accurately the dynamical evolution of a self-gravitating BEC, one must solve the (generalized) GPP equations (3) and (4) numerically. However, an approximate analytical solution can be obtained by making a Gaussian ansatz for the wave function. From the virial theorem, we can obtain a simple differential equation governing the temporal evolution of the typical radius $R(t)$ of the BEC. It is given by [140]

$$\alpha M\frac{d^2R}{dt^2}+\xi\alpha M\frac{dR}{dt}+\alpha\omega_0^2MR=2\sigma\frac{\hbar^2M}{m^2R^3}+3\frac{Mk_BT}{mR}+3\zeta\frac{KM^\gamma}{R^{3(\gamma-1)+1}}-\nu\frac{GM^2}{R^2}. \quad (25)$$

The coefficients are $\alpha=3/2$, $\sigma=3/4$, $\zeta=\pi^{-3(\gamma-1)/2}\gamma^{-3/2}$ and $\nu=1/\sqrt{2\pi}$. At equilibrium ($\dot{R}=\ddot{R}=0$), this equation determines an approximate expression of the mass-radius relation of the self-gravitating BEC. In many cases, this approximate mass-radius relation gives a good agreement with the exact mass-radius relation obtained by solving the GPP equations numerically [78,79]. On the other hand, as illustrated in Fig. 1, the dynamical equation (25) confirms that the system generically relaxes towards the equilibrium state by undergoing damped oscillations.[15]

[14]We note that Eq. (21) is a complicated differential equation because of the presence of the quantum potential that involves derivatives of ρ. It is only in the TF approximation ($Q=0$) that the relationship between ρ and Φ is explicit.

[15]We note that if we make the Gaussian ansatz on the usual GPP equations (1) and (2), we miss the important processes of gravitational cooling and violent relaxation because the resulting differential equation for $R(t)$ does not exhibit damped oscillations (since $\xi=0$) [78] while the GPP equations (1) and (2) do [132–134]. This shows the interest of our heuristic parametrization based on the generalized GPP equations (3) and (4).

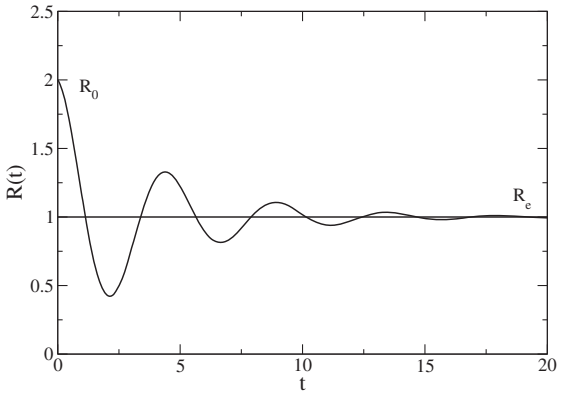

FIG. 1. Damped oscillations of the radius of the self-gravitating BEC during its relaxation towards equilibrium (schematic evolution based on the Gaussian ansatz).

H. Complex pulsation

Close to equilibrium, the complex pulsation can be determined approximately from the Gaussian ansatz. It is given by [140]

$$\omega^2 = \frac{6\Theta_Q + 3(\gamma-1)(3\gamma-2)U + 2W + \omega_0^2 I + 3Nk_BT}{I}. \tag{26}$$

Alternative expressions of the pulsation can be obtained by using the equilibrium form of the free energy and of the virial theorem ($\ddot{I} = \dot{I} = \Theta_c = 0$):

$$F = \Theta_Q + U + W + \frac{1}{2}\omega_0^2 I - TS_B, \tag{27}$$

$$2\Theta_Q + 3\int P d\mathbf{r} + W - \omega_0^2 I = 0. \tag{28}$$

For the equation of state (14), we have $\int P d\mathbf{r} = (\gamma-1)U + Nk_BT$. Particular cases are considered specifically in [140]. In the TF approximation, they agree with the approximate expression of the pulsation given by the Ledoux formula [155].

III. CORE-HALO STRUCTURE OF THE EQUILIBRIUM STATES

A. Fundamental equation of quantum hydrostatic equilibrium

In order to determine the equilibrium states of a self-gravitating BECDM halo, instead of solving the coupled equations (10) and (21), it is more convenient to proceed as follows. We first take the gradient of Eq. (20) and obtain the condition of quantum hydrostatic equilibrium [140]:

$$\frac{\rho}{m}\nabla Q + \nabla P + \rho\nabla\Phi + \rho\nabla\Phi_{\rm ext} = \mathbf{0}. \tag{29}$$

This equation also corresponds to a static state ($\partial_t\rho = 0$, $\mathbf{u} = \mathbf{0}$) of the damped quantum Euler equations (8) and (9). It describes the balance between the quantum potential arising from the Heisenberg uncertainty principle, the pressure due to short-range interactions (scattering), the pressure due to the effective temperature, the gravitational attraction, and the external potential. Combining Eq. (29) with the Poisson equation (10), we obtain the fundamental differential equation of quantum hydrostatic equilibrium [140]:

$$\frac{\hbar^2}{2m^2}\Delta\left(\frac{\Delta\sqrt{\rho}}{\sqrt{\rho}}\right) - \nabla\cdot\left(\frac{\nabla P}{\rho}\right) = 4\pi G\rho + 3\omega_0^2. \tag{30}$$

For the equation of state (12), it takes the form

$$\frac{\hbar^2}{2m^2}\Delta\left(\frac{\Delta\sqrt{\rho}}{\sqrt{\rho}}\right) - \frac{K\gamma}{\gamma-1}\Delta\rho^{\gamma-1} - \frac{k_BT}{m}\Delta\ln\rho = 4\pi G\rho + 3\omega_0^2. \tag{31}$$

This differential equation determines the general equilibrium density profile $\rho(\mathbf{r})$ of a BECDM halo in our model. This profile generically has a core-halo structure with a solitonic core and an isothermal halo (we assume that $\gamma > 1$). In the following, for simplicity, we take $\omega_0 = 0$ and consider spherically symmetric distributions.

B. Solitonic core

In the core, where the density is high, the equation of state (12) is dominated by the polytropic (self-interaction) term and the thermal term can be neglected ($T = 0$). The gravitational attraction is counterbalanced by the quantum potential and by the self-interaction of the bosons. In that case, Eq. (31) reduces to

$$\frac{\hbar^2}{2m^2}\Delta\left(\frac{\Delta\sqrt{\rho}}{\sqrt{\rho}}\right) - \frac{K\gamma}{\gamma-1}\Delta\rho^{\gamma-1} = 4\pi G\rho. \tag{32}$$

The solution of Eq. (32) is called a soliton, being a static state of the ordinary GPP equations (1) and (2).[16] The ground state corresponds to the density profile that has no node.

1. Noninteracting limit

In the noninteracting limit ($K = 0$), the gravitational attraction is counterbalanced by the quantum potential. In that case, Eq. (32) reduces to

[16]In the TF approximation (see below), we will still call the solution of Eq. (32) a soliton although this terminology is abusive since the effect of the quantum potential which usually gives rise to the soliton in the absence of self-interaction is neglected.

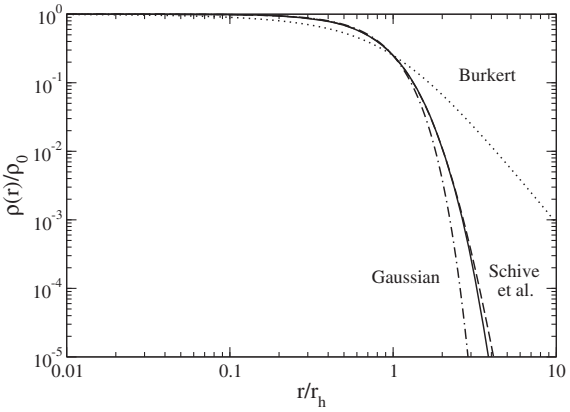

FIG. 2. Normalized density profile of the soliton. It is compared with the Gaussian profile (35) considered in [78], the profile (36) proposed by Schive *et al.* [96,97], and the Burkert profile [6].

$$\frac{\hbar^2}{2m^2}\Delta\left(\frac{\Delta\sqrt{\rho}}{\sqrt{\rho}}\right)=4\pi G\rho. \tag{33}$$

This equation has been solved numerically in [50,79,96,97,111,133,134,156] and the exact density profile has been obtained in these papers. The result of [79] is reproduced in Fig. 2 where the density is normalized by the central density ρ_0 and the radial distance is normalized by the halo radius r_h defined by Eq. (D3). This profile has not a compact support, i.e., it extends to infinity. The exact mass-radius relation is given by [50,78,79]

$$R_{99}=9.946\frac{\hbar^2}{GMm^2}, \tag{34}$$

where R_{99} is the radius of the configuration containing 99% of the mass.

In [78] we have approximated the solitonic density profile by a Gaussian:

$$\rho=\rho_0 e^{-r^2/R^2}. \tag{35}$$

From this distribution, we can obtain the following results. The total mass is given by $M=5.57\rho_0R^3$. The radius containing 99% of the mass is $R_{99}=2.38R$. The halo radius where the central density is divided by 4 is $r_h=1.18R$ and the core radius where the central density is divided by 2 is $r_c=0.833R$. We also find that $M_h/(\rho_0 r_h^3)=1.95$, where M_h is the halo mass defined by Eq. (D5). Using Eq. (34), we obtain $r_h=2.82\hbar^2/(Gm^2M_h)$ and $\rho_0=1.45\hbar^2/(Gm^2r_h^4)$.

On the other hand, Schive *et al.* [96,97] have introduced a fit of a form

$$\rho=\frac{\rho_0}{[1+(r/R)^2]^8}. \tag{36}$$

From this distribution, we can obtain the following results. The total mass is given by $M=0.318\rho_0R^3$. The radius containing 99% of the mass is $R_{99}=1.151R$. The halo radius where the central density is divided by 4 is $r_h=0.435R$ and the core radius where the central density is divided by 2 is $r_c=0.301R$. We also find that $M_h/(\rho_0 r_h^3)=1.91$. Using Eq. (34), we obtain $r_h=1.85\hbar^2/(Gm^2M_h)$ and $\rho_0=0.969\hbar^2/(Gm^2r_h^4)$.

These fits are compared with the exact density profile from [79] in Fig. 2. The Gaussian profile [78] works very well up to the halo radius r_h. The fit of Schive *et al.* [96,97] is valid on a slightly longer distance $\sim 2.5r_h$. For comparison, we have plotted the Burkert profile (see Appendix D 4) that will be considered thereafter.

Remark: We have recently found in Ref. [157] another solution of Eq. (33) which has a compact support.

2. TF approximation

In this section, we assume that the bosons have a repulsive self-interaction ($K>0$). In the TF approximation ($Q=0$), Eq. (32) reduces to

$$-\frac{K\gamma}{\gamma-1}\Delta\rho^{\gamma-1}=4\pi G\rho. \tag{37}$$

This equation is equivalent to the Tsallis-Poisson equation obtained by combining Eqs. (10) and (23). It is also equivalent to the Lane-Emden equation (D28) [158]. It describes the balance between the gravitational attraction and the repulsion due to the short-range interactions.

For the standard BEC model (6), the system is equivalent to a polytrope of index $n=1$. In that case, Eq. (37) becomes

$$\Delta\rho+\frac{Gm^3}{a_s\hbar^2}\rho=0. \tag{38}$$

This equation has a simple analytical solution given by [158]

$$\rho(r)=\rho_0\frac{\sin(\pi r/R)}{\pi r/R}, \tag{39}$$

where ρ_0 is the central density and

$$R=\pi\left(\frac{a_s\hbar^2}{Gm^3}\right)^{1/2} \tag{40}$$

is the radius of the configuration at which the density vanishes (the density profile has a compact support). The radius of a polytrope $n=1$ is independent of its mass [158]. The central density is related to the mass by

$$\rho_0=\frac{\pi M}{4R^3}=\frac{M}{4\pi^2}\left(\frac{Gm^3}{a_s\hbar^2}\right)^{3/2}. \tag{41}$$

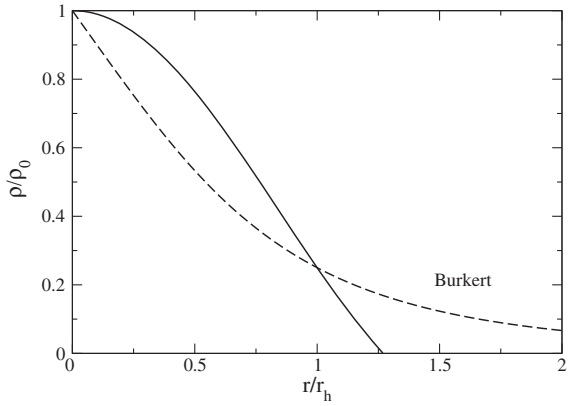

FIG. 3. Density profile of a self-gravitating BEC with a repulsive self-interaction in the TF limit (polytrope $n = 1$). It is compared to the Burkert profile (dashed line).

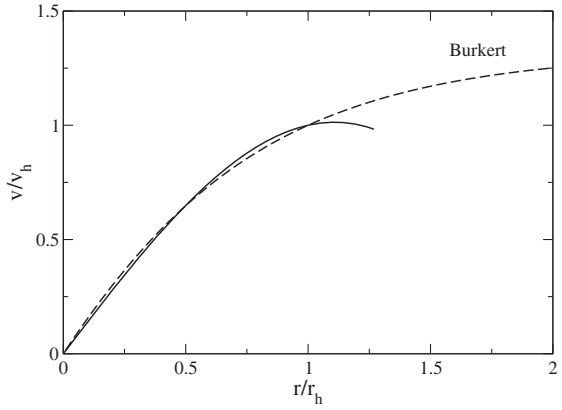

FIG. 4. Same as Fig. 3 for the circular velocity profile.

These results have been derived by several authors in the context of self-gravitating BECs and SFs [53,60,67,69,78,159,160].

Using Eq. (39), we find that the accumulated mass and circular velocity profiles defined by Eqs. (D4) and (D6) are given by

$$M(r) = \frac{4\rho_0 R^3}{\pi^2}\left[\sin\left(\frac{\pi r}{R}\right) - \frac{\pi r}{R}\cos\left(\frac{\pi r}{R}\right)\right], \quad (42)$$

$$v^2(r) = \frac{4G\rho_0 R^2}{\pi}\left[\frac{R}{\pi r}\sin\left(\frac{\pi r}{R}\right) - \cos\left(\frac{\pi r}{R}\right)\right]. \quad (43)$$

For $r \to 0$, the velocity increases linearly with r as for a uniform sphere with density ρ_0: $v(r) \sim (4\pi\rho_0 G/3)^{1/2} r$. For $r \geq R$, we recover the Keplerian law $v(r) = (GM/r)^{1/2}$.

The halo radius, the halo mass, and the circular velocity at the halo radius are given by (see Appendix D 3)

$$\frac{r_h}{R} = 0.788, \qquad \frac{M_h}{\rho_0 r_h^3} = 2.12, \quad (44)$$

$$\frac{v_h^2}{4\pi G\rho_0 r_h^2} = 0.169. \quad (45)$$

The density and circular velocity profiles are plotted in Figs. 3 and 4. For comparison, we have plotted the Burkert profile (see Appendix D 4). We recall that the Burkert profile is empirical. In particular, the Burkert density profile behaves like r instead of r^2 as $r \to 0$, which is not physical for spherically symmetic systems. This explains the disagreement between the two density profiles for $r \leq r_h$. In spite of this difference, the circular velocity profiles are relatively close to each other up to the halo radius r_h. As discussed in Sec. VI F, the solitonic solution of the BECDM model is expected to provide a better description of ultracompact DM halos than the Burkert profile that is more adapted to describe larger DM halos.

3. General case

In the general case, Eq. (32) has been solved numerically in [79,134] for the standard BEC model ($\gamma = 2$). It leads to a general soliton profile taking the quantum potential and the self-interaction into account. This profile is relatively well approximated by a Gaussian distribution, especially when the self-interaction is weak. The solitonic density profile does not diverge at the origin. This may solve the cusp problem of the CDM model. The mass-radius relation of self-gravitating BECs at $T = 0$ (representing the solitonic core of DM halos) has been obtained analytically (approximately) and numerically (exactly) in [78,79] for the standard BEC model ($\gamma = 2$). The case of a self-gravitating BEC with an attractive self-interaction ($a_s < 0$) has also been considered in these papers. It is found that stable configurations only exist below a maximum mass and above a minimum radius given by [78,79]

$$M_{\max} = 1.012\frac{\hbar}{\sqrt{Gm|a_s|}}, \quad (46)$$

$$R_{99} = 5.5\left(\frac{|a_s|\hbar^2}{Gm^3}\right)^{1/2}. \quad (47)$$

C. Isothermal halo

In the halo, where the density is low, the equation of state (12) is dominated by the linear (thermal) term and the self-interaction of the bosons can be neglected ($K = 0$). The quantum potential can also be neglected ($Q = 0$). In that case, Eq. (31) reduces to

$$-\frac{k_B T}{m}\Delta \ln\rho = 4\pi G\rho. \quad (48)$$

This equation is equivalent to the Boltzmann-Poisson equation obtained by combining Eqs. (10) and (22). It is

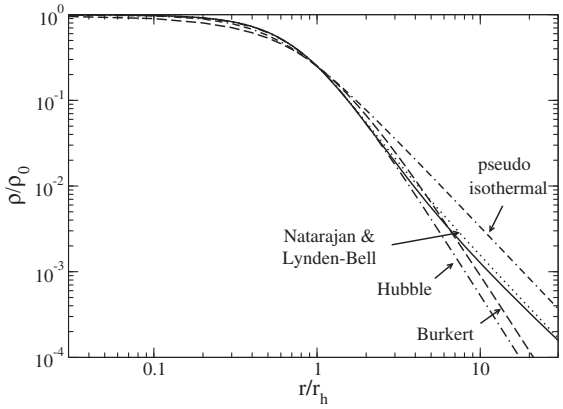

FIG. 5. Normalized isothermal density profile up to $30r_h$. It is compared to the Burkert profile and to other profiles introduced in the literature (see Appendix D).

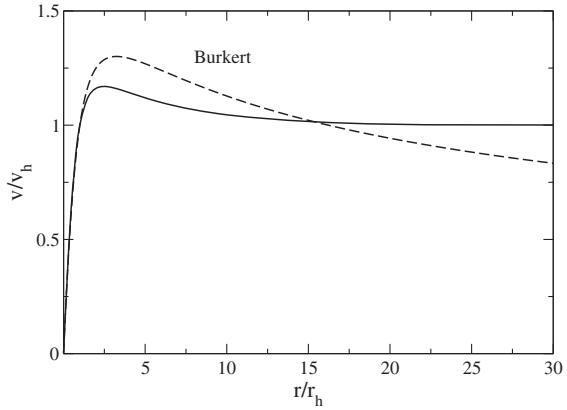

FIG. 6. Normalized circular velocity profile corresponding to the isothermal sphere (the circular velocity reaches its maximum value $v_{\max}/v_h = 1.17$ at $r_*/r_h = 2.48$). It is compared to the Burkert profile ($v_{\max}/v_h = 1.30$ at $r_*/r_h = 3.24$).

also equivalent to the Emden equation (D13) [158].[17] It describes the balance between the gravitational attraction and the thermal pressure. This equation has no simple analytical solution and must be solved numerically. However, its asymptotic behavior is known analytically [158]. The density of a self-gravitating isothermal halo decreases as $\rho(r) \sim k_B T/(2\pi G m r^2)$ for $r \to +\infty$, corresponding to an accumulated mass $M(r) \sim 2k_B \mathrm{Tr}/(Gm)$ increasing linearly with r. This leads to flat rotation curves $v^2(r) = GM(r)/r \to v_\infty^2 = 2k_B T/m$ in agreement with the observations [135].

We note that the isothermal profile has not a compact support so that it extends up to infinity. Furthermore its total mass is infinite [135]. This is why self-gravitating systems have no statistical equilibrium state in an unbounded domain (see [33,154] and footnote 13). In practice, the isothermal equation of state is not valid at arbitrarily large distances and the halo is confined by other effects (see Appendix B). From Eq. (48) we can define a characteristic radius

$$r_0 = \left(\frac{k_B T}{4\pi G \rho_0 m}\right)^{1/2} \tag{49}$$

that we shall call the thermal core radius. It represents the typical core radius of an isothermal halo of central density ρ_0.

The halo mass, the temperature, and the circular velocity at the halo radius are given by (see Appendix D 2)

$$\frac{r_h}{r_0} = 3.63, \qquad \frac{M_h}{\rho_0 r_h^3} = 1.76, \tag{50}$$

$$\frac{k_B T}{G m \rho_0 r_h^2} = 0.954, \qquad \frac{v_h^2}{4\pi G \rho_0 r_h^2} = 0.140. \tag{51}$$

The density and circular velocity profiles of a purely isothermal halo are plotted in Figs. 5 and 6 (see Appendix D 2). For comparison, we have plotted the empirical (observational) Burkert profile [6] (see Appendix D 4). The isothermal profile is close to the Burkert profile up to $r/r_h = 6$. We have also plotted some analytical profiles that have been introduced in the literature to fit the isothermal profile. The pseudo-isothermal profile (see Appendix D 5) provides a good fit of the isothermal profile up to $r/r_h = 1$. The modified Hubble profile [135] (see Appendix D 6) provides a good fit of the isothermal profile up to $r/r_h = 3$. The Natarajan and Lynden-Bell profile [161] (see Appendix D 7) provides a good fit of the isothermal profile for all radii.

Remark: The modified Hubble profile provides a good fit to the isothermal profile for $r/r_h \leq 3$. In particular, it provides a better fit than the pseudo-isothermal profile even though the pseudo-isothermal profile decreases asymptotically as r^{-2}, like the isothermal profile, while the modified Hubble profile decreases asymptotically as r^{-3}. The reason is that, for $r/r_h \leq 3$, we are not in the asymptotic limit where the isothermal density profile displays a logarithmic slope -2. This remark may explain why, in certain circumstances, we observe a density profile with an effective logarithmic slope -3 (like for the observational Burkert profile and for the numerical NFW profile) instead of -2 (corresponding to the isothermal profile predicted by statistical mechanics). Indeed, at intermediate distances $r/r_h \leq 3$, the isothermal profile presents an effective logarithmic slope -3 (see Fig. 5). In this sense, the Burkert and NFW profiles are not in contradiction with the isothermal profile although their

[17]The Boltzmann-Poisson equations and the Emden equation describe the equilibrium state of a classical self-gravitating gas with an isothermal equation of state [158]. They also describe the statistical equilibrium (most probable) state of stellar systems [33,154]. In these two cases, the isothermal distribution results from a collisional relaxation due to strong collisions (gas) or to weak two-body gravitational encounters (stellar systems). By contrast, in the present paper, the effective isothermal halo is justified by Lynden-Bell's statistical mechanics of collisionless violent relaxation [136].

asymptotic slopes (for $r \to +\infty$) are different. This remark is important since the Burkert and NFW profiles are purely empirical while the isothermal profile is justified by statistical mechanics (in the sense of Lynden-Bell). This argument may provide a physical justification of the Burkert and NFW profiles. A detailed comparison between the isothermal and Burkert profiles is made is Sec. VI F.

IV. COMPLETE CORE-HALO SOLUTION

When studying BECDM halos, many authors [47,96,97,122] assume that the bosons are noninteracting ($a_s = 0$). However, cosmological constraints impose that the bosons should have a repulsive self-interaction [46,98]. A repulsive self-interaction may also solve some tensions encountered in the noninteracting model (see the Remark at the end of Appendix D. 4 of [46]). Therefore, a self-interacting SF may be more relevant than a noninteracting SF. In this paper, we consider BECDM halos with a repulsive self-interaction. We assume that the self-interaction is sufficiently strong so that the TF approximation, which amounts to neglecting the quantum potential, is applicable.[18] We shall obtain the complete core-halo profile of BECDM halos in the TF approximation. Other situations (noninteracting bosons, bosons with an attractive self-interaction, fermions, etc.) will be considered in a forthcoming paper [142].

A. Generalized Emden equation

We start from the general equation (31) determining the complete core-halo structure of the system. We consider the standard BEC model (6). We assume that the bosons have a repulsive self-interaction ($a_s > 0$) and we make the TF approximation ($Q = 0$). We also ignore the harmonic potential ($\omega_0 = 0$) and restrict ourselves to spherically symmetric configurations. In that case, Eq. (31) reduces to

$$-\frac{4\pi a_s \hbar^2}{m^3}\Delta\rho - \frac{k_B T}{m}\Delta \ln\rho = 4\pi G\rho. \tag{52}$$

This equation is equivalent to the equation obtained by combining Eq. (21) with the Poisson equation (10). We write

$$\rho = \rho_0 e^{-\psi} \quad \text{and} \quad \xi = \frac{r}{r_0}, \tag{53}$$

where ρ_0 is the central density and r_0 is the thermal core radius defined by Eq. (49). We also introduce the dimensionless parameter

$$\chi = \frac{4\pi a_s \hbar^2 \rho_0}{m^2 k_B T}, \tag{54}$$

which is a measure of the central density ρ_0 for a given value of the temperature T. We call it the concentration parameter. Equation (52) then takes the form of a generalized Emden equation

$$\Delta\psi + \chi\nabla\cdot(e^{-\psi}\nabla\psi) = e^{-\psi}. \tag{55}$$

The ordinary Emden equation (D13) is recovered for $\chi = 0$. Another transformation in which Eq. (52) takes the form of a generalized Lane-Emden equation is proposed in Appendix E. For a spherically symmetric configuration, the generalized Emden equation (55) takes the form

$$\frac{1}{\xi^2}\frac{d}{d\xi}\left(\xi^2\frac{d\psi}{d\xi}\right) + \frac{\chi}{\xi^2}\frac{d}{d\xi}\left(\xi^2 e^{-\psi}\frac{d\psi}{d\xi}\right) = e^{-\psi}, \tag{56}$$

or, equivalently,

$$\frac{d^2\psi}{d\xi^2} + \frac{2}{\xi}\frac{d\psi}{d\xi} = \frac{\chi(\frac{d\psi}{d\xi})^2 + 1}{\chi + e^{\psi}}. \tag{57}$$

For a given value of χ, this equation can be solved numerically with the boundary conditions $\psi(0) = \psi'(0) = 0$. We note that $\psi''(0) = 1/[3(1+\chi)]$. The density profile is plotted in Fig. 7 for $\chi = 20$.

B. Mass and circular velocity profiles

According to Eqs. (53) and (D4), the mass contained within a sphere of radius r is

$$M(r) = \rho_0 r_0^3 \int_0^{\xi} e^{-\psi} 4\pi\xi'^2 d\xi'. \tag{58}$$

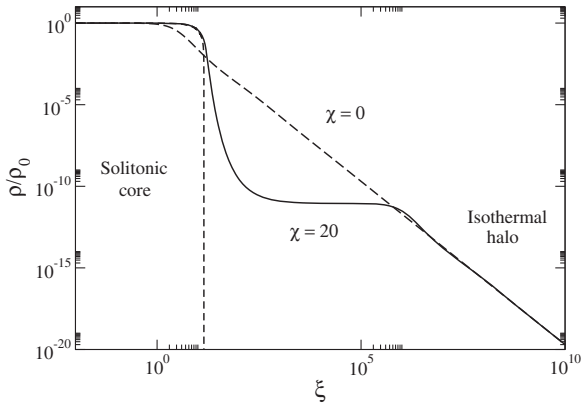

FIG. 7. Normalized density profile corresponding to $\chi = 20$. It presents a core-halo structure with a solitonic core and an isothermal halo (see Sec. V). The long-dashed line corresponds to a pure isothermal halo ($\chi = 0$) decreasing as $\rho/\rho_0 \sim 2/\xi^2$. The short-dashed line corresponds to a pure solitonic profile whose analytical expression is $\rho/\rho_0 = (\sqrt{\chi}/\xi)\sin(\xi/\sqrt{\chi})$.

[18]The considerations developed in Appendix D. 4 of [46] indicate that DM halos with an attractive self-interaction may be just at the transition between the noninteracting regime and the TF regime. Therefore, the TF approximation may be just marginally applicable. In principle, we should take into account both the quantum potential and the self-interaction of the bosons as done in [78,79] for the self-gravitating BEC model at $T = 0$. In this paper, for simplicity, we ignore the contribution of the quantum potential.

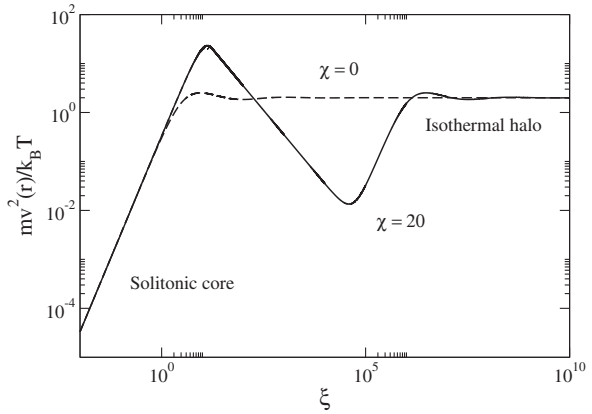

FIG. 8. Normalized circular velocity profile corresponding to $\chi = 20$. It displays a dip due to the presence of the solitonic core (see Sec. V). The long-dashed line corresponds to a pure isothermal profile ($\chi = 0$) tending to $mv^2/k_BT \to 2$. The short-dashed line corresponds to a pure solitonic profile whose analytical expression is $mv^2/k_BT = \chi[(\sqrt{\chi}/\xi)\sin(\xi/\sqrt{\chi}) - \cos(\xi/\sqrt{\chi})]$ (it can hardly be distinguished from the solid line up to the border of the soliton).

Using the generalized Emden equation (56), we get

$$\frac{M(r)}{4\pi\rho_0 r_0^3} = \xi^2\psi'(\xi)[1+\chi e^{-\psi(\xi)}]. \tag{59}$$

The circular velocity defined by Eq. (D6) is given by

$$\frac{v^2(r)}{4\pi G\rho_0 r_0^2} = \xi\psi'(\xi)[1+\chi e^{-\psi(\xi)}]. \tag{60}$$

Using Eq. (49), we find that the temperature satisfies the relation

$$\frac{k_BT}{m} = 4\pi G\rho_0 r_0^2. \tag{61}$$

Therefore, we can rewrite Eq. (60) as

$$\frac{mv^2(r)}{k_BT} = \xi\psi'(\xi)[1+\chi e^{-\psi(\xi)}]. \tag{62}$$

The circular velocity profile is plotted in Fig. 8 for $\chi = 20$.

C. Normalized halo parameters

The halo radius defined by Eq. (D3) is given by

$$r_h = \xi_h r_0, \tag{63}$$

where the function $\xi_h(\chi)$ is determined by the equation

$$e^{-\psi(\xi_h)} = \frac{1}{4}. \tag{64}$$

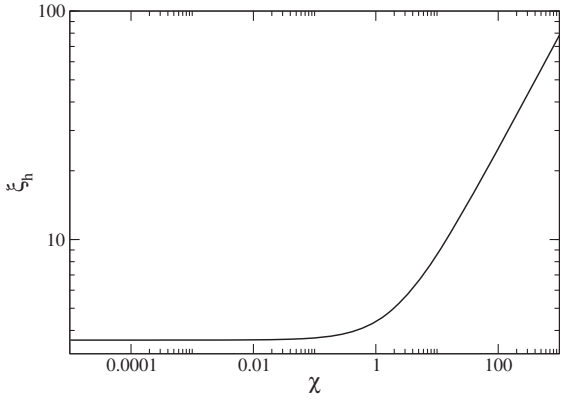

FIG. 9. Normalized halo radius ξ_h vs χ. For $\chi \to 0$, $\xi_h \to 3.63$. For $\chi \to +\infty$, $\xi_h \sim 2.47\sqrt{\chi}$.

Using Eqs. (59) and (63) the halo mass defined by Eq. (D5) is given by

$$\frac{M_h}{\rho_0 r_h^3} = 4\pi\frac{\psi'(\xi_h)}{\xi_h}[1+\chi e^{-\psi(\xi_h)}]. \tag{65}$$

Using Eqs. (60) and (63) the circular velocity at the halo radius defined by Eq. (D7) is given by

$$\frac{v_h^2}{4\pi G\rho_0 r_h^2} = \frac{\psi'(\xi_h)}{\xi_h}[1+\chi e^{-\psi(\xi_h)}]. \tag{66}$$

Finally, using Eqs. (61) and (63), the normalized temperature satisfies the relation

$$\frac{k_BT}{Gm\rho_0 r_h^2} = \frac{4\pi}{\xi_h^2}. \tag{67}$$

The normalized halo radius $\xi_h = r_h/r_0$ and the normalized halo mass $M_h/\rho_0 r_h^3$ are plotted as a function of χ in Figs. 9 and 10. The evolution with χ of the normalized circular velocity at the halo radius $v_h^2/4\pi G\rho_0 r_h^2$ and the

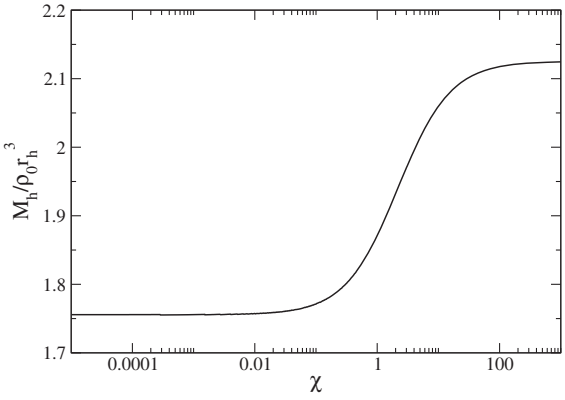

FIG. 10. Normalized halo mass $M_h/\rho_0 r_h^3$ vs χ. It slightly changes from the value 1.76 corresponding to the isothermal profile ($\chi \to 0$) to the value 2.125 corresponding to the solitonic profile ($\chi \to +\infty$).

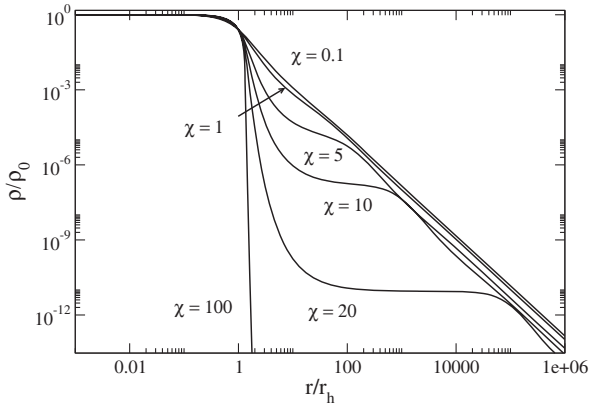

FIG. 11. Normalized density profiles for different values of χ. For $\chi \to 0$ we recover the purely isothermal profile of Fig. 5 (the density profiles with $\chi \leq \chi_* = 0.1$ are indistinguishable from the isothermal profile). For $\chi \to +\infty$ we recover the purely solitonic profile of Fig. 3. For intermediate values of χ, the density profiles have a core-halo structure (see Sec. V).

evolution with χ of the normalized temperature $k_B T/G m \rho_0 r_h^2$ can be easily deduced from these curves.

The normalized density profile $\rho(r)/\rho_0$ and the normalized circular velocity profile $v(r)/v_h$ are plotted as a function of the normalized radial distance

$$\frac{r}{r_h} = \frac{\xi}{\xi_h} \tag{68}$$

in Figs. 11 and 12.

A purely isothermal halo ($a_s = 0$) corresponds to $\chi \to 0$. In that limit, we recover the results of Sec. III C. We also have (see Appendix D 2):

$$\xi_h \to 3.63 \qquad (\chi \to 0). \tag{69}$$

A pure soliton (polytrope of index $n = 1$ with $T = 0$) corresponds to $\chi \to +\infty$. In that limit, we recover the

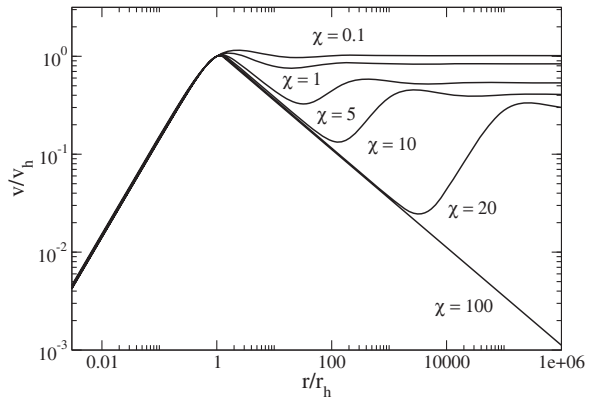

FIG. 12. Normalized circular velocity profiles for different values of χ. For $\chi \to 0$ we recover the purely isothermal profile of Fig. 6. For $\chi \to +\infty$ we recover the purely solitonic profile of Fig. 4. For intermediate values of χ, the circular velocity profiles present a dip due to the presence of the solitonic core (see Sec. V).

results of Sec. III B 2. We must be careful that the definition of ξ adopted in the present section differs from the one used in Appendix D 3. It is easy to see that they are related to each other by $\xi = \tilde{\xi}\sqrt{\chi}$, where $\tilde{\xi}$ refers to the ξ used in Appendix D 3. Since $\tilde{\xi}_h = 2.4746$ (see Appendix D 3), we get

$$\xi_h \sim 2.4746\sqrt{\chi} \quad (\chi \to +\infty). \tag{70}$$

V. SEMIANALYTICAL DESCRIPTION OF THE CORE-HALO STRUCTURE

In the previous section, the differential equation (31) has been solved numerically in the TF approximation. The corresponding density and circular velocity profiles are plotted in Figs. 11 and 12. They present a striking core-halo structure with a solitonic core and an isothermal halo. The presence of the core solves the cusp problem of the CDM model. The presence of the isothermal atmosphere leads to flat rotation curves in agreement with the observations. The circular velocity profile shows a dip due to the presence of the solitonic core.

A. A short history

Historically, this core-halo structure was first obtained in models where DM is made of fermions. In that case, the core corresponds to a fermion ball which is a completely degenerate nucleus at $T = 0$ in which the gravitational attraction is balanced by the quantum pressure arising from the Pauli exclusion principle. In the nonrelativistic limit, the fermion ball is equivalent to a polytrope of index $n = 3/2$ and its mass-radius relation is given by $R = 0.114h^2/(Gm^{8/3}M^{1/3})$ [158]. The fermion ball is surrounded by an isothermal halo in which the gravitational attraction is balanced by thermal pressure. An isothermal halo, with a true thermodynamic temperature $T_{\rm th}$, corresponds to the statistical equilibrium state of a gas of self-gravitating fermions resulting from a collisional relaxation. However, the collisional relaxation time is generally much larger than the age of the Universe. This is a problem to justify the Fermi-Dirac distribution in a cosmological context. However, a quasistationary state having a core-halo structure made of an effective fermion ball surrounded by an isothermal halo with an effective temperature T may also be justified by the statistical mechanics of violent relaxation [136] which takes place on a much shorter timescale. This may be the correct justification of the Fermi-Dirac distribution in a cosmological context as proposed in [26,39,40] (see footnote 4).

The core-halo structure of the self-gravitating Fermi gas at nonzero temperature, in the nonrelativistic and relativistic regimes, was found by numerous authors.[19]

[19]We focus our review on papers that explicitly display density profiles similar to those reported in Fig. 11. For a more general bibliography, see Refs. [14–44].

The density profiles of a partially degenerate gas of self-gravitating fermions at nonzero temperature (like electrons in white dwarfs, neutrons in neutron stars, or massive neutrinos in DM halos) were first computed by Wares [162], Margrave [163], Hertel and Thirring [164], Bludman and Van Riper [165], Edwards and Merilan [166], and Edwards [167] in the context of stellar structure; by Ruffini and Stella [15], Chau *et al.* [17], Ingrosso and Ruffini [19], Gao *et al.* [20], Merafina [21] and Ingrosso *et al.* [22] in the context of DM made of massive neutrinos; and by Chavanis and Sommeria [26] in the context of Lynden-Bell's theory of violent relaxation. Bilic *et al.* [30,31] considered a general relativistic Fermi gas at nonzero temperature, obtained a core-halo profile, and proposed that the fermion ball may mimic a SMBH at the centers of the galaxies. This idea was taken up again recently by Ruffini *et al.* [38] and further developed by Argüelles *et al.* [42]. Chavanis *et al.* [40] studied phase transitions in the fermionic King model and obtained a core-halo profile similar to that of Fig. 11 with a confinement due to tidal effects.

A similar core-halo profile was obtained by Slepian and Goodman [168] in a model where DM is made of bosons with a repulsive self-interaction (see also the figures in [140,141]). In that case, the core corresponds to a soliton which is the ground state of the self-gravitating BEC at $T=0$. In the TF limit, it is equivalent to a polytrope of index $n=1$ with a radius $R=\pi(a_s\hbar^2/Gm^3)^{1/2}$ independent of its mass. The solitonic core is surrounded by an isothermal halo.[20] This core-halo structure was also observed in the numerical simulations of Schive *et al.* [96,97] for noninteracting bosons. In that case, the halo is fitted by a NFW profile. In the very recent works of Lin *et al.* [169] and Mocz *et al.* [170], it is shown that the halo is relatively close to an isothermal distribution or to a fermionic King distribution [40,138] in which the degeneracy is due to Lynden-Bell's type of exclusion principle, as suggested in [140,141].

In the following subsections, we provide a semianalytic description of the core-halo structure of self-gravitating bosons at nonzero temperature by analogy with our previous work on fermions [26]. We assume that $\chi\gg 1$ so that a clear separation exists between the core and the halo marked by the presence of a plateau (see Sec. VII).

B. Properties of the density profile

We first consider the density profile. In the core, thermal effects are negligible as compared to quantum effects (self-interaction) so the system is equivalent to a pure soliton with central density ρ_0, radius R_c and mass M_c (see Sec. III B 2). The soliton radius is given by

$$R_c=\pi\left(\frac{a_s\hbar^2}{Gm^3}\right)^{1/2} \tag{71}$$

and the soliton mass is given by

$$M_c=\frac{4}{\pi}\rho_0 R_c^3. \tag{72}$$

At larger distances, quantum effects are negligible as compared to thermal effects so the system presents an isothermal halo with a density profile [see Eq. (22)]:

$$\rho=Ae^{-\beta m\Phi}. \tag{73}$$

Close to the core, the gravitational potential Φ is dominated by the contribution of the central body (soliton) so that

$$\Phi\sim -\frac{GM_c}{r}. \tag{74}$$

Therefore, the density profile can be approximated by

$$\rho=B\rho_0 e^{\beta GM_c m(\frac{1}{r}-\frac{1}{R_c})}, \tag{75}$$

where B is a dimensionless prefactor of order unity which can be obtained numerically (see below).

When $r\to R_c$, the foregoing equation reduces to

$$\rho=B\rho_0 e^{\beta GM_c m(R_c-r)/R_c^2}. \tag{76}$$

Therefore, at the contact with the solitonic core, the density decreases exponentially rapidly, and the system develops a *spike* (see Fig. 7) on a typical length scale

$$l=\frac{R_c^2}{\beta GM_c m}. \tag{77}$$

[20]In the study of Slepian and Goodman [168] the isothermal halo is justified by ordinary thermodynamics. This, however, poses a timescale problem, related to the establishment of a statistical equilibrium state by collisional relaxation on a relevant timescale (shorter than the Hubble time) as discussed above in the case of fermions. This also implies that the temperature in their model is the true thermodynamic temperature $T_{\rm th}$. As a result, in order to derive the equation of state of the boson gas, Slepian and Goodman [168] must consider the case where the bosons are condensed ($\rho>\rho_c$) or not ($\rho<\rho_c$). The resulting equation of state (see their Fig. 1) presents a plateau after ρ_c for weakly self-interacting bosons ($\theta\ll 1$) leading to an impossibility to construct BECDM halos that match the observations (see Appendix F). In our approach, the isothermal halo has a different origin. We assume since the start that the true thermodynamic temperature is rigorously equal to zero, or $T_{\rm th}\ll T_c$ (see Appendix G), so the bosons are always condensed and the fundamental equations are the GPP equations at $T_{\rm th}=0$. The core-halo structure of the system (with a solitonic core and a effective isothermal halo) is then an out-of-equilibrium virialized structure justified by the process of gravitational cooling and violent relaxation as explained in the Introduction. As a result, the problems raised by Slepian and Goodman [168] do not arise in our model since the two models are physically different.

The spike extends up to $R_s = R_c + l$. From Eqs. (54), (71), (72), and (77), we get

$$\frac{l}{R_c} = \frac{1}{\chi}. \tag{78}$$

We note that $l \to 0$ when $\chi \to +\infty$ (pure soliton) so that $R_s \simeq R_c$ in that limit.

When $r \to +\infty$, the density profile given by Eq. (75) tends to a constant

$$\rho_c = B\rho_0 e^{-\beta G M_c m/R_c}. \tag{79}$$

Therefore, when $r > R_s$, the density profile forms a *plateau* (see Fig. 7) with a constant density ρ_c.[21] Using Eq. (77), this density may be rewritten as

$$\rho_c = B\rho_0 e^{-R_c/l}. \tag{82}$$

From Eqs. (78) and (82) we get

$$\frac{\rho_c}{\rho_0} = Be^{-\chi}. \tag{83}$$

We have numerically computed the ratio ρ_c/ρ_0 as a function of χ and found an excellent agreement with the theoretical prediction from Eq. (83). This numerical study (not reported) allows us to obtain the value of the prefactor:

$$B = 4.24 \times 10^{-3}. \tag{84}$$

Equation (83) is valid for $\chi \gg 1$. Actually, our numerical study shows that Eq. (83) with B given by Eq. (84) is valid in good approximation for $\chi \gtrsim 1$. For $\chi \lesssim 1$ the separation between a core and a halo is not clear cut (the plateau disappears) so Eq. (83) does not really make sense. In order to connect the result $\rho_c = \rho_0$ when $\chi = 0$ (no solitonic core) to the result from Eq. (83) when $\chi \gg 1$, we introduce a convenient interpolation formula of the form

$$\frac{\rho_c}{\rho_0} = B(\chi)e^{-\chi} \tag{85}$$

with

$$B(\chi) = 1 + (B-1)\tanh(\chi). \tag{86}$$

This interpolation formula is of course purely *ad hoc* but it has the correct limiting behaviors and it will facilitate the analysis of Sec. VII.

The plateau extends from R_s up to a distance R_p after which it is not possible to neglect the self-gravity of the halo as compared to the attraction of the core. Therefore, R_p is determined by the condition

$$\frac{4}{3}\pi\rho_c(R_p^3 - R_s^3) \simeq M_c. \tag{87}$$

Making the approximation $R_p \gg R_s$ valid for $\chi \gg 1$, we get

$$R_p = \left(\frac{3M_c}{4\pi\rho_c}\right)^{1/3}. \tag{88}$$

From Eqs. (72), (83) and (88), we obtain

$$\frac{R_p}{R_c} = \left[\frac{3}{B(\chi)\pi^2}\right]^{1/3} e^{\chi/3}. \tag{89}$$

When $r \gg R_p$, we can neglect the gravitational attraction of the solitonic core. In that case, the system is asymptotically equivalent to a purely isothermal halo with a density profile decreasing as $\rho \sim k_B T/(2\pi G m r^2)$ with damped oscillations superimposed [158,171].

In conclusion, the density profile represented in Fig. 7 can be divided in four regions:

(i) a purely solitonic core of almost constant density,
(ii) a spike,
(iii) a plateau of constant density,
(iv) a purely isothermal halo where the density decreases as r^{-2} with some oscillations.

This core-halo structure is similar to the one discussed in the case of self-gravitating fermions [26] with the difference that the solitonic core replaces the degenerate fermion ball.

C. Properties of the circular velocity profile

We now consider the circular velocity profile. In the solitonic core, the density is approximately constant with value ρ_0. Therefore, the mass contained within the sphere of radius r is $M(r) \simeq (4/3)\pi\rho_0 r^3$. This leads to a circular velocity profile of the form

$$v^2(r) \sim \frac{4}{3}\pi G\rho_0 r^2. \tag{90}$$

[21] We emphasize that ρ_c is different from the transition density

$$\rho_i = \frac{k_B T m^2}{2\pi a_s \hbar^2} \tag{80}$$

obtained by equating the pressure $P = 2\pi a_s\hbar^2\rho^2/m^3$ in the solitonic core and the pressure $P = \rho k_B T/m$ in the isothermal halo. When $\rho \gg \rho_i$ the thermal pressure can be neglected and when $\rho \ll \rho_i$ the quantum pressure can be neglected (the transition temperature for a given density is $k_B T_i = 2\pi a_s\hbar^2\rho/m^2$). This is similar to the Sommerfeld criterion for fermions. We note that

$$\frac{\rho_i}{\rho_0} = \frac{2}{\chi}. \tag{81}$$

We also note that $\rho_i = (\pi/4)v_\infty^2/GR_c^2$, where $v_\infty^2 = 2k_B T/m$ is the constant circular velocity in an isothermal halo.

The circular velocity increases linearly with the distance (see Fig. 8).

In the spike and at the beginning of the plateau, the mass almost does not change so that $M(r) \simeq M_c$. This leads to a circular velocity profile of the form

$$v^2(r) \sim \frac{GM_c}{r}. \tag{91}$$

The circular velocity has a Keplerian decay $\propto r^{-1/2}$ (see Fig. 8).

On the plateau, the density is constant with value ρ_c. Therefore, at the end of the plateau where we can ignore the contribution of the central mass M_c, the mass contained within the sphere of radius r is $M(r) \simeq (4/3)\pi\rho_c r^3$. This leads to a circular velocity profile of the form

$$v^2(r) \sim \frac{4}{3}\pi G\rho_c r^2. \tag{92}$$

The circular velocity increases linearly with the distance as in the core (see Fig. 8).

At large distances, the system is purely isothermal and the mass increases as $M(r) \sim 2k_B\mathrm{Tr}/Gm$ leading to flat rotation curves:

$$v^2(r) \to \frac{2k_BT}{m}. \tag{93}$$

In conclusion, the circular velocity profile represented in Fig. 8 can be divided in four regions:

(i) a region where $v \propto r$ associated with the purely solitonic core,
(ii) a region where $v \propto r^{-1/2}$ associated with the spike,
(iii) a region where $v \propto r$ associated with the plateau,
(iv) a region where the velocity tends to a constant after some oscillations associated with the purely isothermal halo.

This profile reflects the core-halo structure of the system. In particular, it presents a dip due to the presence of the solitonic core.

VI. MASS-RADIUS RELATION OF DM HALOS AND THEIR PHYSICAL CHARACTERISTICS (MODEL I)

In this section, we express the previous results in terms of physical variables appropriate to make a detailed comparison with observations. We determine the mass-radius relation of DM halos and discuss their physical characteristics.

A. The constant surface density

It is an observational evidence that the surface density of DM halos is independent of their mass and size and has a universal value [172–174]:

$$\Sigma_0 = \rho_0 r_h = 141^{+83}_{-52} M_\odot/\mathrm{pc}^2. \tag{94}$$

This result is valid for all the galaxies even if their sizes and masses vary by several orders of magnitude (up to 14 orders of magnitude in luminosity). The reason for this universality is not known but it is crucial to take this result into account in any modeling of DM halos. Therefore, we shall assume this relation as an empirical fact.

B. Ultracompact halos: Solitonic profile (ground state)

Ultrasmall DM halos such as dwarf spheroidal galaxies (dSphs) like Fornax ($R \sim 1$ kpc and $M \sim 10^8\ M_\odot$) are very compact and do not have an atmosphere, or they have just a tiny one. The BECDM model predicts that there exists a minimum halo radius and a minimum halo mass corresponding to a pure soliton without atmosphere ($T = 0$). This is the ground state of the GPP equations (1) and (2). In the TF approximation, the soliton radius R_c where the density vanishes is given by Eq. (71) and the soliton mass M_c is given by Eq. (72). The halo radius r_h and the halo mass M_h are given by Eq. (44) where $R = R_c$. The halo radius is entirely determined by the physical properties of the bosons through the ratio a_s/m^3. The halo mass depends on the central density ρ_0. However, since the central density is determined by the halo radius according to Eq. (94), we find that the halo mass is determined by the ratio a_s/m^3 and by the universal value of Σ_0. Therefore, in the BECDM model, the minimum halo radius and the minimum halo mass are given by

$$(r_h)_{\min} = 0.788R_c, \qquad (M_h)_{\min} = 1.32\Sigma_0 R_c^2. \tag{95}$$

Using Eqs. (45) and (94), we find that the maximum central density and the minimum halo circular velocity are

$$(\rho_0)_{\max} = 1.27\frac{\Sigma_0}{R_c}, \qquad (v_h^2)_{\min} = 1.67G\Sigma_0 R_c. \tag{96}$$

They can be explicitly rewritten as

$$(r_h)_{\min} = 2.47\left(\frac{a_s\hbar^2}{Gm^3}\right)^{1/2}, \tag{97}$$

$$(M_h)_{\min} = 13.0\frac{a_s\hbar^2\Sigma_0}{Gm^3}, \tag{98}$$

$$(\rho_0)_{\max} = 0.404\left(\frac{Gm^3\Sigma_0^2}{a_s\hbar^2}\right)^{1/2}, \tag{99}$$

$$(v_h^2)_{\min} = 5.25\left(\frac{a_s\hbar^2G\Sigma_0^2}{m^3}\right)^{1/2}. \tag{100}$$

If we know the parameters m and a_s of the DM particle, we can determine the minimum halo radius $(r_h)_{\min}$ and the

minimum halo mass $(M_h)_{\rm min}$ from the foregoing expressions. However, we shall proceed the other way around. We assume that the smallest halo that we know (say Fornax to fix the ideas) represents the ground state of the GPP equations (pure soliton without atmosphere) and we determine the characteristics of the DM particle from the observed parameters of this halo. For convenience, we adopt the following value for its radius[22]:

$$R_c = 1 \text{ kpc}. \tag{101}$$

Using Eqs. (94), (95), (96), and (101), we get

$$(r_h)_{\rm min} = 788 \text{ pc}, \qquad (M_h)_{\rm min} = 1.86\times 10^8\ M_\odot, \tag{102}$$

$$(\rho_0)_{\rm max} = 0.179\ M_\odot/\text{pc}^3, \quad (v_h)_{\rm min} = 31.9 \text{ km/s}. \tag{103}$$

The ratio a_s/m^3 characterizing the DM particle can then be obtained from Eq. (71) yielding

$$\frac{a_s}{\text{fm}}\left(\frac{\text{eV}/c^2}{m}\right)^3 = 3.28\times 10^3. \tag{104}$$

Inversely, if we assume that DM halos are made of bosons with a ratio a_s/m^3 given by Eq. (104), we then find that the minimum halo radius and the minimum halo mass (ground state) are given by Eq. (102). These values are consistent with the mass and size of dSphs like Fornax.[23]

Remark: If we use the same reasoning for noninteracting bosons and for fermions we get $m = 2.92\times 10^{-22}$ eV$/c^2$ and $m = 170$ eV$/c^2$ respectively (see Appendix D of [46]). The order of magnitude of these values is consistent with the values obtained by other authors using more precise methods. We stress that, in this paper, we are more interested in developing a general theory of DM halos (and presenting basic ideas) rather than determining the characteristics of the DM particle accurately. Therefore, orders of magnitudes are sufficient for our purposes.

[22]It is not clear whether Fornax really corresponds to the ground state of the GPP equations (there may be a little atmosphere due to quantum interferences of excited states). Furthermore, its radius R_c is not exactly given by Eq. (101). Therefore, the values of $(r_h)_{\rm min}$, $(M_h)_{\rm min}$, $(\rho_0)_{\rm max}$, $(v_h)_{\rm min}$ and of a_s/m^3 that we obtain in this paper are approximate. However, a more accurate characterization of the ground state of DM halos will not crucially affect our results, nor change our general scenario.

[23]In the BECDM model, the order of magnitude of the minimum halo mass $(M_h)_{\rm min}$ and minimum halo radius $(r_h)_{\rm min}$ can be determined by a Jeans stability analysis as detailed in Ref. [127]. This point is further discussed in [142,175]. On the other hand, the maximum mass $(M_h)_{\rm max}\sim 10^{13}\ M_\odot$ of the DM halos (superclusters) may be connected to the maximum Jeans mass at the transition between the ultrarelativistic regime and the nonrelativistic regime (see Appendix F. 7 of [127]).

C. Large halos: Isothermal profile

For large halos like the medium spiral ($R\sim 10$ kpc and $M\sim 10^{11}\ M_\odot$), the mass of the solitonic core is negligible (see below) and it is a good approximation to assume that the halo is purely isothermal. In that case, using Eqs. (50), (51), and (94), we get

$$M_h = 1.76\Sigma_0 r_h^2, \qquad \frac{k_BT}{m} = 0.954 G\Sigma_0 r_h, \tag{105}$$

$$v_h^2 = 1.76 G\Sigma_0 r_h, \qquad \rho_0 = \frac{\Sigma_0}{r_h}. \tag{106}$$

We can rewrite these equations as

$$\frac{M_h}{\Sigma_0 R_c^2} = 1.76\left(\frac{r_h}{R_c}\right)^2, \qquad \frac{k_BT}{mG\Sigma_0 R_c} = 0.954\frac{r_h}{R_c}, \tag{107}$$

$$\frac{v_h^2}{G\Sigma_0 R_c} = 1.76\frac{r_h}{R_c}, \qquad \frac{\rho_0}{\Sigma_0/R_c} = \frac{R_c}{r_h}. \tag{108}$$

The halo mass scales with the size as $M_h\propto r_h^2$ and the temperature as $k_BT/m\propto r_h$ (basically, these scalings stem from the universality of the surface density of DM halos $M_h/r_h^2\sim\Sigma_0$ and from the virial theorem $k_BT/m\sim GM_h/r_h\sim G\Sigma_0 r_h$). For a halo of mass $M_h = 10^{11}\ M_\odot$, we find $r_h = 20.1$ kpc, $\rho_0 = 7.02\times 10^{-3}\ M_\odot/\text{pc}^3$, $(k_BT/m)^{1/2} = 108$ km/s, and $v_h = (GM_h/r_h)^{1/2} = 146$ km/s (we also have $v_\infty = 153$ km/s). We stress that these results are independent of the characteristics of the DM particle.

Remark: If we consider an ultralight boson of mass $m\sim 10^{-22}$ eV$/c^2$, we find that the temperature of large halos such as the medium spiral is $T\sim 10^{-25}$ K. Such a small temperature may not be physical. This strongly suggests that T is not the true thermodynamic temperature. It may rather represent an effective temperature as we have argued in the Introduction.

D. Small halos: Core-halo profile

We now consider the general case where the DM halos have a core-halo profile with a solitonic core (polytrope $n = 1$) and an isothermal halo. We shall determine r_h, ρ_0, M_h, v_h and $(k_BT/m)^{1/2}$ as a function of χ (see Sec. IV). We shall express these quantities in units of R_c, Σ_0/R_c, $\Sigma_0R_c^2$ and $(G\Sigma_0R_c)^{1/2}$ in order to be general [recall that R_c can itself be expressed in terms of a_s/m^3 according to Eq. (71)]. However, for numerical applications we will use the values of Σ_0 and R_c given by Eqs. (94) and (101) yielding

$$R_c = 1 \text{ kpc}, \qquad \Sigma_0/R_c = 0.141\ M_\odot/\text{pc}^3, \tag{109}$$

$$\Sigma_0R_c^2 = 1.41\times 10^8\ M_\odot, \qquad (G\Sigma_0R_c)^{1/2} = 24.6 \text{ km/s}. \tag{110}$$

1. The thermal core radius

Using Eqs. (49), (54), and (71), the concentration parameter χ can be rewritten as

$$\chi = \frac{1}{\pi^2}\left(\frac{R_c}{r_0}\right)^2. \tag{111}$$

It can be seen as the ratio between the soliton radius R_c and the thermal core radius r_0. Therefore, the thermal core radius is given in terms of χ by

$$\frac{r_0}{R_c} = \frac{1}{\pi\sqrt{\chi}}. \tag{112}$$

Since $\xi = r/r_0$, the normalized radial distance can be expressed as

$$\frac{r}{R_c} = \frac{\xi}{\pi\sqrt{\chi}}. \tag{113}$$

2. The halo radius

Using Eq. (113), we find that the halo radius is given by

$$\frac{r_h}{R_c} = \frac{\xi_h}{\pi\sqrt{\chi}}, \tag{114}$$

where ξ_h is defined in Sec. IV. For $\chi \to 0$,

$$\frac{r_h}{R_c} \sim \frac{1.16}{\sqrt{\chi}}, \tag{115}$$

where we have used Eq. (69). For $\chi \to +\infty$,

$$\frac{r_h}{R_c} \to 0.788, \tag{116}$$

where we have used Eq. (70). The halo radius is represented as a function of χ in Fig. 13. We see that large halos correspond to small values of χ (i.e., they are isothermal) and small halos correspond to large values of χ (i.e., they are solitonic).

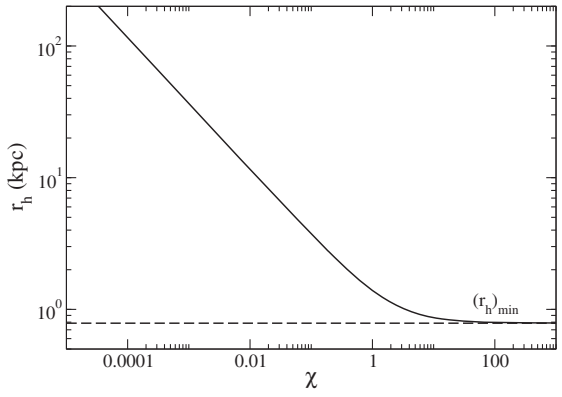

FIG. 13. Halo radius as a function of χ. We note, parenthetically, that $r_h = R_c$ for $\chi = 3.44$.

3. The central density

The central density can be obtained from Eqs. (94) and (114) giving

$$\frac{\rho_0 R_c}{\Sigma_0} = \frac{\pi\sqrt{\chi}}{\xi_h}. \tag{117}$$

For $\chi \to 0$,

$$\frac{\rho_0 R_c}{\Sigma_0} = 0.865\sqrt{\chi}. \tag{118}$$

For $\chi \to +\infty$,

$$\frac{\rho_0 R_c}{\Sigma_0} \to 1.27. \tag{119}$$

The central density is represented as a function of χ in Fig. 14. Large halos (small χ) have lower central densities than small halos (large χ).

4. The halo mass

Using Eqs. (65), (94), and (114), the halo mass is given by

$$\frac{M_h}{\Sigma_0 R_c^2} = \frac{4\psi'(\xi_h)\xi_h}{\pi\chi}[1 + \chi e^{-\psi(\xi_h)}]. \tag{120}$$

For $\chi \to 0$,

$$\frac{M_h}{\Sigma_0 R_c^2} \sim \frac{2.34}{\chi}. \tag{121}$$

For $\chi \to +\infty$,

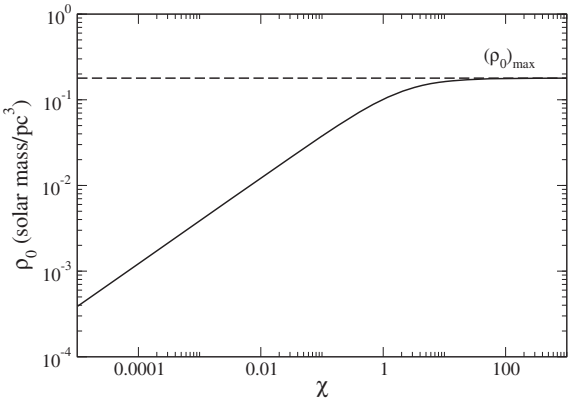

FIG. 14. Central density as a function of χ.

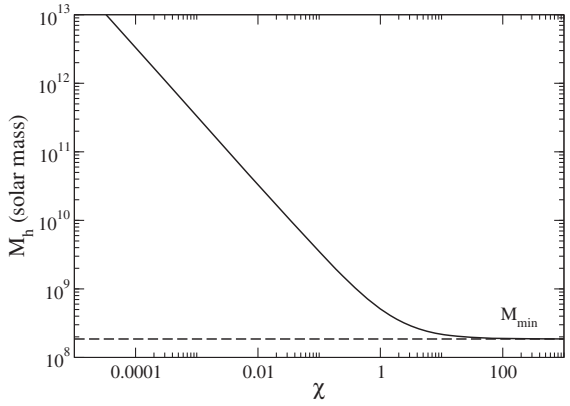

FIG. 15. Halo mass as a function of χ.

$$\frac{M_h}{\Sigma_0 R_c^2} \to 1.32. \tag{122}$$

The halo mass is represented as a function of χ in Fig. 15. Large halos (small χ) have a larger mass than small halos (large χ).

From Eqs. (114) and (120) we can obtain the mass-radius relation $M_h(r_h)$ of the DM halos in parametric form (with parameter χ). It is represented in Fig. 16. It starts from $(r_h)_{\rm min} = 788$ pc and $(M_h)_{\rm min} = 1.86 \times 10^8\ M_\odot$ (ground state) and behaves as $M_h \sim 1.76\Sigma_0 r_h^2$ for $r_h \to +\infty$ (large halos). Taking $r_h = (r_h)_{\rm min} = 788$ pc and using the isothermal mass-radius relation $M_h \sim 1.76\Sigma_0 r_h^2$ [see Eq. (105)], we find $M_h = 1.54 \times 10^8\ M_\odot$ which is very close to the value of the ground state $(M_h)_{\rm min} = 1.86 \times 10^8\ M_\odot$ [see Eq. (102)]. Therefore, the difference between the exact mass-radius relation and its asymptotic behavior given by Eq. (105), corresponding to purely isothermal halos, is imperceptible in a log-log plot. It is only close to the ground state $[(r_h)_{\rm min}, (M_h)_{\rm min}]$ that quantum effects (producing a solitonic core) are appreciable. Actually, the main effect of quantum mechanics is to provide an origin (see the bullet in Fig. 16) to the mass-radius relation, corresponding to a "minimum halo" (ground state). In comparison, there is no minimum halo in the ΛCDM model.

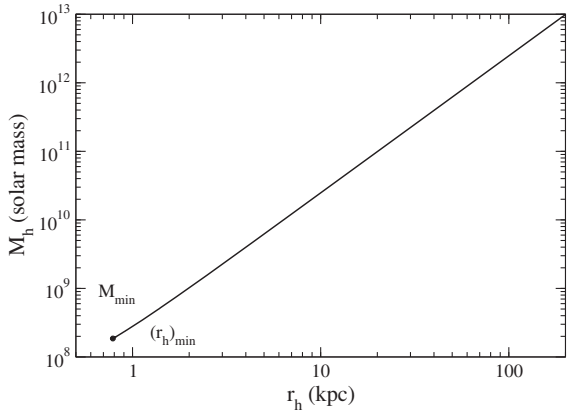

FIG. 16. Mass-radius relation of BECDM halos. Quantum mechanics is important only close to the ground state (bullet) where the halos have a solitonic core. Larger halos are purely isothermal without a solitonic core.

5. The circular velocity

Using Eqs. (66), (94), and (114), the halo velocity is given by

$$\frac{v_h^2}{G\Sigma_0 R_c} = \frac{4\psi'(\xi_h)}{\sqrt{\chi}}[1 + \chi e^{-\psi(\xi_h)}]. \tag{123}$$

For $\chi \to 0$,

$$\frac{v_h^2}{G\Sigma_0 R_c} \sim \frac{2.03}{\sqrt{\chi}}. \tag{124}$$

For $\chi \to +\infty$,

$$\frac{v_h^2}{G\Sigma_0 R_c} \to 1.67. \tag{125}$$

The halo velocity is represented as a function of χ in Fig. 17. Large halos (small χ) have a larger velocity than small halos (large χ).

6. The effective temperature

Using Eqs. (67), (94), and (114), the effective temperature of the halos is given by

$$\frac{k_B T}{Gm\Sigma_0 R_c} = \frac{4}{\xi_h \sqrt{\chi}}. \tag{126}$$

For $\chi \to 0$,

$$\frac{k_B T}{Gm\Sigma_0 R_c} \sim \frac{1.10}{\sqrt{\chi}}. \tag{127}$$

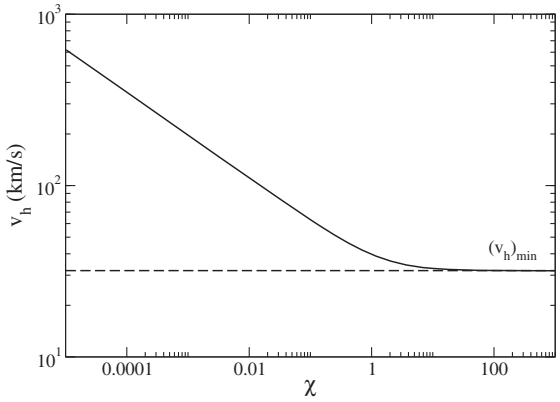

FIG. 17. Circular velocity as a function of χ.

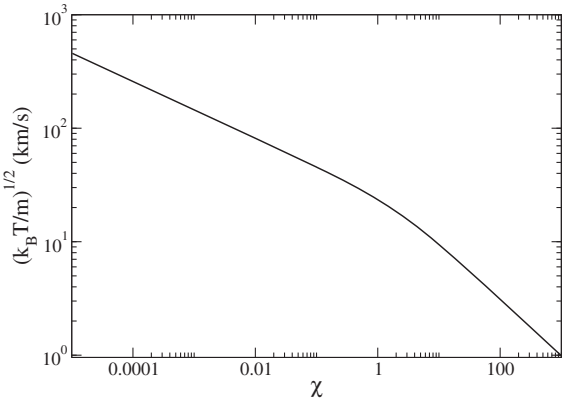

FIG. 18. Effective temperature as a function of χ.

For $\chi \to +\infty$,

$$\frac{k_BT}{Gm\Sigma_0 R_c} \sim \frac{1.62}{\chi}. \tag{128}$$

The effective temperature of the halo is represented as a function of χ in Fig. 18. Large halos (small χ) have a larger effective temperature than small halos (large χ). Actually, the temperature tends to zero when $\chi \to +\infty$ (ground state).

From Eqs. (114) and (126) we can obtain the temperature-radius relation $T(r_h)$ in parametric form (with parameter χ). It is represented in Fig. 19. It starts from $(r_h)_{\rm min} = 788$ pc and $T_{\rm min} = 0$ (ground state) and behaves as $k_BT/m \sim 0.954G\Sigma_0 r_h$ for $r_h \to +\infty$ (large halos).

7. The soliton radius and the soliton mass

The size of the solitonic core R_c is given by Eq. (71). We note that the solitonic core always has the same radius, whatever the halo mass M_h, since it only depends on the ratio a_s/m^3 which is a property of the DM particle. The soliton mass M_c is given by Eq. (72). The soliton mass depends on the halo mass M_h since it is proportional to the central density ρ_0. From Eqs. (72) and (117), we find that the soliton mass is given by

$$\frac{M_c}{\Sigma_0 R_c^2} = \frac{4\sqrt{\chi}}{\xi_h}. \tag{129}$$

For $\chi \to 0$,

$$\frac{M_c}{\Sigma_0 R_c^2} \sim 1.10\sqrt{\chi}. \tag{130}$$

For $\chi \to +\infty$,

$$\frac{M_c}{\Sigma_0 R_c^2} \to 1.62. \tag{131}$$

The evolution of the soliton mass M_c as a function of χ can be easily deduced from Fig. 14 since $M_c \propto \rho_0$. Large halos (small χ) have a less massive solitonic core than small halos (large χ). For large halos, using Eqs. (121) and (130) we find that

$$\frac{M_c}{\Sigma_0 R_c^2} \sim 1.68\sqrt{\frac{\Sigma_0 R_c^2}{M_h}}. \tag{132}$$

According to this relation, the soliton mass decreases as $M_c \propto M_h^{-1/2}$ with the halo mass. Actually, for $\chi \lesssim 0.1$, there is no well-defined solitonic core (see below) so that the relation from Eq. (132) is meaningless. Large DM halos are purely isothermal, without a solitonic core. In that case, Eq. (132) essentially gives the mass of the isothermal core within a sphere of radius R_c.

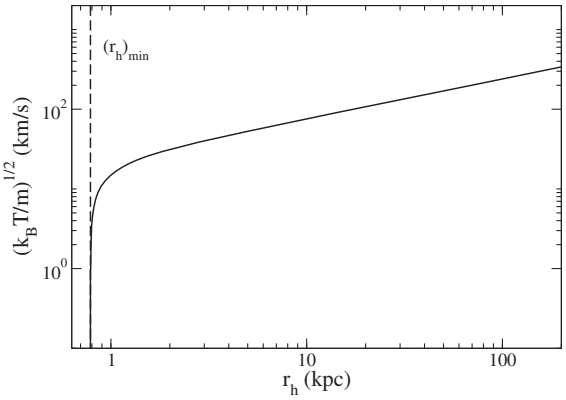

FIG. 19. Temperature-radius relation. A fit for $r_h \to (r_h)_{\rm min}$ gives $k_BT/Gm\Sigma_0 R_c \sim 1.42[(r_h - (r_h)_{\rm min})/R_c]^{0.888}$.

8. The mass M_{300}

It is an observational evidence that all dwarf spheroidal galaxies of the Milky Way have the same total DM mass contained within a radius $r_u = 300$ pc. From the observations, Strigari *et al.* [176] obtained $\log(M_{300}/M_\odot) = 7.0^{+0.3}_{-0.4}$. Let us see how this result compares with our model.

Using Eqs. (59), (94), (112) and the relation $\xi_h = r_h/r_0$ we obtain

$$\frac{M_{300}}{\Sigma_0 R_c^2} = \left(\frac{r_u}{R_c}\right)^2 \frac{4\pi}{\xi_h}\psi'\left(\frac{r_u\pi\sqrt{\chi}}{R_c}\right)[1+\chi e^{-\psi(r_u\pi\sqrt{\chi}/R_c)}]. \tag{133}$$

For $\chi \to 0$,

$$\frac{M_{300}}{\Sigma_0 R_c^2} \sim \frac{4\pi^2}{3}\left(\frac{r_u}{R_c}\right)^3 \frac{\sqrt{\chi}}{\xi_h} \sim 0.0979\sqrt{\chi}. \tag{134}$$

For $\chi \to +\infty$,

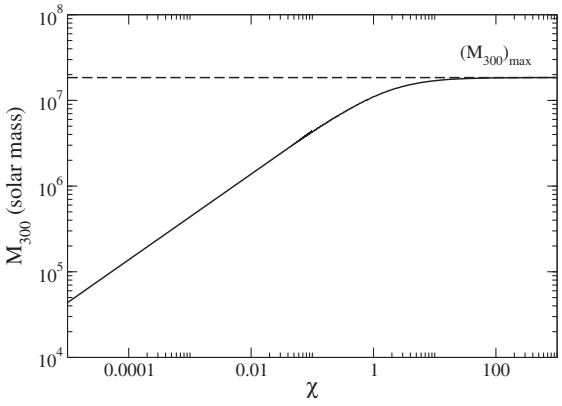

FIG. 20. Mass within a sphere of radius 300 pc as a function of χ.

$$\frac{M_{300}}{\Sigma_0 R_c^2} \to \frac{4R_c}{\pi^2 r_h}\left[\sin\left(\frac{\pi r_u}{R_c}\right) - \frac{\pi r_u}{R_c}\cos\left(\frac{\pi r_u}{R_c}\right)\right] = 0.131. \tag{135}$$

To obtain Eq. (134) we used $\psi \sim \xi^2/6$ when $\xi \to 0$ [158] and to obtain Eq. (135) we used Eqs. (42) and (94).

The evolution of the mass M_{300} as a function of χ is represented in Fig. 20. We note that M_{300} decreases as the halo size increases (χ decreases). For small halos ($\chi \to +\infty$), we get $(M_{300})_{\rm max} = 0.131\Sigma_0 R_c^2 = 0.0992(M_h)_{\rm min} = 1.85\times 10^7\, M_\odot$. Therefore $\log((M_{300})_{\rm max}/M_\odot) = 7.27$ in good agreement with the upper bound of the observational result of Strigari *et al.* [176] quoted above.[24] For large halos ($\chi \to 0$), using Eqs. (105), (121), and (134) we find that

$$\frac{M_{300}}{\Sigma_0 R_c^2} \sim 0.150\sqrt{\frac{\Sigma_0 R_c^2}{M_h}} \sim 0.114\frac{R_c}{r_h}. \tag{136}$$

According to this relation, M_{300} decreases as $M_{300} \propto M_h^{-1/2} \propto r_h^{-1}$ with the halo mass and halo radius.

Remark: We note that, for large (isothermal) halos,

$$M_{300} \sim 5.54\frac{\Sigma_0^{3/2} r_u^3}{M_h^{1/2}} \sim \frac{4\pi}{3}\frac{\Sigma_0 r_u^3}{r_h}. \tag{137}$$

The second equivalent can be obtained directly from the relation $M_{300} \sim (4\pi/3)\rho_0 r_u^3$ and Eq. (94).

9. Transition between small and large halos

In our model, a DM halo is entirely characterized by the concentration parameter χ. Indeed, for a given value of χ, we can obtain all the characteristics of the halo such as r_h, ρ_0, M_h, v_h and T.[25] Small halos (that contain a solitonic core) correspond to $\chi \gg 1$. Large halos (that are essentially isothermal without a solitonic core) correspond to $\chi \ll 1$. The transition between large and small halos ($\chi_t = 1$) corresponds to

$$(r_h)_t = 1.39R_c = 1.39\ \text{kpc}, \tag{138}$$

$$(M_h)_t = 3.63\Sigma_0 R_c^2 = 5.12\times 10^8\ M_\odot, \tag{139}$$

$$(\rho_0)_t = 0.716\Sigma_0/R_c = 0.101\ M_\odot/\text{pc}^3, \tag{140}$$

$$(v_h)_t = 1.61(G\Sigma_0 R_c)^{1/2} = 39.7\ \text{km/s}, \tag{141}$$

$$(k_B T/m)_t^{1/2} = 0.955(G\Sigma_0 R_c)^{1/2} = 23.5\ \text{km/s}. \tag{142}$$

We see that the transition is very close to the ground state $(r_h)_{\rm min} = 788$ pc and $(M_h)_{\rm min} = 1.86\times 10^8\ M_\odot$. This means that most of the DM halos are purely isothermal, except the dwarf halos that are very close to the ground state. This is in agreement with our previous observation (see Fig. 16).

10. Physical density profiles

Using the preceding results, the physical density and circular velocity profiles of a BECDM halo characterized by the concentration parameter χ can be written as

$$\frac{\rho(r)}{\Sigma_0/R_c} = \frac{\rho(\xi)}{\rho_0}\frac{\pi\sqrt{\chi}}{\xi_h}, \tag{143}$$

$$\frac{v^2(r)}{G\Sigma_0 R_c} = \frac{v^2(\xi)}{4\pi G\rho_0 r_0^2}\frac{4}{\xi_h\sqrt{\chi}}, \tag{144}$$

$$\frac{r}{R_c} = \frac{\xi}{\pi\sqrt{\chi}}, \tag{145}$$

where $\rho(\xi)/\rho_0$, $v^2(\xi)/4\pi G\rho_0 r_0^2$, and $\xi_h(\chi)$ are given by Eqs. (53), (60) and (64).

These profiles are represented in Figs. 21 and 22 for different values of χ. For $\chi \to 0$, we obtain a purely isothermal halo without solitonic core. For $\chi \to +\infty$, we obtain a pure soliton without isothermal halo (ground state). For intermediate values of χ, the profile has a core-halo structure with a solitonic core and an isothermal halo. At each value of χ corresponds a halo whose characteristics $(M_h, r_h \ldots)$ can be determined from the equations given in the previous sections. The transition

[24] Our theoretical result is valid up to $\chi \sim 1$ corresponding to a halo mass $(M_h)_t = 5.12\times 10^8\ M_\odot$ (see below).

[25] Physically, we can choose to characterize a halo by its mass M_h. The corresponding value of χ is then determined by Eq. (120). From the knowledge of χ we can determine the other characteristics of the halo. Therefore, a DM halo is entirely characterized by its mass M_h. In this sense, there is no free parameter in our model except for the value of the ratio a_s/m^3 which determines the minimum halo radius from Eq. (97).

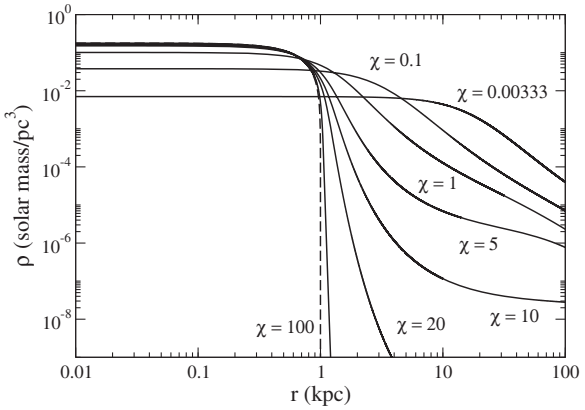

FIG. 21. Density profiles of different halos characterized by the concentration parameter χ. For $\chi = 0.00333$ $(M_h = 10^{11}\ M_\odot)$ and $\chi = 0.1$ $(M_h = 3.30 \times 10^9\ M_\odot)$ the halo is essentially isothermal without a solitonic core (large halos). For $\chi = 1$ $(M_h = 5.12 \times 10^8\ M_\odot)$ and $\chi = 5$ $(M_h = 2.50 \times 10^8\ M_\odot)$ the density profiles present a core-halo structure (small halos). For $\chi = 10$ $(M_h = 2.18 \times 10^8\ M_\odot)$, $\chi = 20$ $(M_h = 2.02 \times 10^8\ M_\odot)$, and $\chi = 100$ $(M_h = 1.89 \times 10^8\ M_\odot)$ the halo is dominated by the solitonic core (ultracompact halos). The dashed line corresponds to the pure soliton with $\chi \to +\infty$ $((M_h)_{\rm min} = 1.86 \times 10^8\ M_\odot)$ representing the ground state of the BECDM model.

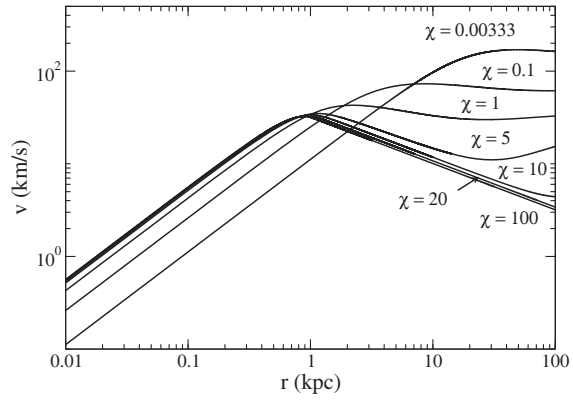

FIG. 22. Same as Fig. 21 for the circular velocity profiles.

between small and large halos corresponds to $\chi_t = 1$ (see Sec. VI D 9). On the other hand, as indicated in the caption of Fig. 11, large halos with $\chi \leq \chi_* = 0.1$ are almost indistinguishable from a purely isothermal profile without a solitonic core. This corresponds to

$$(r_h)_* = 3.67 R_c = 3.67\ \text{kpc}, \tag{146}$$

$$(M_h)_* = 23.4 \Sigma_0 R_c^2 = 3.30 \times 10^9\ M_\odot, \tag{147}$$

$$(\rho_0)_* = 0.2735 \Sigma_0 / R_c = 0.0386\ M_\odot/\text{pc}^3, \tag{148}$$

$$(v_h)_* = 2.53 (G \Sigma_0 R_c)^{1/2} = 62.2\ \text{km/s}, \tag{149}$$

$$(k_B T/m)_*^{1/2} = 1.865 (G \Sigma_0 R_c)^{1/2} = 45.9\ \text{km/s}. \tag{150}$$

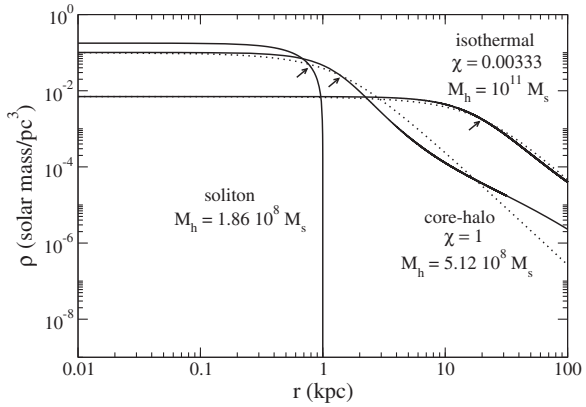

FIG. 23. Density profiles of DM halos of different mass. We have represented the purely solitonic profile (ground state of the BEC model) which is similar to an ultracompact halo like Fornax $[(M_h)_{\rm min} = 1.86 \times 10^8\ M_\odot]$, the core-halo profile of a small halo $(M_h = 5.12 \times 10^8\ M_\odot)$, and the almost isothermal profile of a large halo like the medium spiral $(M_h = 10^{11}\ M_\odot)$. In each case, we have indicated the halo radius r_h (where the central density is divided by 4) by an arrow. We have also plotted the Burkert profile for comparison (dotted lines).

E. The three types of DM halos in model I

In this section, we illustrate the previous results by showing examples of BECDM halos with a purely solitonic core (ultracompact halo), a core-halo structure (small halo), and a purely isothermal halo (large halo). Their density and circular velocity profiles are represented in Figs. 23 and 24.

Let us first consider a small DM halo with a concentration parameter $\chi = 1$. Its physical characteristics obtained from our model are $r_h = 1.39$ kpc, $M_h = 5.12 \times 10^8\ M_\odot$, $\rho_0 = 0.101\ M_\odot/\text{pc}^3$, $v_h = 39.7$ km/s, and $(k_B T/m)^{1/2} = 23.5$ km/s. This DM halo has a core-halo structure with a solitonic core and an isothermal atmosphere. The solitonic core has a radius $R_c = 1$ kpc and a mass $M_c = 1.29 \times 10^8\ M_\odot$. We note that the velocity profile exhibits a small dip due to the presence of the solitonic core. Nonmonotonic velocity profiles (oscillations) are sometimes observed in

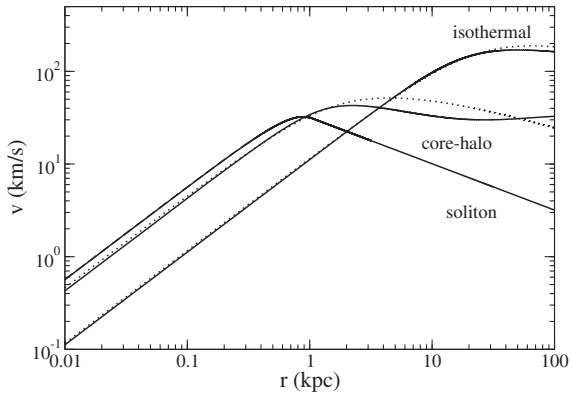

FIG. 24. Rotation curves of DM halos of different mass (the conventions are the same as in Fig. 23).

real rotation curves of galaxies. We suggest that they could, in certain cases, be the manifestation of a solitonic core.

For comparison, we have plotted the density and velocity profiles of the DM halo with the minimum mass corresponding to the ground state of the BECDM model. This ultracompact DM halo ($\chi \to +\infty$) is a pure soliton, without isothermal atmosphere ($T = 0$). Its physical characteristics obtained from our model are $(r_h)_{\rm min} = 788$ pc, $(M_h)_{\rm min} = 1.86 \times 10^8\ M_\odot$, $(\rho_0)_{\rm max} = 0.179\ M_\odot/{\rm pc}^3$, and $(v_h)_{\rm min} = 31.9$ km/s similar to the characteristics of dSphs like Fornax. We note that the density profile of the soliton has a larger central density than the profile of the DM halo with a core-halo structure.

Finally, we have plotted the density and velocity profiles corresponding to a large DM halo with a concentration parameter $\chi = 3.33 \times 10^{-3}$. In that case, there is no solitonic core and the profiles coincide with those of the isothermal sphere. For large DM halos, the flat density core (for $r \to 0$) is due to the effective temperature, not to the self-interaction of the bosons (see Appendix A). The physical characteristics of this halo obtained from our model are $r_h = 2.01 \times 10^4$ pc, $M_h = 10^{11}\ M_\odot$, $\rho_0 = 7.02 \times 10^{-3}\ M_\odot/{\rm pc}^3$, $v_h = (GM_h/r_h)^{1/2} = 146\,{\rm km/s}$, and $(k_B T/m)^{1/2} = 108$ km/s similar to the medium spiral. We note that the density profile of the purely isothermal halo has a smaller central density than the profile of the DM halo with a core-halo structure.

Remark: As soon as $M_h > (M_h)_{\rm min}$ (i.e., $T > 0$) the soliton is surrounded by an extended isothermal halo whose density decreases slowly as $\rho \propto r^{-2}$. This yields an infinite mass if it is extended to infinity. In practice, the halo is tidally truncated (see Appendix B).

F. Comparison with observations

In this section, we make a first comparison between the results of our model and observations. A more detailed comparison will be made in future works.

1. Preliminary remarks

Classical numerical simulations of CDM lead to DM halos that are well fitted by the NFW profile [5]:

$$\rho(r) \propto \frac{1}{\frac{r}{r_s}(1+\frac{r}{r_s})^2}, \tag{151}$$

where r_s is a scale radius that varies from halo to halo. The density decreases as r^{-3} for $r \to +\infty$ and diverges as r^{-1} for $r \to 0$. This singular behavior is not consistent with observations that reveal that DM halos possess a core, not a cusp. Observed DM halos are better fitted by the Burkert profile [6]:

$$\rho(r) = \frac{\rho_0}{(1+\frac{r}{r_h})(1+\frac{r^2}{r_h^2})}, \tag{152}$$

where ρ_0 is the central density and r_h is the halo radius defined by Eq. (D3). This density profile decreases as r^{-3} for $r \to +\infty$, like the NFW profile, but displays a flat core for $r \to 0$ instead of a cusp. In the following, we shall compare the theoretical profiles of BECDM halos obtained from our model with the Burkert profile that fits a lot of observations.

Some preliminary remarks can be made:

(i) The Burkert profile is empirical and does not rely on a theory. It is therefore important to see if this profile is consistent with a profile obtained from a theoretical model such as the one presented in this paper.

(ii) The profiles of DM halos are not expected to be universal. Small halos, with a mass $\sim 10^8\ M_\odot$, are very compact. In the BECDM model, they correspond to the solitonic solution of the GPP equations (ground state). This solution is substantially different from the Burkert profile (see below). However, the solitonic profile may be closer to the observations of ultracompact DM halos than the Burkert profile. The Burkert profile is expected to be valid only for relatively large halos.

(iii) The DM halos of our model behave as the isothermal sphere at large distances so their density profiles decrease as r^{-2} for $r \to +\infty$ while the Burkert profile decreases as r^{-3} for $r \to +\infty$. Therefore, if we compare the halos of our model with the Burkert profile at arbitrarily large distances, we will clearly find a difference of slope. However, in practice, the halos do not extend to infinity so that both the isothermal profile and the Burkert profile cease to be valid above a certain distance. Furthermore, observational data are only obtained within a limited range of radial distances: $0 \leq r \leq r_{\rm max}$. Therefore, we must take this constraint into account when comparing the DM halos of our model with the Burkert profile.

2. Large halos: Isothermal profile

We first consider large DM halos that are essentially isothermal with a negligible solitonic core. As we have seen in Sec. VI D 10, these halos have a mass $M_h \geq (M_h)_* = 3.30 \times 10^9\ M_\odot$ corresponding to $\chi \leq \chi_* = 0.1$. The intrinsic isothermal profile giving the density normalized by the central density ρ/ρ_0 as a function of the distance normalized by the halo radius r/r_h is represented in Fig. 5 together with the intrinsic Burkert profile (and other profiles that we do not consider here). The rotation curves of DM halos are usually measured up to a typical distance $r_{\rm max} = 100$ kpc. Therefore, for a large DM halo characterized by a concentration parameter $\chi \leq \chi_* = 0.1$, we have to make the comparison between the intrinsic isothermal profile and the intrinsic Burkert profile up to a maximum normalized distance $r_{\rm max}/r_h = 86.5\sqrt{\chi}$, where we have used Eq. (115). The smallest purely isothermal halo, corresponding to

$\chi_* = 0.1$, has a mass $(M_h)_* = 3.30 \times 10^9\ M_\odot$. For this halo, we have to make the comparison with the Burkert profile up to $(r_{\rm max}/r_h)_* = 27.3$. For larger halos, we have to make the comparison up to a smaller normalized distance $r_{\rm max}/r_h = 86.5\sqrt{\chi} \leq 27.3$. This is why we have plotted the intrinsic density profiles in Fig. 5 up to $30r_h$ in order to cover all possibilities. In Fig. 5, we see that the isothermal profile is very close to the Burkert profile for $r/r_h \leq 6$ and that it departs from it for $r/r_h \geq 6$. Therefore, for large DM halos such that $\chi \leq \chi_c = (6/86.5)^2 = 0.00481$, corresponding to

$$(r_h)_c = 16.7R_c = 16.7\ \text{kpc}, \tag{153}$$

$$(M_h)_c = 486\Sigma_0 R_c^2 = 6.86 \times 10^{10}\ M_\odot, \tag{154}$$

$$(\rho_0)_c = 0.0600\Sigma_0/R_c = 0.00846\ M_\odot/\text{pc}^3, \tag{155}$$

$$(v_h)_c = 5.41(G\Sigma_0 R_c)^{1/2} = 133\ \text{km/s}, \tag{156}$$

$$(k_B T/m)_c^{1/2} = 3.98(G\Sigma_0 R_c)^{1/2} = 98.0\ \text{km/s}, \tag{157}$$

the isothermal profile is almost indistinguishable from the Burkert profile up to the maximum distance of observation $r_{\rm max} = 100$ kpc. By contrast, for smaller isothermal halos with $\chi_c = 0.00481 \leq \chi \leq \chi_* = 0.1$, corresponding to a mass range $(M_h)_* = 3.30 \times 10^9\ M_\odot \leq M_h \leq (M_h)_c = 6.86 \times 10^{10}\ M_\odot$, we can see a difference between the isothermal profile and the Burkert profile at large distances. This difference appears at $r/r_h > 6$, corresponding to $r > 6.96\chi^{-1/2}$ kpc. Beyond this distance, the isothermal profile decreases as r^{-2} while the Burkert profile descreases as r^{-3}.[26] These results are illustrated in Fig. 25 where we have represented the isothermal and Burkert density profiles in physical scales for halos of different mass (see also Figs. 23 and 24).

3. Small halos: Core-halo profile

We now consider small halos with a core-halo profile. As we have seen in Sec. VI D 10, they have a mass $(M_h)_{\rm min} = 1.86 \times 10^8\ M_\odot < M_h \leq (M_h)_* = 3.30 \times 10^9\ M_\odot$ corresponding to $\chi_* = 0.1 \leq \chi < +\infty$. In that case, the difference between the core-halo profile and the Burkert profile is very significant at large distances as shown in Figs. 23 and 24 for $\chi = 1$ corresponding to $M_h = 5.12 \times 10^8\ M_\odot$.

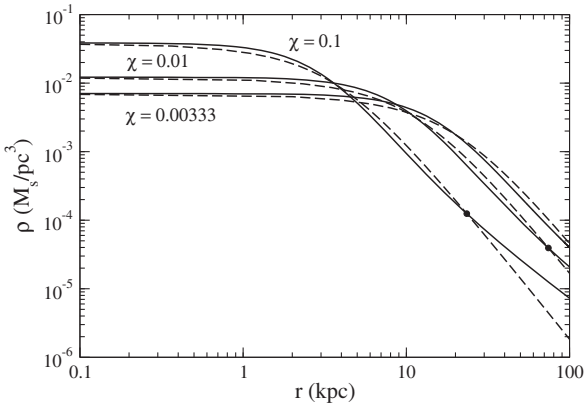

FIG. 25. Comparison between the purely isothermal profile (solid lines) valid for $M_h > (M_h)_* = 3.30 \times 10^9\ M_\odot$ ($\chi \leq \chi_* = 0.1$) and the Burkert profile (dashed lines) in the range $0 \leq r \leq 100$ kpc corresponding to the observations. For a large halo of mass $M_h = 10^{11}\ M_\odot$ ($\chi = 0.00333 < \chi_c = 0.00481$) corresponding to the medium spiral, the two profiles are almost indistinguishable. For a smaller halo of mass $M_h = 3.30 \times 10^{10}\ M_\odot$ ($\chi = 0.01 \gtrsim \chi_c = 0.00481$), a deviation starts to appear close to the maximum distance of observation (in the present case at $r = 69.6$ kpc). For a halo of mass $(M_h)_* = 3.30 \times 10^9\ M_\odot$ ($\chi_* = 0.1 > \chi_c = 0.00481$), the difference becomes very pronounced at large distances where we clearly see the two slopes r^{-2} (isothermal) and r^{-3} (Burkert). The difference appears at $r = 22.0$ kpc (see the bullet). For smaller halos with a core-halo profile, the disagreement is even more pronounced (see Fig. 23). However, for small DM halos, the BEC profile may be more relevant than the Burkert profile.

However, for small DM halos, the BEC profile may be more relevant than the Burkert profile.

4. Ultracompact halos: Ground state

Ultracompact halos close to the ground state $(M_h)_{\rm min} = 1.86 \times 10^8\ M_\odot$, corresponding to $\chi \to +\infty$, have no atmosphere (they are purely solitonic) so it is not relevant to compare their density profile with the Burkert profile at large distances ($r_{\rm max} = 100$ kpc) since the density drops to zero at $R_c = 1$ kpc. For these halos, the solitonic profile should provide a better agreement with observations than the Burkert profile. We note, however, that the two profiles (soliton and Burkert) are relatively close to each other, especially for what concerns the rotation curve, up to the halo radius r_h (see Figs. 3 and 4).[27] At larger distances, the density of the soliton drops to zero and the circular velocity decreases according to the Kepler law, so it is no more relevant to continue the comparison.

5. Conclusion

In conclusion, our results are qualitatively consistent with the observations. Quantum mechanics explains why

[26] This difference of slope may be explained by incomplete violent relaxation, tidal effects and stochastic forcing, as discussed in Refs. [39,40] in the context of the King model (see also Appendix B). In the present model, the logarithmic slope of the density profile could be corrected heuristically by tuning the external potential ω_0 in the generalized GPP equations (3) and (4). This may be a simple way to take into account tidal effects and other nonideal effects.

[27] This is also true for the larger halos considered previously.

there is a minimum halo mass $(M_h)_{\rm min} = 1.86 \times 10^8\ M_\odot$ and a minimum halo radius $(r_h)_{\rm min} = 788$ pc (ground state). On the other hand, the isothermal density profile of large DM halos $[M_h > (M_h)_c = 6.86 \times 10^{10}\ M_\odot]$ is indistinguishable from the empirical Burkert [6] profile up to 100 kpc (see Figs. 23–25). Therefore, these profiles quantitatively agree with the structure of the observed halos, at least in an average sense (recall that the Burkert profile is obtained by averaging over many rotation curves of galaxies). One interest of our model is that there is no arbitrary (free) parameter. For a given halo mass M_h, all the parameters can be determined from our equations. It would be therefore important to carry out a more detailed comparison of our model with observations. This will be considered in future works.

VII. ANOTHER FAMILY OF SOLUTIONS WITH A PERSISTENT SOLITONIC CORE AND A PLATEAU (MODEL II)

In the model developed in the previous section (model I), we have seen that the solitonic core disappears progressively as the halo mass increases so that large DM halos are purely isothermal without a solitonic core. In the present section, we develop another model (model II) in which large DM halos present a persistent solitonic core and a plateau.

A. A new definition of the halo radius

In Secs. IV–VI, we have defined the halo radius r_h by Eq. (D3). However, in the case where there is a strong separation between a small solitonic core and a large isothermal halo ($\chi \gg 1$), as in Fig. 7, it is more relevant to define the halo radius r_h by

$$\frac{\rho(r_h)}{\rho_c} = \frac{1}{4}, \tag{158}$$

where ρ_c is the density of the plateau given by Eq. (85), not the central density ρ_0. Similarly, the (universal) surface density of DM halos should be defined by

$$\Sigma_0 = \rho_c r_h = 141\ M_\odot/{\rm pc}^2 \tag{159}$$

instead of Eq. (94). Indeed, when the size of the soliton is small with respect to the size of the halo, the soliton may not be sufficiently well resolved in observations and what we regard as being the "central" density is actually the density of the plateau ρ_c, not the density of the soliton ρ_0. As we shall see, this change of definition leads to a new family of solutions that appears above a critical mass $(M_h)_b \sim 10^9\ M_\odot$. Contrary to the family of solutions constructed in Sec. VI this new family of solutions presents a persistent solitonic core as the halo mass increases. In a sense, it corresponds to a bifurcation from the branch of solutions of model I. In Sec. VIII we shall interpret this bifurcation in relation to phase transitions in a thermal self-gravitating boson gas in a box.

B. Physical parameters: Exact expressions

We can easily generalize the results of Sec. VI with the new definition of the halo radius from Eq. (158). The halo radius r_h is now given by

$$\frac{r_h}{R_c} = \frac{\xi_h}{\pi\sqrt{\chi}}, \tag{160}$$

where the function $\xi_h(\chi)$ is determined by the equation

$$e^{-\psi(\xi_h)} = \frac{B(\chi)e^{-\chi}}{4}. \tag{161}$$

The density of the plateau is given by

$$\frac{\rho_c R_c}{\Sigma_0} = \frac{\pi\sqrt{\chi}}{\xi_h}. \tag{162}$$

The halo mass is given by

$$\frac{M_h}{\Sigma_0 R_c^2} = \frac{4\psi'(\xi_h)\xi_h e^{\chi}}{B(\chi)\pi\chi}[1 + \chi e^{-\psi(\xi_h)}]. \tag{163}$$

The halo velocity is given by

$$\frac{v_h^2}{G\Sigma_0 R_c} = \frac{4\psi'(\xi_h)e^{\chi}}{B(\chi)\sqrt{\chi}}[1 + \chi e^{-\psi(\xi_h)}]. \tag{164}$$

The effective temperature of the halo is given by

$$\frac{k_B T}{Gm\Sigma_0 R_c} = \frac{4e^{\chi}}{B(\chi)\xi_h\sqrt{\chi}}. \tag{165}$$

From Eqs. (85) and (162), we find that the central density is given by

$$\frac{\rho_0 R_c}{\Sigma_0} = \frac{\pi\sqrt{\chi}}{B(\chi)\xi_h} e^{\chi}. \tag{166}$$

From Eq. (72), we find that the soliton mass is given by

$$\frac{M_c}{\Sigma_0 R_c^2} = \frac{4\sqrt{\chi}}{B(\chi)\xi_h} e^{\chi}. \tag{167}$$

For a DM halo characterized by its concentration parameter χ, all the halo parameters r_h, ρ_c, M_h, v_h, T, ρ_0, and M_c are determined by Eqs. (160)–(167).

C. Physical parameters: Approximate analytical expressions

Actually, it is possible to obtain approximate analytical expressions of these parameters. Indeed, for large halos, the

solitonic core is small compared to the halo radius so that, from the "outside," everything happens as if the halo were purely isothermal (i.e., we do not "see" the soliton). Said differently, the solitonic core is not expected to affect the properties of the halo at sufficiently large distances $r \gg R_c$. Therefore, the "external" halo parameters ρ_c, M_h, v_h, and T should be given in good approximation by the purely isothermal expressions

$$\frac{M_h}{\Sigma_0 R_c^2} = 1.76\left(\frac{r_h}{R_c}\right)^2, \qquad \frac{k_B T}{mG\Sigma_0 R_c} = 0.954\,\frac{r_h}{R_c}, \tag{168}$$

$$\frac{v_h^2}{G\Sigma_0 R_c} = 1.76\,\frac{r_h}{R_c}, \qquad \frac{\rho_c}{\Sigma_0/R_c} = \frac{R_c}{r_h}, \tag{169}$$

as in the absence of the soliton (see Sec. VI C and note that ρ_0 has been replaced by ρ_c). In particular, the temperature of the halo should not depend whether there is a solitonic core or not. Identifying Eqs. (165) and (168), and using Eq. (160), we obtain

$$\xi_h = \frac{3.63}{\sqrt{B(\chi)}}\,e^{\chi/2}. \tag{170}$$

We then find that the halo radius is given by

$$\frac{r_h}{R_c} = \frac{1.155}{\sqrt{B(\chi)}}\,\frac{e^{\chi/2}}{\sqrt{\chi}}. \tag{171}$$

Using Eqs. (168), (169) and (171), we get

$$\frac{M_h}{\Sigma_0 R_c^2} = \frac{2.35}{B(\chi)}\,\frac{e^{\chi}}{\chi}, \tag{172}$$

$$\frac{v_h^2}{G\Sigma_0 R_c} = \frac{2.03}{\sqrt{B(\chi)}}\,\frac{e^{\chi/2}}{\sqrt{\chi}}, \tag{173}$$

$$\frac{k_B T}{Gm\Sigma_0 R_c} = \frac{1.10}{\sqrt{B(\chi)}}\,\frac{e^{\chi/2}}{\sqrt{\chi}}, \tag{174}$$

$$\frac{\rho_c R_c}{\Sigma_0} = 0.866\sqrt{B(\chi)}\sqrt{\chi}e^{-\chi/2}. \tag{175}$$

Finally, from Eqs. (166), (167), and (170), we find that

$$\frac{\rho_0 R_c}{\Sigma_0} = \frac{0.866}{\sqrt{B(\chi)}}\sqrt{\chi}e^{\chi/2}, \tag{176}$$

$$\frac{M_c}{\Sigma_0 R_c^2} = \frac{1.10}{\sqrt{B(\chi)}}\sqrt{\chi}e^{\chi/2}. \tag{177}$$

These functions are plotted in Figs. 26–32. We see that they define two branches of solutions. For $\chi < 1$, the system is equivalent to a purely isothermal halo without solitonic core. For $\chi > 1$ the system has a core-halo structure with a small solitonic core and an extended isothermal atmosphere. They are separated by a plateau. If we add the branch of solutions obtained in Sec. VI (model I), we see that a sort of bifurcation occurs at a typical mass[28]

$$(M_h)_b \sim 10^9\ M_\odot. \tag{178}$$

When $M_h = (M_h)_{\rm min}$ the DM halo is a pure soliton (ground state). When $(M_h)_{\rm min} < M_h < (M_h)_b$ the DM halo has the form of a soliton with a tenuous isothermal halo. There is no plateau between them. When $M_h > (M_h)_b$ two types of solutions are possible: a solution where the DM halo is purely isothermal without central soliton (it corresponds to the branch studied in Sec. VI and recovered in the

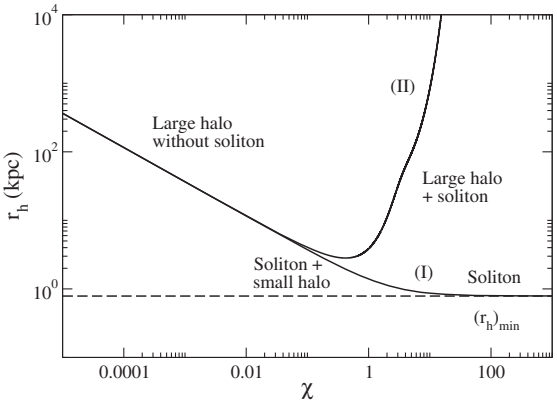

FIG. 26. Halo radius r_h as a function of χ for model II. We have also plotted the curve corresponding to model I.

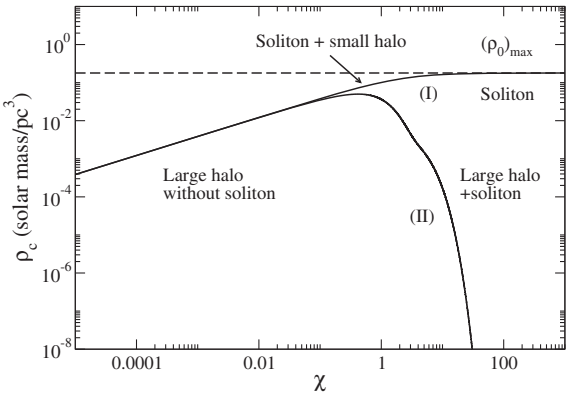

FIG. 27. Plateau density ρ_c as a function of χ for models I and II. When there is no plateau, ρ_c represents the central density ρ_0.

[28]The precise value of $(M_h)_b$ should not be given too much importance since it partly relies on the (*ad hoc*) fitting procedure used in Sec. V B to estimate $B(\chi)$ for small χ. It is sufficient to say that $(M_h)_b$ is larger than $(M_h)_{\rm min}$ by about one order of magnitude, i.e., $(M_h)_b/(\Sigma_0 R_c^2) \sim 10$. It is convenient to identify $(M_h)_b$ to $(M_h)_*$ so that the halo parameters at the bifurcation point are given by Eqs. (146)–(150).

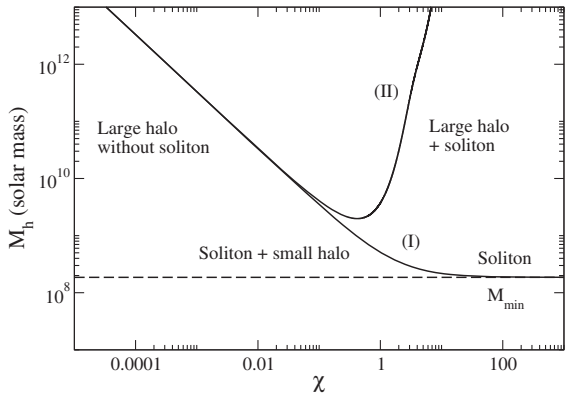

FIG. 28. Halo mass M_h as a function of χ for models I and II.

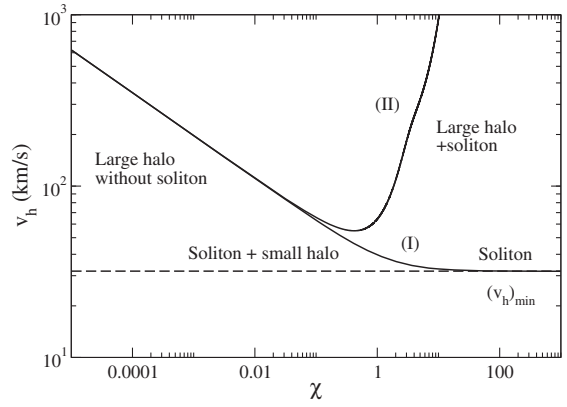

FIG. 29. Circular velocity v_h as a function of χ for models I and II.

present analysis for $\chi \lesssim 1$) and a solution where the DM halo has a core-halo structure with a small solitonic core and an extended isothermal atmosphere separated by a plateau.

The DM halo parameters corresponding to the purely isothermal branch [for $M_h > (M_h)_b$] are given analytically

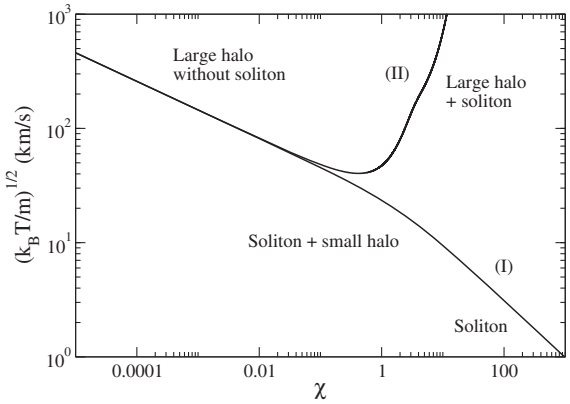

FIG. 30. Effective temperature T as a function of χ for models I and II.

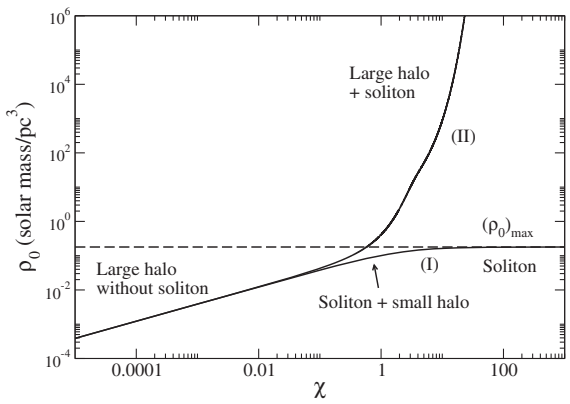

FIG. 31. Central density ρ_0 as a function of χ for models I and II.

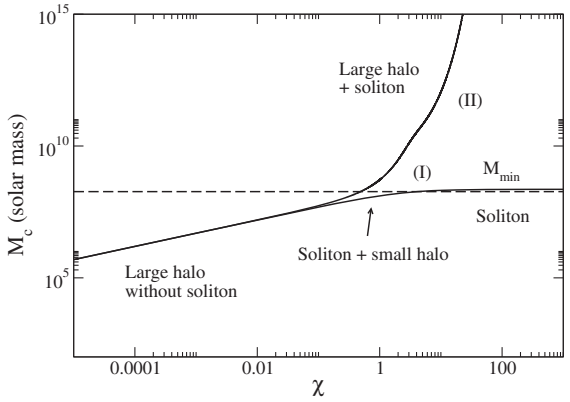

FIG. 32. Soliton mass as a function of χ for models I and II.

in terms of r_h by Eqs. (168) and (169) with $\rho_c = \rho_0$, i.e., by Eqs. (107) and (108).

The DM halo parameters corresponding to the core-halo branch [for $M_h > (M_h)_b$] are given analytically in terms of r_h by Eqs. (168) and (169) for what concerns their external structure (isothermal halo), and by

$$\frac{\rho_0 R_c}{\Sigma_0} = 1.50 \frac{r_h}{R_c} \ln\left(\frac{r_h}{R_c}\right), \tag{179}$$

$$\frac{M_c}{\Sigma_0 R_c^2} = 1.90 \frac{r_h}{R_c} \ln\left(\frac{r_h}{R_c}\right), \tag{180}$$

for what concerns their "internal" structure (soliton). These latter equations, which determine the soliton density and the soliton mass have been obtained by eliminating χ from Eqs. (171), (176), and (177).[29] It is interesting to note that, apart from logarithmic corrections, these formulas are independent of B. Therefore, we can consider that these results have been obtained in a purely analytical manner

[29]We have neglected sublogarithmic corrections and taken $\chi \sim 2\ln(r_h/R_c)$ at leading order.

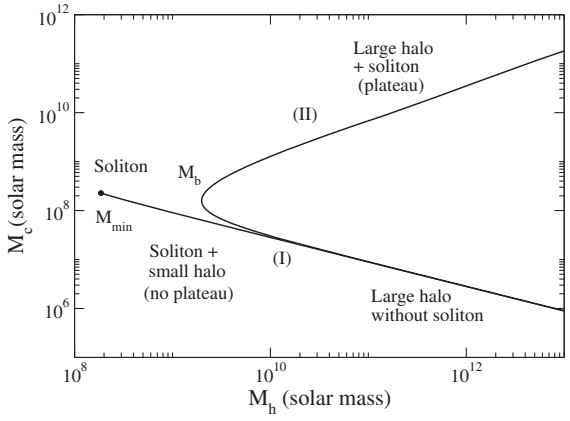

FIG. 33. Relation between the soliton mass M_c and the halo mass M_h [according to Eq. (181) we approximately have $M_c/M_\odot \sim 8.54 \times 10^3 (M_h/M_\odot)^{1/2}$].

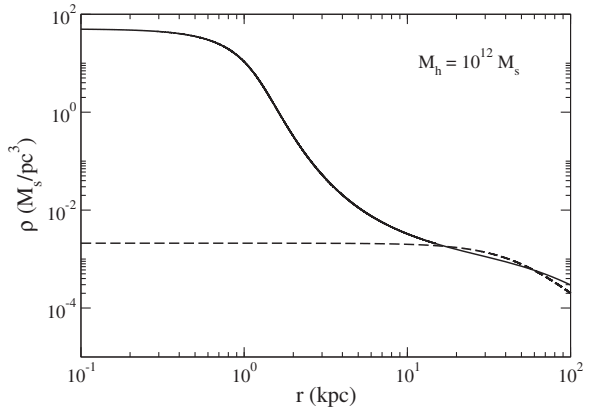

FIG. 34. Density profile of a DM halo of mass $M_h = 10^{12}\ M_\odot$. The full line corresponds to the core-halo solution of model II. The concentration parameter $\chi = 4.54$ is not very large. As a result, the plateau is not very clear cut and the definition of the "plateau density" ρ_c is a bit ambiguous. It approximately corresponds to the inflexion point of the core-halo profile. The dashed line corresponds to the purely isothermal solution without soliton. We see that the two profiles approximately match each other for $r \gtrsim 10$ kpc.

since we only used the numerics in Sec. V B to determine the constant B and we do not need its value here.

D. The relation between the soliton mass and the halo mass

From Eqs. (168) and (180), we can obtain the relation between the soliton mass and the halo mass:

$$\frac{M_c}{\Sigma_0 R_c^2} = 0.719 \left(\frac{M_h}{\Sigma_0 R_c^2}\right)^{1/2} \ln\left(\frac{M_h}{\Sigma_0 R_c^2}\right). \quad (181)$$

It is plotted in Fig. 33. Introducing the minimum halo mass $(M_h)_{\rm min} = 1.32\Sigma_0 R_c^2 = 1.86 \times 10^8\ M_\odot$, we can rewrite the foregoing equation as

$$\frac{M_c}{(M_h)_{\rm min}} = 0.626 \left(\frac{M_h}{(M_h)_{\rm min}}\right)^{1/2} \ln\left(\frac{M_h}{(M_h)_{\rm min}}\right). \quad (182)$$

We also note that

$$M_c = 0.719 R_c \sqrt{\Sigma_0 M_h} \ln\left(\frac{M_h}{\Sigma_0 R_c^2}\right). \quad (183)$$

These relations are valid on the core-halo branch for $M_h > (M_h)_b$ and sublogarithmic corrections have been neglected. At leading order, the core mass increases as $M_c \propto M_h^{1/2}$. Logarithmic corrections may slightly change the apparent scaling exponent.

The bifurcation is clearly visible in Fig. 33. When $(M_h)_{\rm min} < M_h < (M_h)_b$ there is only one solution which corresponds to a solitonic core surrounded by a small isothermal halo without plateau. For $M_h > (M_h)_b$ there are two solutions: a large isothermal halo without soliton and a large isothermal halo with a solitonic core and a plateau.

Remark: In a recent work, Lin *et al.* [169] found that "small" halos ($M_h < 10^{10}\ M_\odot$) have a core-halo structure without a plateau while "large halos" ($M_h > 10^{10}\ M_\odot$) have a core-halo structure exhibiting a plateau. This is qualitatively similar to the bifurcation that we have independently obtained in our study.

E. Astrophysical consequences: Formation of a solitonic bulge

Let us study the astrophysical consequences of these results. For a large DM halo of mass $M_h = 10^{12}\ M_\odot$, considering the core-halo solution, we find that $\chi = 4.54$. Then, we get $r_h = 61.9$ kpc, $v_h = 263$ km/s, $\sqrt{k_B T/m} = 246$ km/s, $\rho_c = 2.27 \times 10^{-3}\ M_\odot/{\rm pc}^3$, $\rho_0 = 50.2\ M_\odot/{\rm pc}^3$, and $M_c = 6.39 \times 10^{10}\ M_\odot$.[30] Considering now a purely isothermal DM halo ($\chi = 0$) with the same mass and using Eqs. (107) and (108), we find that $r_h = 63.5$ kpc, $v_h = 260$ km/s, $\sqrt{k_B T/m} = 191$ km/s, and $\rho_c = 2.22 \times 10^{-3}\ M_\odot/{\rm pc}^3$ (the differences between the external parameters r_h, v_h, T/m, and ρ_c in the two cases are due to the fact that χ is relatively small). The density and velocity profiles are represented in Figs. 34 and 35.

Our model II predicts that a large DM halo of mass $M_h = 10^{12}\ M_\odot$, such as the one surrounding our Galaxy, should possess a solitonic core of radius $R_c = 1$ kpc, mass $M_c = 6.39 \times 10^{10}\ M_\odot$, and central density $\rho_0 = 50.2\ M_\odot/{\rm pc}^3$ (see Fig. 34). In the solitonic core, the circular velocity is much larger than for a purely isothermal distribution (see Fig. 35). Let us consider different implications of this prediction.

[30]To determine these values, we have used the exact expressions from Eqs. (160)–(167), not the approximate analytical expressions from Eqs. (171)–(177) because χ is not large enough to fully justify their validity.

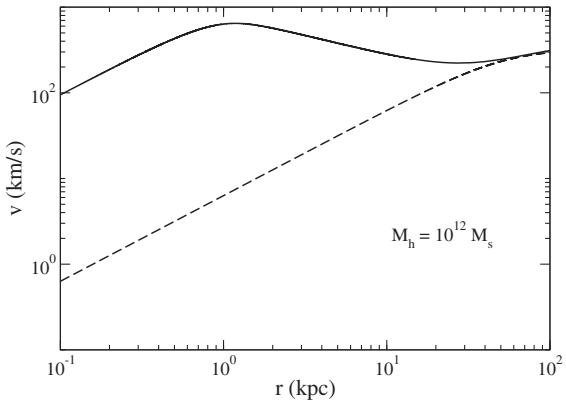

FIG. 35. Same as Fig. 34 for the circular velocity.

In the most favorable scenario, the solitonic core is physical. This scenario is supported by the numerical simulations of Schive *et al.* [96,97] that reveal the presence of an extended solitonic core at the centres of DM halos.[31] For real galaxies, this solitonic core may still exist now or may have existed only in the past and has disappeared since then (see below). Because of its deep gravitational potential, the solitonic core could have acted as a "seed" for the formation of early spheroids and quasars. It could have helped forming a stellar bulge or a galactic nucleus.[32] Indeed, the gravitational force created by the soliton can quickly attract a large amount of gas into a small central region, thereby creating an ultradense gas favorable for major starbursts and for the formation of SMBHs [96,97]. We shall show in the following section that this core-halo solution is thermodynamically unstable in the canonical ensemble. Therefore, the solitonic core may have formed only temporarily in the past, but long enough to constitute a stellar bulge (possibly triggering the formation of a black hole and a quasar), before disappearing on a longer timescale.[33]

In the most defavorable scenario, the solitonic core is not physical. Indeed, the solitonic core should produce a clear signature on the velocity curves marked by the presence of a dip (see Fig. 35). Apparently, this dip has not been clearly observed as argued by Slepian and Goodman [168] (see, however, the Remark at the end of this section). Assuming that this is not a problem of measurement (or that the dip/soliton has not disappeared during the evolution of the halo), this raises the following possibilities:

(i) The first possibility is that the BECDM model with a repulsive self-interaction is ruled out. This is essentially the conclusion of Slepian and Goodman [168].

(ii) There is, however, another possibility. The core-halo solution forms just one possible solution of the self-gravitating BEC model. Another solution exists in which the DM halo is purely isothermal without solitonic core. It is possible that this purely isothermal solution is selected instead of the core-halo one. We shall show in the following section that the purely isothermal solution is stable (minimum of free energy at fixed mass) while the core-halo solution is thermodynamically unstable in the canonical ensemble (saddle point of free energy). From these thermodynamical considerations, the purely isothermal solution with no soliton is more probable than the core-halo one (assuming that the canonical ensemble rather than the microcanonical ensemble applies to our problem).

Clearly, the confirmation of the presence or the absence of a "solitonic" bulge of mass $M_c = 6.39 \times 10^{10}\ M_\odot$ and size $R_c = 1$ kpc at the center of DM halos of mass $M_h = 10^{12}\ M_\odot$ and size $r_h = 61.9$ kpc would be of considerable interest. This is a challenge for astrophysical observations.

Remark: During the redaction of our manuscript, we came across the recent paper of De Martino *et al.* [177] who show that the central motion of bulge stars in the Milky Way implies the presence of a DM core of mass $\simeq 10^9\ M_\odot$ and radius $\simeq 100$ pc that they interpret as a soliton. Their result is based on the measures of dispersion velocity by Zoccali *et al.* [178] and Portail *et al.* [179] who construct a fully dynamical model of the bulge and find the need for a compact mass of $\simeq 2 \times 10^9\ M_\odot$. These results are qualitatively consistent with our model which predicts a large solitonic core of radius $R_c = 1$ kpc and mass $M_c = 6.39 \times 10^{10}\ M_\odot$ in a DM halo of mass $M_h = 10^{12}\ M_\odot$. The values of M_c and R_c are different from De Martino *et al.* [177] because our model is different: we are considering self-interacting bosons in the TF limit while De Martino *et al.* [177] consider noninteracting bosons. Furthermore, our DM halo of mass $M_h = 10^{12}\ M_\odot$ is more massive than the DM halo of the Milky Way implying a larger soliton mass. Neverthless, this qualitative agreement is encouraging and shows that a solitonic core can really be present, even now, at the centers of the galaxies (from a thermodynamical point of view this would imply that the microcanonical ensemble is more relevant than the canonical one, see footnote 33). It will be important to extend our model to the case of noninteracting bosons [142] to see if the agreement with De Martino *et al.* [177] improves. This may help discriminating between different types of bosons, i.e., noninteracting bosons versus self-interacting bosons.

[31] These simulations apply to a noninteracting BEC but similar results should be obtained for a self-interacting BEC.

[32] In this respect, we note that the mass $M_c = 6.39 \times 10^{10}\ M_\odot$ and the size $R_c = 1$ kpc of the soliton are compatible with the mass and size of stellar bulges and galactic nuclei.

[33] Note that the core-halo solution is dynamically stable so that it is relatively persistent. It is also thermodynamically stable in the microcanonical ensemble (see Secs. VIII D 5 and IX). This may increase its lifetime if the microcanonical ensemble is the correct ensemble to consider in our problem. Therefore, it is very likely that the core-halo solution is physically relevant (see the Remark at the end of this section).

F. Can the soliton mimic a SMBH?

There is strong observational evidence that very massive objects reside at the centers of galaxies. These objects are usually considered to be SMBHs. For example, Sagittarius A* (Sgr A*), a bright and very compact astronomical radio source that resides at the center of our Galaxy is thought to be the location of a SMBH of mass $M = 4.2 \times 10^6\ M_\odot$ and Schwarzschild radius $R_S = 4.02 \times 10^{-7}$ pc. Whatever the object may be, it must be enclosed within a radius $R_P = 6 \times 10^{-4}$ pc ($R_P = 1492 R_S$), the S2 star pericenter [180].[34] Similar objects are expected to reside at the centers of most spiral and elliptical galaxies, in active galactic nuclei. Although it is commonly believed that these objects are SMBHs [180–183], this is not yet established on a firm observational basis in all cases. As an alternative to the black hole hypothesis, it has been proposed that such objects could be fermion balls [24,27,30,31,38,42] or boson stars [184,185] that could mimic a black hole. Let us consider this possibility in the framework of the present model. More precisely, let us investigate if a solitonic core can mimic a SMBH at the center of the Milky Way.

To be specific, let us consider a DM halo of mass $M_h = 10^{11}\ M_\odot$ similar to the one that surrounds the Milky Way. Using the results of Sec. VII C, we find that this halo should contain a solitonic core of mass $M_c = 1.77 \times 10^{10}\ M_\odot$ and radius $R_c = 1$ kpc. Clearly, the soliton is too extended to mimic a black hole. As discussed in Sec. VII E the solitonic core is more likely to represent a bulge which is either present now or which, in the past, may have triggered the formation of a black hole.

Nevertheless, let us try to push our model to its limits by relaxing certain assumptions. We relax the value of $R_c = 1$ kpc that was fixed by the size of ultracompact DM halos (see Sec. VI B) and we impose that $M_h = 10^{11}\ M_\odot$ and $M_c = 4.2 \times 10^6\ M_\odot$. Using the relation $M_h/M_c = (2.14/\sqrt{B(\chi)})e^{\chi/2}/\chi^{3/2}$ obtained from Eqs. (172) and (177) we obtain $\chi = 22.5$. Then, we find from Eq. (172) that $R_c = 0.652\sqrt{B(\chi)\chi}e^{-\chi/2}(M_h/\Sigma_0)^{1/2}$, giving $R_c = 6.98 \times 10^{-2}$ pc.[35] Finally, Eqs. (171), (173), (174), (175), and (176) imply $r_h = 2.00 \times 10^4$ pc, $\rho_c = 7.03 \times 10^{-3}\ M_\odot/\mathrm{pc}^3$, $(k_B T/m)^{1/2} = 108$ km/s, $v_h = (GM_h/r_h)^{1/2} = 146$ km/s, and $\rho_0 = 9.80 \times 10^9\ M_\odot/\mathrm{pc}^3$. The values of the external parameters exactly match the values of a purely isothermal halo (see Sec. VI C). This is because $\chi \gg 1$ making our approximate analytical expressions accurate. As a result, we obtain a core-halo profile (see Figs. 36 and 37) that is consistent with the observations from the outside, and that contains a solitonic core of mass $M_c = 4.2 \times 10^6\ M_\odot$ similar to the mass of the compact object at the center of the Galaxy. Unfortunately, the radius of the soliton, $R_c = 6.98 \times 10^{-2}$ pc, is 100 times larger than the maximum size of this object, $R_P = 6 \times 10^{-4}$ pc, deduced from the observations.[36] More generally, we show in Appendix H that the solitonic core is never relativistic so it can never mimic a SMBH.

In addition to being unable to mimic a central black hole, there is another problem with the profile constructed

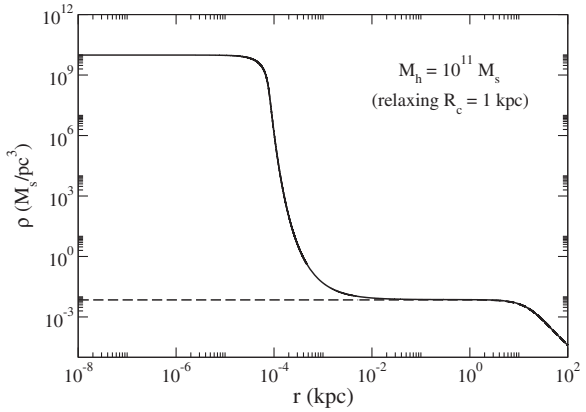

FIG. 36. Core-halo density profile in the framework of model II corresponding to a DM halo of mass $M_h = 10^{11}\ M_\odot$ and concentration parameter $\chi = 22.5$ when the condition $R_c = 1$ kpc is (arbitrarily) relaxed. It is compared with a purely isothermal profile (dashed line). The solitonic core cannot model a SBH because it is nonrelativistic and, above all, its radius is too large.

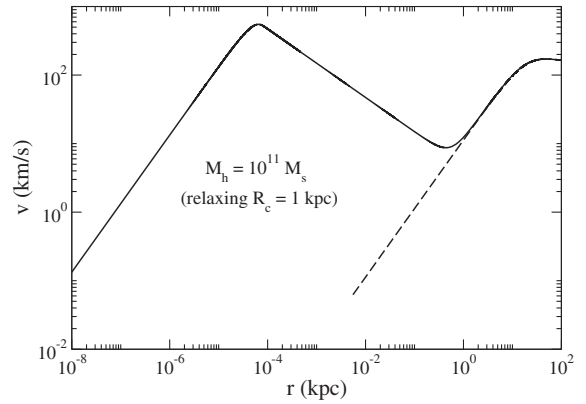

FIG. 37. Same as Fig. 36 for the circular velocity.

[34]The radius of the compact object must satisfy $R_* \leq R_P$ from the observations. This implies $R_*/R_S \leq 1492$. This object is not necessarily a black hole unless its radius is much smaller than $R_P = 6 \times 10^{-4}$ pc, namely $R_* \sim R_S = 4.02 \times 10^{-7}$ pc.

[35]This corresponds to a ratio $a_s/m^3 = 1.60 \times 10^{-5}\ \mathrm{fm}/(\mathrm{eV}/\mathrm{c}^2)^3$ of the DM particle parameters [see Eq. (71)].

[36]Instead of imposing the core mass, we could impose the core radius $R_c = 6 \times 10^{-4}$ pc. From Eq. (172) with $M_h/(\Sigma_0 R_c^2) = 1.97 \times 10^{15}$, we obtain $\chi = 32.4$. Then, Eq. (171) and Eqs. (173)–(177) give $r_h = 2.02 \times 10^4$ pc, $\rho_c = 6.95 \times 10^{-3}\ M_\odot/\mathrm{pc}^3$, $(k_B T/m)^{1/2} = 108$ km/s, $v_h = (GM_h/r_h)^{1/2} = 147$ km/s, $\rho_0 = 1.93 \times 10^{14}\ M_\odot/\mathrm{pc}^3$, and $M_c = 5.30 \times 10^4\ M_\odot$. This time, the core mass $M_c = 5.30 \times 10^4\ M_\odot$ is about 100 times smaller than the mass of the central object $M = 4.2 \times 10^6\ M_\odot$ estimated from the observations.

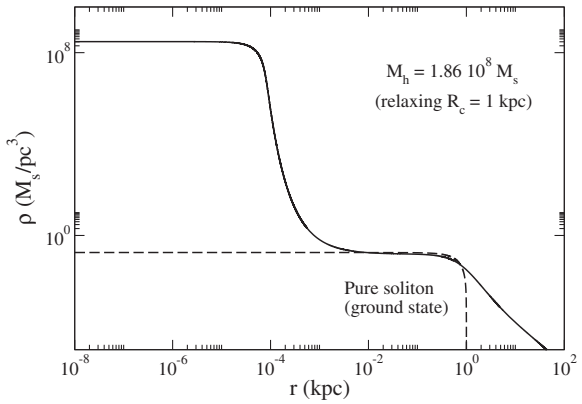

FIG. 38. Core-halo density profile in the framework of model II corresponding to a DM halo of mass $M_h = 1.86 \times 10^8\ M_\odot$ (such as Fornax) and concentration parameter $\chi = 15.9$ when the condition $R_c = 1$ kpc is (arbitrarily) relaxed. As explained in the text, this profile has to be rejected in favor of the pure soliton (dashed line) corresponding to the ground state of the BECDM model.

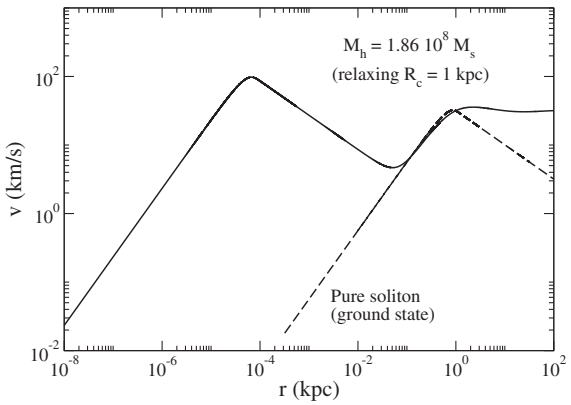

FIG. 39. Same as Fig. 38 for the circular velocity.

previously. Since we have changed the value of $R_c = 6.98 \times 10^{-2}$ pc with respect to its original value $R_c = 1$ kpc in order to impose a core mass $M_c = 4.2 \times 10^6\ M_\odot$, the ground state of the self-gravitating BEC model has been changed accordingly. For $R_c = 6.98 \times 10^{-2}$ pc, the ground state now corresponds to $(r_h)_{\rm min} = 5.50 \times 10^{-2}$ pc and $(M_h)_{\rm min} = 0.906\ M_\odot$ [see Eq. (95)]. The minimum halo radius and the minimum halo mass are much smaller than the radius and the mass of typical dSphs like Fornax. Such small halos are not observed, suggesting that the ground state of DM halos is at a much larger scale, of the order of 1 kpc, as we have initially assumed (see Sec. VI B). If we ignore this difficulty and nevertheless apply the model with $R_c = 6.98 \times 10^{-2}$ pc to a halo of mass $M_h = 1.86 \times 10^8\ M_\odot$ (such as Fornax) we find from Eq. (172) that $\chi = 15.9$. We then obtain from Eq. (171) and Eqs. (173)–(177) that $r_h = 880\,{\rm pc}$, $\rho_c = 0.160\,M_\odot/{\rm pc}^3$, $(k_B T/m)^{1/2} = 22.5$ km/s, $v_h = (GM_h/r_h)^{1/2} = 30.6$ km/s, $\rho_0 = 3.04 \times 10^8\ M_\odot/{\rm pc}^3$, and $M_c = 1.31 \times 10^5\ M_\odot$. This DM halo has a core-halo structure with a very small nucleus of mass $M_c = 1.31 \times 10^5\ M_\odot$ and radius $R_c = 6.98 \times 10^{-2}$ pc, and an extended isothermal halo (see Figs. 38 and 39). This is very different from the structure that we have considered in Sec. VI B consisting of a pure soliton of mass $M_h = 1.86 \times 10^8\ M_\odot$ and radius $r_h = 788$ pc (see the pure soliton in Figs. 23 and 24).

The previous arguments (and the results of Appendix H) lead to the conclusion that the solitonic core of model II cannot mimic a SMBH. The solitonic core is more likely to represent a large central bulge or a galactic nucleus (see Sec. VII E). This conclusion is important in view of the different attempts that have been made in the past to describe the compact object that resides at the center of our Galaxy, presumably a SMBH [180–183], by an object of another nature like a fermion ball [24,27,30,31,38,42] or a boson star [184,185].[37] In future works [142], we shall adapt our model to the case of noninteracting bosons and self-gravitating fermions to see whether we reach the same conclusion. We will then decide whether the boson star or fermion ball scenario (as a SMBH mimicker) is ruled out or if we need to modify our model. Any definite conclusion is premature for the moment.

[37]Bilic *et al.* [31] developed a model of fermionic DM (with a fermion mass $m = 15\ {\rm keV/c^2}$) that describes both the center and the halo of the Galaxy. They found a (nonrelativistic) fermion ball of mass $M = 2.27 \times 10^6\ M_\odot$ and radius $R = 18$ mpc. Unfortunately, its radius is larger by a factor 100 than the bound $R_P = 6 \times 10^{-4}$ pc set by later observations [180]. The same problem was encountered by Ruffini *et al.* [38] who developed a similar model with a fermion mass $m \sim 10\ {\rm keV/c^2}$. Very recently, Argüelles *et al.* [42] considered the fermionic King model [40] (accounting for a tidal confinement) with a fermion mass $m = 48\ {\rm keV/c^2}$ and found a core-halo solution with a (nonrelativistic) fermion ball of mass $M = 4.2 \times 10^6\ M_\odot$ and radius $R = R_P = 6 \times 10^{-4}$ pc consistent with the observations. This core-halo state is dynamically (Vlasov) stable. Therefore, if we "prepare" the system in this state, it will remain in this state for a very long time. However, we have argued in [40,186] (see also Sec. VIII D 5) that this core-halo solution is thermodynamically unstable in all statistical ensembles. As a result, it is very unlikely to appear *spontaneously* in a thermodynamical sense. The fermion ball of the core-halo state corresponds to a sort of "critical droplet" or "critical nucleus" (saddle point of entropy) in the language of phase transitions and nucleation which has a very low probability of occurrence. Furthermore, the model of Argüelles *et al.* [42] faces the "ground state problem" reported in the fourth paragraph of this section. Assuming that Fornax is the ground state of the self-gravitating Fermi gas imposes that $m = 170\ {\rm eV/c^2}$ (see the Remark at the end of Sec. VI B). This mass is much smaller than the mass $m = 48\ {\rm keV/c^2}$ taken in Ref. [42]. If we object that Fornax may not be the ground state of the self-gravitating Fermi gas this would imply that (i) much smaller halos should exist, (ii) Fornax should have a core-halo structure with a small central fermion ball (possibly mimicking a SMBH). To our knowledge, these two features have not been observed.

VIII. PHASE TRANSITIONS OF A THERMAL SELF-GRAVITATING BOSON GAS IN A BOX

In this section, we study the nature of phase transitions in a self-gravitating BEC described by the equation of state (14). This system generically has a core-halo structure with a solitonic core and an isothermal halo. Since the halo is isothermal, the density decreases at large distances as r^{-2}. This implies that the total mass of the system is infinite. A solution to avoid the infinite mass problem is to confine the system within a spherical box of radius R. This box model will allow us to recover the bifurcation between the purely isothermal state and the core-halo state obtained in the preceding section and to interpret this bifurcation in terms of a phase transition related to the existence of a canonical critical point. It will also allow us to show that purely isothermal configurations are thermodynamically stable (minima of free energy) while core-halo configurations are thermodynamically unstable in the canonical ensemble (saddle points of free energy). We will also discuss their microcanonical stability and the notion of ensembles inequivalence [33,154,187].

A. Basic equations

The equilibrium states of a self-gravitating BEC described by the equation of state (14) are determined by the generalized Emden equation (56). Let us denote by α the value of ξ at the box radius R. According to Eqs. (49) and (53), the normalized box radius α is given by

$$\alpha = (4\pi G\rho_0\beta m)^{1/2}R. \tag{184}$$

We then have $r = \xi R/\alpha$. The total mass enclosed within the box is $M = M(R)$. From Eq. (59) we find that the normalized inverse temperature

$$\eta = \frac{\beta GMm}{R} \tag{185}$$

is given by

$$\eta = \alpha[1 + \chi e^{-\psi(\alpha)}]\psi'(\alpha). \tag{186}$$

Let us introduce the control parameter[38]

$$\mu = \frac{Gm^3R^2}{a_s\hbar^2}. \tag{187}$$

Using Eq. (71), it can be written as

$$\mu = \pi^2\left(\frac{R}{R_c}\right)^2. \tag{188}$$

It measures the size of the system (represented by R) as compared to the size R_c of the solitonic core. We note that the condition $R > R_c$ corresponds to $\mu > \mu_{\rm min} = \pi^2 = 9.87$. From Eqs. (54) and (184), we find that

$$\mu = \frac{\alpha^2}{\chi}. \tag{189}$$

On the other hand, combining Eqs. (184), (185) and (189), we find that the normalized central density is given by

$$\frac{4\pi\rho_0R^3}{M} = \frac{\alpha^2}{\eta} = \frac{\mu\chi}{\eta}. \tag{190}$$

Then, combining Eqs. (72), (188) and (190), we find that the mass of the solitonic core is given by

$$\frac{M_c}{M} = \frac{\pi\chi}{\eta\sqrt{\mu}}. \tag{191}$$

Finally, the density profile from Eq. (53) can be written as

$$\frac{4\pi R^3}{M}\rho = \frac{\alpha^2}{\eta}e^{-\psi(\alpha r/R)}. \tag{192}$$

B. Series of equilibria

Let us prescribe a value of μ. For a given value of χ we can solve the generalized Emden equation (56) up to the normalized box radius $\alpha = \sqrt{\mu\chi}$ [see Eq. (189)]. The corresponding normalized inverse temperature η is then given by Eq. (186). By varying the value of χ from 0 to $+\infty$, we can obtain the series of equilibria $\eta(\chi)$ for a fixed value of μ. Examples of such curves are given in Fig. 40. For a given value of the inverse temperature η there may exist one or several solutions with different values of the concentration parameter χ. This multiplicity of solutions leads to bifurcations and phase transitions. Among all possible solutions, we must select the stable ones, i.e., those that correspond to (local) minima of free energy.[39] Similarly to the case of self-gravitating fermions [33], we find the existence of a canonical critical point (see Fig. 40):

$$\mu_{\rm CCP} \simeq 130 \tag{193}$$

above which phase transitions appear in the canonical ensemble. As we shall see, this canonical critical point is

[38]This parameter is the counterpart of the degeneracy parameter $\mu = \eta_0\sqrt{512\pi^4G^3MR^3}$ with $\eta_0 = gm^4/h^3$ (where $g = 2s + 1$ is the spin multiplicity of the quantum states) introduced in the study of self-gravitating fermions [33].

[39]In this section, we work in the canonical ensemble. The microcanonical ensemble is considered in Sec. VIII D 5.

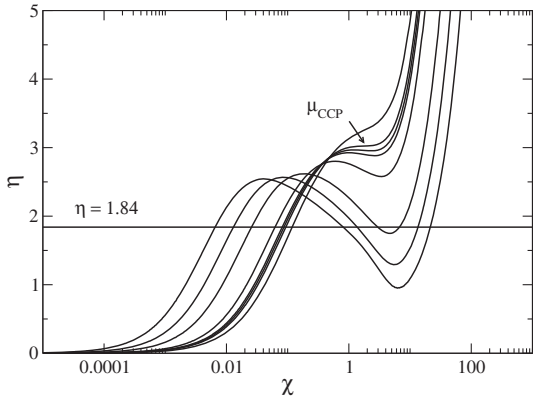

FIG. 40. Series of equilibria $\eta(\chi)$ for different values of μ (we have taken $\mu = 100, 130, 140, 150, 200, 500, 1000, 2000$—top to bottom—for illustration). We find the existence of a canonical critical point $\mu_{\rm CCP} \simeq 130$ above which bifurcations and phase transitions appear. They are associated with a multiplicity of solutions for the same value of the inverse temperature η.

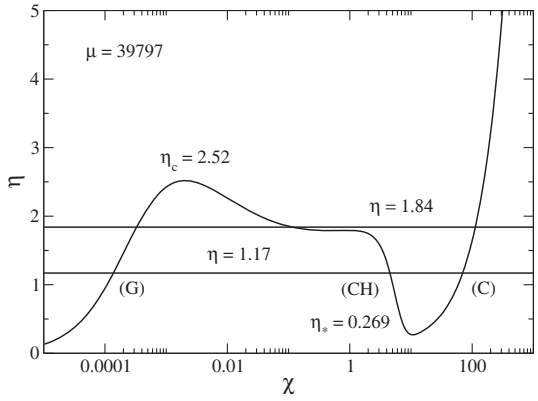

FIG. 42. Series of equilibria $\eta(\chi)$ for $\mu > \mu_{\rm CCP} \simeq 130$ not too large (here $\mu = 39797$). For $\eta = 1.17$ and $\eta = 1.84$ there are three equilibrium states: (G) is the stable gaseous phase, (C) is the stable condensed phase, and (CH) is the unstable core-halo phase.

connected to the bifurcation observed in Sec. VII. Below, we provide a preliminary study of phase transitions in the thermal self-gravitating boson gas, limiting ourselves to the canonical ensemble (fixed T). A more detailed study will be the object of a future paper.

1. $\mu < \mu_{\rm CCP}$

When $\mu < \mu_{\rm CCP} \simeq 130$ there is only one equilibrium state for each temperature (see Fig. 41). It corresponds to a pure soliton surrounded by a tiny isothermal atmosphere (quantum phase Q). This structure is thermodynamically stable. There is no phase transition.

2. $\mu > \mu_{\rm CCP}$

When $\mu > \mu_{\rm CCP} \simeq 130$ there is a canonical phase transition associated with a multiplicity of equilibrium states with the same temperature. Let us first consider the case where μ is not too large. We take $\mu = 39797$ (see Fig. 42). This value of μ corresponds to a DM halo of mass $M = 10^{12}\ M_\odot$ and size $R = 63.5$ kpc similar to the DM halo that surrounds the Milky Way (see Sec. VII E and Sec. VIII D 1 below). For the inverse temperature $\eta = 1.17$ (the choice of this value is explained in Sec. VIII D 1 below) there are three solutions with different concentration parameters χ. Their density profiles are represented in Fig. 43. For each of these solutions, the core mass M_c can be determined by Eq. (191).

The first solution (G) with $\chi^{(\rm G)} = 1.37 \times 10^{-4}$ and $M_c^{(\rm G)}/M = 1.84 \times 10^{-6} \ll 1$ corresponds to an isothermal halo having a negligible solitonic core. This is the gaseous phase.

The third solution (C) with $\chi^{(\rm C)} = 69.8$ and $M_c^{(\rm C)}/M = 0.939$ corresponds to a very compact halo (pure solitonic core) having a negligible atmosphere. This is the condensed phase.

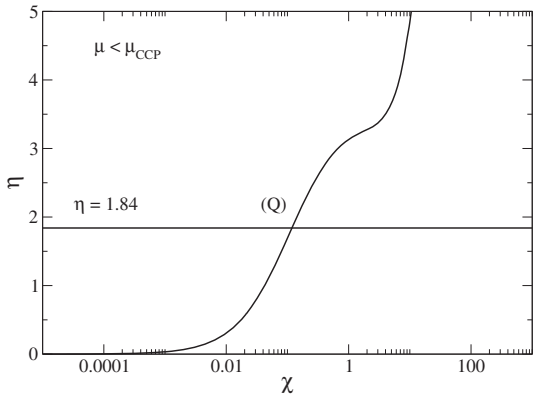

FIG. 41. Series of equilibria $\eta(\chi)$ for $\mu < \mu_{\rm CCP} \simeq 130$ (here $\mu = 100$). There is only one equilibrium state for each temperature.

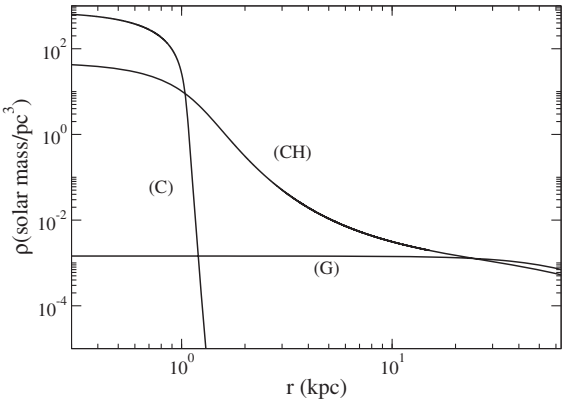

FIG. 43. Density profiles of the three solutions corresponding to the inverse temperature $\eta = 1.17$ for $\mu = 39797$. They correspond to a DM halo of mass $M = 10^{12}\ M_\odot$ and size $R = 63.5$ kpc.

Finally, the second solution (CH) with $\chi^{(\mathrm{CH})} = 4.54$ and $M_c^{(\mathrm{CH})}/M = 0.0611$ has a core-halo structure with a relatively massive solitonic core and a large isothermal atmosphere. This is the core-halo phase.

Using the Poincaré turning point criterion [188,189],[40] we can deduce from Fig. 42 that, in the canonical ensemble, the solutions (G) and (C) are thermodynamically stable (minima of free energy at fixed mass) while the solution (CH) is thermodynamically unstable (saddle point of free energy at fixed mass). It represents a critical droplet or a critical nucleus creating a barrier of free energy that the system must cross in order to trigger a phase transition from the gaseous phase (G) to the condensed phase (C).

We note that the multiplicity of the solutions depends on the temperature. When $\eta < \eta*$ there is only one solution: the gaseous phase (G). When $\eta > \eta_c$ there is only one solution: the condensed phase (C). When $\eta_* < \eta < \eta_c$ there are three solutions: the gaseous phase (G), the core-halo phase (CH) and the condensed phase (C).

There exists a transition temperature η_t (not represented) such that when $\eta < \eta_t$ the gaseous state is fully stable (global minimum of free energy) and the condensed phase is metastable (local minimum of free energy). When $\eta > \eta_t$ the situation is reversed (see [33] for a detailed discussion of phase transitions in the case of self-gravitating fermions). However, for systems with long-range interactions such as self-gravitating systems, the metastable states have a very long lifetime scaling as e^N where N is the number of particles (this is because the probability to spontaneously create a critical nucleus in order to trigger the phase transition is a very low—rare event—scaling as e^{-N}). This lifetime is generally much larger than the age of the Universe so that metastable states can be as much, or even more, relevant than fully stable states [190]. Therefore, the first order phase transition at η_t does not take place in practice. As a result, we shall not distinguish between fully stable and metastable states. The selection of the gaseous or condensed phase depends on the initial conditions and on a notion of basin of attraction [33].

3. $\mu \gg \mu_{\mathrm{CCP}}$

For very large values of μ, new equilibrium states may appear in a certain range of temperatures. For example, when $\mu = 10^5$, we have five solutions at $\eta = 1.84$ (see Fig. 44). Using the Poincaré turning point criterion, we can show that (G) is stable, (CH") has one mode of instability, (CH') has two modes of instability, (CH) has one mode of instability, and (C) is stable.

As before, the multiplicity of the solutions depends on the value of η. When $\eta < \eta_*$, there is only one solution: the gaseous phase (G). When $\eta > \eta_c$ there is only one solution: the condensed phase (C). When $\eta_* < \eta < \eta_2$ there are three solutions: the gaseous phase (G), the core-halo phase (CH), and the condensed phase (C). When $\eta_2 < \eta < \eta_c$ there are three or more solutions.

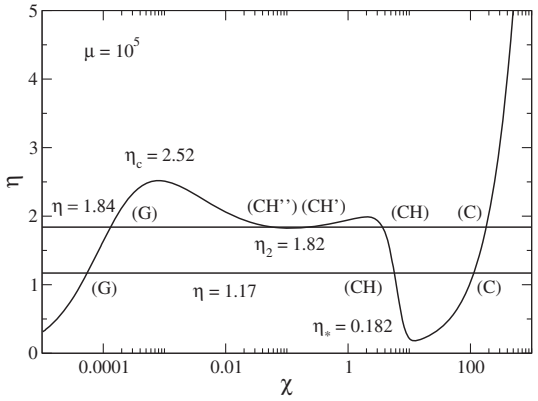

FIG. 44. Series of equilibria $\eta(\chi)$ for $\mu \gg \mu_{\mathrm{CCP}}$ (here $\mu = 10^5$). For $\eta = 1.84$ there are five intersections: (G) is the gaseous phase, (C) is the condensed phase, and (CH), (CH'), and (CH") are unstable phases with a core-halo structure. (CH) is the less unstable of them. For $\eta = 1.17$ there are only three solutions as before.

C. Caloric curves

We can also visualize the multiplicity of the solutions by plotting the caloric curves $\eta(\Lambda)$ giving the inverse temperature $\eta = \beta GMm/R$ as a function of the opposite of the energy $\Lambda = -ER/GM^2$. The caloric curves of a thermal self-gravitating BEC will be given in a forthcoming paper but they are similar to those obtained in the case of self-gravitating fermions [33].

When $\mu < \mu_{\mathrm{CCP}}$, the caloric curve is monotonic (see Fig. 14 of [33]) leading to the results of Sec. VIII B 1.

When $\mu > \mu_{\mathrm{CCP}}$ is not too large, the caloric curve has an N-shape structure (see Fig. 31 of [33]) leading to the results of Sec. VIII B 2.

When $\mu \gg \mu_{\mathrm{CCP}}$, the caloric curve has a more complicated structure, corresponding to a thick spiral (see Fig. 22 of [33]). We call it "thick" because it is made of two branches that almost superimpose: a direct spiral and an inverse spiral. This leads to the results of Sec. VIII B 3. For $\eta \simeq 2$, corresponding to the center of the spiral (see below), the number of solutions increases (up to an infinity) as μ increases.

When $\mu \to +\infty$, we recover the classical spiral (see Fig. 8 of [33]).[41] In that case, the direct and inverse branches exactly superimpose. We get $\eta_* \to 0$, $\eta_c \to 2.52$ (maximum of the classical isothermal spiral), $\eta_2 \to 1.84$ (minimum of the classical isothermal spiral), and $\eta_s \to 2$ (center of the spiral).

[40] See [33] for an application of the Poincaré turning point criterion in the case of self-gravitating fermions.

[41] The quantum caloric curves with a finite value of μ described previously correspond to the unwiding of the classical spiral (see Fig. 14 of [33]).

D. Application to real DM halos

In this section, we apply the box model to real DM halos. We shall recover from the box model the bifurcation obtained in Sec. VII C and the relation between the core mass M_c and the halo mass M_h obtained in Sec. VII D.

1. Connection to astrophysical parameters

In order to apply the box model to real DM halos, we identify the box radius R with the halo radius r_h and the mass M with the halo mass M_h. For a given DM halo, we can compute the parameter μ given by Eq. (188).[42] We have previously seen that large DM halos appear "from the outside" as being essentially isothermal (the solitonic core—if there is any—does not affect their external structure). As a result, the halo mass is related to the halo radius by the relation

$$M_h = 1.76\Sigma_0 r_h^2. \tag{194}$$

As in Sec. VII E, we consider a halo of mass $M = 10^{12}\ M_\odot$ and radius $R = 63.5$ kpc similar to the DM halo that surrounds the Milky Way. For such a halo we get $\mu = 39797$. The corresponding series of equilibria $\eta(\chi)$ is represented in Fig. 42.

Using Eqs. (D21) and (D23), we find that the normalized inverse temperature of the halo is[43]

$$\frac{\beta G M_h m}{r_h} = \xi_h \psi'_h = 1.84. \tag{195}$$

Therefore, if we want to make the connection between the box model and real DM halos, we should consider a value of η equal to 1.84. The intersection between the series of equilibria $\eta(\chi)$ and the line level $\eta = 1.84$ determines the possible equilibrium states. It is reassuring to note that $\eta = 1.84$ is smaller than $\eta_c \simeq 2.52$ (corresponding to the maximum of the classical isothermal spiral) implying that there always exists a gaseous equilibrium state (G). Actually, we should not give too much importance on the precise value of η. It is sufficient to consider that η is of the order of 1–2. This is essentially a consequence of the virial theorem. Considering Fig. 42, we see that the gaseous solution (G) and the condensed solution (C) do not strongly depend on η in the interval $\eta \sim 1$–2 while the core-halo solution (CH) is more sensitive to its precise value. This is even more true for the case considered in Fig. 44, with a larger value of μ, where several core-halo solutions (CH), (CH'), (CH") may exist at the same temperature. In order to always clearly identify the less unstable core-halo solution (corresponding to the last but one intersection), we find it convenient to select a value of η smaller than η_2. In this manner, we are guaranteed to have at most three solutions: a gaseous solution (G), a core-halo solution (CH), and a condensed solution (C). To be specific, and guided by the results obtained in Sec. VII E, we choose $\eta = 1.17$. In that case, the core-halo solution for $\mu = 39797$ has $\chi^{(\mathrm{CH})} = 4.54$ (see Fig. 42) as in Sec. VII E.

2. The critical mass $(M_h)_{\mathrm{CCP}}$ for the onset of the bifurcation

We have seen in Sec. VIII B that phase transitions (associated with the multiplicity of the solutions for a given temperature) appear for $\mu > \mu_{\mathrm{CCP}} \simeq 130$. If we identify R with r_h in Eq. (188), we get

$$\frac{r_h}{R_c} = \frac{\sqrt{\mu}}{\pi}. \tag{196}$$

Combining Eqs. (194) and (196), we obtain

$$M_h = 1.76\Sigma_0 \frac{\mu}{\pi^2} R_c^2. \tag{197}$$

Therefore, the halo mass corresponding to the canonical critical point is

$$\frac{(M_h)_{\mathrm{CCP}}}{\Sigma_0 R_c^2} = 1.76\frac{\mu_{\mathrm{CCP}}}{\pi^2} \simeq 23.2. \tag{198}$$

Using Eq. (110), we obtain

$$(M_h)_{\mathrm{CCP}} = 3.27 \times 10^9\ M_\odot. \tag{199}$$

When $M_h < (M_h)_{\mathrm{CCP}}$ there is only one equilibrium state corresponding to a solitonic core surrounded by a tiny isothermal atmosphere (quantum phase Q). When $M_h > (M_h)_{\mathrm{CCP}}$ there are generically three equilibrium states with the same temperature: a purely isothermal halo (gaseous phase G), an almost purely solitonic halo (condensed phase C), and an isothermal halo containing a small but relatively massive solitonic core (core-halo phase CH). Eliminating the almost purely solitonic solution which is not consistent with the observations of large DM halos, it remains the gaseous solution (G) and the core-halo solution (CH). Therefore, the box model predicts a bifurcation similar to the one predicted in Sec. VII C from different arguments. We note that the critical mass $(M_h)_{\mathrm{CCP}} = 3.27 \times 10^9\ M_\odot$ obtained in the present section is relatively close to the critical mass $(M_h)_{\mathrm{b}} \sim 10^9$ obtained in Sec. VII C indicating that the two approaches are consistent. The critical mass $(M_h)_{\mathrm{CCP}} = 3.27 \times 10^9\ M_\odot$ is also extremely close to $(M_h)_* = 3.30 \times 10^9\ M_\odot$. Therefore, it is convenient to identify $(M_h)_*$, $(M_h)_b$, and $(M_h)_{\mathrm{CCP}}$. As a result, the halo parameters at the bifurcation are given by Eqs. (146)–(150).

[42] We note that for the model of BECDM considered in this paper μ depends only on R, not on M.

[43] Remarkably, this value turns out to be very close to the value $\eta_2 = 1.84$ corresponding to the minimum inverse temperature of the classical isothermal spiral (see Sec. VIII C).

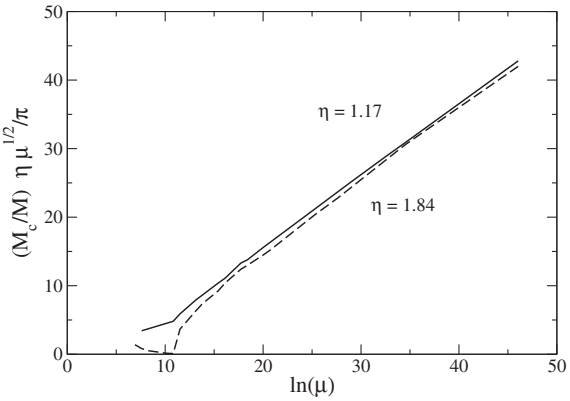

FIG. 45. Relation between the solitonic core mass normalized by the total mass, M_c/M, and the size of the system measured by the dimensionless parameter $\mu = \pi^2(R/R_c)^2$ for two different values of the dimensionless temperature η in the framework of the box model. This curve shows that the concentration parameter $\chi^{(\mathrm{CH})}$ of the core-halo phase behaves as $\ln\mu$. This leads to the scaling given by Eq. (200).

Remark: Using Eq. (197), we note that the halo mass associated with $\mu_{\min} = \pi^2 = 9.87$ is $M_h = 1.76\Sigma_0 R_c^2 = 2.48\times 10^8\ M_\odot$ which can be identified with the minimum halo mass $(M_h)_{\min} = 1.32\Sigma_0 R_c^2 = 1.86\times 10^8\ M_\odot$ obtained in Sec. VI B.

3. The $M_c - M_h$ relation

The $M_c - M_h$ relation can be obtained from the box model as follows. For $\eta = 1.17$ and for a given value of μ, we can determine the concentration parameter $\chi^{(\mathrm{CH})}$ of the core-halo solution by the intersections illustrated in Fig. 42. Then, we can obtain the solitonic core mass normalized by the total mass M_c/M from Eq. (191). We can repeat this procedure for different values of μ and obtain the curve M_c/M as a function of μ. In Fig. 45, we plot $(M_c/M)\eta\sqrt{\mu}/\pi = \chi^{(\mathrm{CH})}(\mu)$ as a function of $\ln\mu$. In the dominant approximation, we numerically find that[44]

$$\frac{M_c}{M} \sim \frac{\pi}{\eta}\frac{\ln\mu}{\mu^{1/2}}. \tag{200}$$

We have repeated the same procedure with $\eta = 1.84$ being careful to define $\chi^{(\mathrm{CH})}$ as being the last but one intersection in Fig. 44. Although the results differ for small values of μ (showing the sensibility of the core-halo solution with η mentioned previously), we find essentially the same scaling for large values of μ. From this scaling law, identifying M with the halo mass and using Eqs. (188) and (194), we find that

$$\frac{M_c}{\Sigma_0 R_c^2} = \frac{1.33}{\eta}\ln\left(\frac{M_h}{\Sigma_0 R_c^2}\right)\left(\frac{M_h}{\Sigma_0 R_c^2}\right)^{1/2}, \tag{201}$$

with $\eta \sim 1$–2. This returns the scaling $M_c \propto M_h^{1/2}$ obtained in Sec. VII D from a different method. The prefactor is also consistent with the one obtained from Eq. (181), displaying a logarithmic correction. Since the core mass increases with the halo mass, the solitonic core is persistant in the core-halo phase of large DM halos.

Performing the same study with the concentration parameter $\chi^{(\mathrm{G})}$ of the gaseous phase, we numerically find that

$$\frac{M_c}{M} \sim \frac{14.7}{\mu^{3/2}}, \tag{202}$$

leading to

$$\frac{M_c}{\Sigma_0 R_c^2} \sim 1.11\sqrt{\frac{\Sigma_0 R_c^2}{M_h}}, \tag{203}$$

in qualitative agreement with Eq. (132) of model I. Since the core mass decreases with the halo mass, there is no solitonic core in the gaseous phase of large DM halos.

Finally, performing the same study with the concentration parameter $\chi^{(\mathrm{C})}$ of the condensed phase, we numerically find that

$$\frac{M_c}{M} \simeq 1 \tag{204}$$

meaning that all the mass is in the solitonic core. As previously mentioned this solution is not in agreement with the observed structure of large DM halos and must be rejected.

4. Simple analytical model

In Appendix I we develop a simple analytical model of self-gravitating BECs with an isothermal atmosphere in a box. In that model, the mass of the solitonic core M_c is obtained by extremizing the free energy $F(M_c)$ for a given value of T, M, and R. We find that, above a canonical critical point μ_{CCP}, the free energy $F(M_c)$ has generically three extrema in agreement with the results of Sec. VIII B:

(i) A minimum at $M_c = 0$ corresponding to an isothermal halo without solitonic core (gaseous phase G). This solution is thermodynamically stable.

(ii) A minimum at some $M_c \simeq M$ corresponding to a soliton without halo (condensed phase C). This solution is thermodynamically stable.

[44]This scaling law can be understood analytically as follows. We have found in Sec. VII that $\chi \sim 2\ln(r_h/R_c)$ (see footnote 29). From Eq. (188), we have $\mu = \pi^2(r_h/R_c)^2$. Combining these two relations, we get $\chi \sim \ln\mu$. Substituting this result into Eq. (191) yields Eq. (200).

(iii) A maximum at some M_c satisfying

$$\frac{M_c}{M} \propto \frac{1}{\mu^{1/2}}, \tag{205}$$

corresponding to a solitonic core surrounded by a large isothermal halo (core-halo phase CH). This solution is thermodynamically unstable in the canonical ensemble. We note that the scaling law from Eq. (205) is consistent with the numerical result from Eq. (200) up to logarithmic corrections offering therefore an alternative derivation of this result. The analytical study of Appendix I also confirms that the core-halo solution is thermodynamically unstable in the canonical ensemble in agreement with the result obtained in Sec. VIII B from the Poincaré turning point criterion.

5. Ensembles inequivalence

In the previous sections, we have worked in the canonical ensemble. This is the statistical ensemble associated with the generalized (coarse-grained) GPP equations (3) and (4) where the temperature T is fixed. However, the microcanonical ensemble, where the energy E is fixed, may also be relevant. Actually, it may even be more relevant than the canonical ensemble since the total energy should be conserved as in the original (fine-grained) GP equations (1) and (2). As explained in Appendix I of [140], the GPP equations (3) and (4) could be modified in order to conserve the energy. In that case, the statistical ensemble associated to these equations would be the microcanonical one.

The equilibrium states in the microcanonical ensemble are the same as in the canonical ensemble (an extremum of entropy at fixed mass and energy is also an extremum of free energy at fixed mass) [191]. However, their stability may be different in the canonical and in the microcanonical ensembles. An equilibrium state that is canonically stable is always microcanonically stable, but the converse is wrong (a minimum of free energy at fixed mass is always a maximum of entropy at fixed mass and energy but a maximum of entropy at fixed mass and energy is not necessarily a minimum of free energy at fixed mass) [191]. This corresponds to the concept of ensembles inequivalence for systems with long-range interaction [33,154,187]. In particular, the core-halo states (CH) that we have found previously are always unstable in the canonical ensemble but they may be stable in the microcanonical ensemble. This is the case in particular if there is no turning point of energy in the caloric curve, or if the core-halo state stands before the first turning point of energy. In that case, the core-halo state has a negative specific heat $C < 0$. This is forbidden in the canonical ensemble but this is allowed in the microcanonical ensemble [33,154,187].

There exists a microcanonical critical point

$$\mu_{\rm MCP} \sim 10^5 \tag{206}$$

above which the caloric curve presents at least one turning point of energy.[45] Using Eq. (197) it corresponds to a halo mass

$$\frac{(M_h)_{\rm MCP}}{\Sigma_0 R_c^2} = 1.76\frac{\mu_{\rm MCP}}{\pi^2} \sim 2\times 10^4. \tag{207}$$

Using Eq. (110), we obtain

$$(M_h)_{\rm MCP} \sim 2\times 10^{12}\ M_\odot. \tag{208}$$

When $\mu < \mu_{\rm MCP}$, the caloric curve $\eta(\Lambda)$ is univalued. All the equilibrium states are stable in the microcanonical ensemble, even the core-halo states that are unstable in the canonical ensemble. This is the case in particular for the value $\mu = 39797$ corresponding to a DM halo of mass $M = 10^{12}\ M_\odot$ (see Sec. VIII D 1). Therefore, the solitonic core of mass $M_c = 6.39\times 10^{10}\ M_\odot$ (bulge) that this halo may harbor (see Sec. VII E) is part of a core-halo structure that is stable in the microcanonical ensemble while being unstable in the canonical ensemble. When $\mu > \mu_{\rm MCP}$, the caloric curve has a Z-shape structure (see Fig. 21 of [33]). Only the equilibrium states before the first turning point of energy and after the last turning point of energy are stable in the microcanonical ensemble (see [33] for details). Using these arguments, we can show that the core-halo configurations with a large value of χ (high central density) constructed in Sec. VII F are unstable both in the canonical and in the microcanonical ensembles[46] (see the similar discussion for fermions in Secs. VI–VIII of [40]). Therefore, not only the solitonic core cannot mimic a black hole (see the arguments given in Sec. VII F) but the core-halo configuration to which it belongs is unstable in all thermodynamical ensembles.

E. Core-halo solution: Critical droplet or true equilibrium state

Among the possible equilibrium states discussed previously, the core-halo solution (CH) with a quantum core surrounded by an isothermal atmosphere is the most important one. It appears for $M_h > (M_h)_{\rm CCP}$. Its stability

[45]For bosonic DM, we have not computed the microcanonical critical point $\mu_{\rm MCP}$ precisely but its value should be close to the situation where the caloric curve presents three turning points of temperature. Therefore, according to Figs. 42 and 44 we have $39797 < \mu_{\rm MCP} < 10^5$. To be specific, we shall take $\mu_{\rm MCP} \sim 10^5$.

[46]For a halo of mass $M_h = 10^{11}\ M_\odot$ and radius $r_h = 20.1$ kpc, taking $R_c = 6.98\times 10^{-2}$ pc as in Sec. VII F we get $\mu = 8.18\times 10^{11} \gg \mu_{\rm MCP}$. Taking $R_c = 6\times 10^{-4}$ pc as in footnote 36, we get $\mu = 1.11\times 10^{16} \gg \mu_{\rm MCP}$. Since μ is large in the two cases, the caloric curve has a complex structure (see Fig. 44 of [40]) and the core-halo configurations with a large value of χ considered in Sec. VII F are located between the first and the last turning points of energy. As a result, they are thermodynamically unstable in all ensembles.

depends on the statistical ensemble. In the canonical ensemble, the core-halo solution (CH) is always unstable (saddle point of free energy at fixed mass). It represents a critical droplet or a critical nucleus creating a barrier of free energy that the system must cross in order to trigger a phase transition from the gaseous phase (G) to the condensed phase (C). This is a very rare event. In the microcanonical ensemble, the core-halo solution (CH) is stable (maximum of entropy at fixed mass and energy) if $M_h < (M_h)_{\rm MCP}$. It may describe DM halos with a quantum core (representing a large bulge) and an isothermal atmosphere. However, it is unstable (saddle point of entropy at fixed mass and energy) if $M > M_{\rm MCP}$. In that case, it is replaced by a SMBH as discussed in the following section.

IX. ASTROPHYSICAL APPLICATIONS

We now discuss several potential scenarios that are suggested by the previous results.

A. Small DM halos with $(M_h)_{\rm min} < M_h < (M_h)_{\rm CCP}$: Solitonic core + tenuous isothermal atmosphere (quantum solution)

We consider a small DM halo with $(M_h)_{\rm min} = 1.86\times 10^8\, M_\odot < M_h < (M_h)_{\rm CCP} = 3.27\times 10^9\, M_\odot$. Since $\mu_{\rm min} < \mu < \mu_{\rm CCP}$ the caloric curve is monotonic (see Fig. 46).[47] The DM halo is made of a solitonic core surrounded by a tenuous isothermal atmosphere. This quantum solution (Q) is thermodynamically stable.

B. Large DM halos with $(M_h)_{\rm CCP} < M_h < (M_h)_{\rm MCP}$

We consider a large DM halo with $(M_h)_{\rm CCP} = 3.27\times 10^9\, M_\odot < M_h < (M_h)_{\rm MCP} \sim 2\times 10^{12}\, M_\odot$. Specifically, we consider a DM halo of mass $M = 10^{12}\, M_\odot$ and size $R = 63.5$ kpc similar to the one that surrounds our Galaxy. Since $\mu_{\rm CCP} < \mu < \mu_{\rm MCP}$ the caloric curve has an N-shape structure (see Fig. 47).

1. Isothermal halo + solitonic bulge possibly triggering the formation of a SMBH (core-halo solution)

We first assume that the DM halo is in the core-halo (CH) phase (see Fig. 47).[48] It is therefore made of a solitonic core of mass $M_c = 6.39\times 10^{10}\, M_\odot$ and size $R_c = 1$ kpc surrounded by an isothermal halo (see Sec. VII E). We have shown in Secs. VIII B and VIII D 4 that this core-halo solution is thermodynamically unstable in the canonical ensemble in the sense that it is a saddle point of free energy, not a (local) minimum of free energy. However, the timescale for the development of the instability may be very large (possibly larger than the age of the Universe) so that this core-halo structure may be long-lived.[49] Actually, these core-halo structures are observed in the numerical simulations of Schive *et al.* [96,97] so they appear to be robust and physical. In the case of real galaxies, the solitonic core may have existed in the past as a temporary state, or may still possibly exist. We have mentioned in Secs. VII E and VII F that the solitonic core cannot mimic a SMBH. However, it can represent a large bulge providing a favorable environment for triggering the formation of a SMBH.[50] The final outcome of this scenario would be an isothermal halo containing either a solitonic bulge or a SMBH that would be the remnant of the original solitonic bulge.

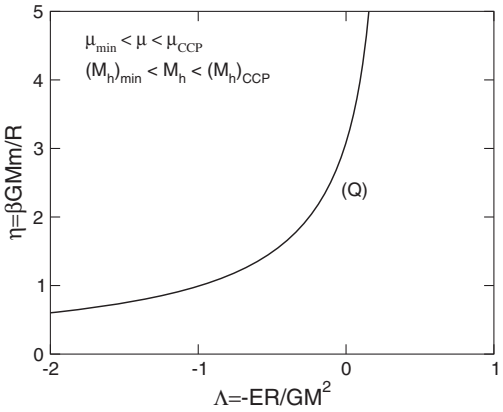

FIG. 46. For $(M_h)_{\rm min} < M_h < (M_h)_{\rm CCP}$, the caloric curve is monotonic. The quantum solutions (Q) are stable.

2. Isothermal halo without solitonic core (gaseous solution)

We now assume that the DM halo is in the gaseous (G) phase (see Fig. 47). In that case, it has the form of a purely isothermal halo without solitonic core. This gaseous solution is thermodynamically stable. In this sense, this is the most probable state in the canonical ensemble. A first possibility is that the DM halo remains in this phase. This is not inconsistent with the observations since we have shown

[47] In this section, the series of equilibria are indicative. They have been taken from our previous work [33] related to self-gravitating fermions but similar curves would be obtained for self-gravitating bosons in the framework of the present model [142].

[48] The system may reach this core-halo phase directly from a process of collisionless violent relaxation or, more slowly, from a collisional evolution as discussed in Sec. IX B 4 and in the caption of Fig. 47.

[49] A saddle point of free energy can persist for a long time as long as the fluctuations (or the environment) have not generated the dangerous perturbations that destabilize it (see an explicit illustration of this process in Ref. [192] in the context of two-dimensional turbulence). Moreover, as discussed in Sec. VIII D 5, this core-halo solution (with a negative specific heat) is stable in the microcanonical ensemble while being unstable in the canonical ensemble. Therefore, it is fully stable with respect to perturbations that conserve the energy.

[50] In that context, the solitonic core would be a sort of critical droplet (in the canonical ensemble) allowing for the transition to a more compact structure, e.g., a SMBH.

in Sec. VI F that, in many cases, an isothermal halo is almost indistinguishable from the observational Burkert profile, especially if we account for tidal effects (see Appendix B and [39,40]). However, this scenario does not account for the presence of a compact object, such as a SMBH, at the centers of the galaxies. Of course, we can always add "by hands" a primordial SMBH at the center of our isothermal halo but this is almost assuming the result. In order to explain the presence of the black hole we consider another possibility. Following our previous works [39,40], we assume that the DM halo evolves dynamically due to collisions between DM particles. These collisions are not two-body gravitational encounters because the relaxation time would be too long, but they can have another origin.[51] Because of this dynamical evolution, the central density of the halo increases until it (possibly) reaches a critical value at which the halo becomes thermodynamically unstable and undergoes a gravitational collapse. Since the statistical ensembles are inequivalent for self-gravitating systems we have to consider two possibilities (canonical and microcanonical) as detailed in the following sections.

3. Canonical evolution: Isothermal collapse from the gaseous phase to the condensed phase

In the canonical ensemble, the control parameter is the temperature. Because of collisions and evaporation the central density increases and the temperature decreases. The series of equilibria becomes unstable at the turning point of temperature T_c (see Fig. 47). At that point, the halo undergoes an isothermal collapse [194] which is eventually halted by quantum mechanics (in the present model by the repulsive self-interaction of the bosons). This takes the system from the gaseous phase (G) to the condensed phase (C) in which almost all the mass of the halo forms a compact soliton (see the analogous discussion for fermions in [33]). The final outcome of this scenario is therefore a pure soliton of radius $R_c = 1$ kpc and mass $M_c \sim 10^{12}\ M_\odot$ without atmosphere. Such a structure, which is reminiscent of an hypernova, is not observed [a pure soliton is expected to have a much smaller mass $(M_h)_{\rm min} = 1.86 \times 10^8\ M_\odot$ corresponding to the ground state of the BECDM model] so this scenario should be rejected. A possible reason for the failure of this scenario is that the canonical ensemble is not relevant for our model (see Sec. VIII D 5). Therefore, the microcanonical evolution discussed in the next section may be more relevant.

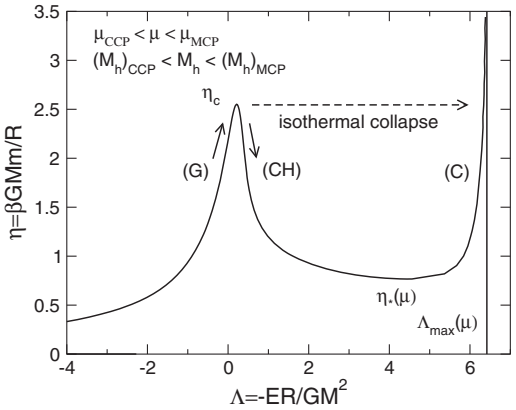

FIG. 47. For $(M_h)_{\rm CCP} < M_h < (M_h)_{\rm MCP}$, the caloric curve has an N-shape structure. In the canonical ensemble, the gaseous phase (G) and the condensed phase (C) are stable while the core-halo phase (CH) is unstable. The system can evolve collisionally in the gaseous phase (G) up to the turning point of temperature T_c and collapse in the condensed phase (C). This corresponds to an isothermal collapse (dotted arrow). As explained in the text, this canonical scenario does not seem to be realistic for large DM halos. In the microcanonical ensemble, all the equilibrium states are stable. The system can evolve collisionally (solid arrows) from the gaseous solution (G) to the core-halo solution (CH). It can also directly reach the (CH) phase through a process of collisionless violent relaxation (Jeans instability or free fall).

Remark: This scenario (isothermal collapse) could be valid in a different context in order to explain the formation of a supermassive boson star from the gravitational collapse of a dilute gaseous cloud of bosons (see Appendices J and K). The boson star could mimic a SMBH (without DM halo) of mass $\sim 10^9\ M_\odot$ at the center of an elliptical galaxy. In that case, we have to change the values of the model parameters (i.e., the characteristics of the DM particle) and take general relativity into account. The possibility of this scenario presupposes that DM may be made of different types of bosons which is not impossible. A similar scenario can also be developed for fermions as discussed in Refs. [33,186].

4. Microcanonical evolution: From the gaseous solution to the core-halo solution

In the microcanonical ensemble, the control parameter is the energy. Because of collisions and evaporation the

[51] In the context of BECDM this collisional evolution may be due to the formation of "granules" or "quasiparticles" (arising from the wave nature of the system [96,97]) which can lead to a collisonal relaxation as suggested by Hui *et al.* [122]. This scenario has been developed very recently by Bar-Or *et al.* [193] who showed that the DM halos behave similarly to classical N-body systems like globular clusters. We note that these results give further support to our study in which we model the halo as an isothermal gas following [140,141]. We argued that this isothermal halo arises from a process of violent collisionless relaxation but it can also be due to (or maintained by) "collisions" of quasiparticles. The process of violent collisionless relaxation (or gravitational cooling) may explain the rapid formation of a core-halo (CH) structure with a solitonic core (bulge) and an isothermal halo, or simply the formation of an isothermal halo (G). The process of collisional relaxation may justify why the halo evolves slowly along a series of equilibria because of collisions among pseudoparticles and evaporation (tidal effects), possibly leading to the formation of a solitonic core (see Sec. IX B 4). Finally, we note that the self-interaction of the bosons ($a_s > 0$) may also be responsible for a collisional evolution of the system and justify a (quasi-)isothermal distribution (see footnote 52).

central density increases and the energy decreases. The temperature first decreases in the region of positive specific heat ($C = dE/dT > 0$) then increases as the system enters in the region of negative specific heat ($C = dE/dT < 0$). The whole series of equilibria represented in Fig. 47 is stable. Therefore, if the system evolves microcanonically under the effect of collisions, the DM halo can go smoothly from the gaseous phase (G) to the core-halo phase (CH). This may be a mechanism which explains how the system reaches the core-halo phase (CH). The core-halo phase contains a solitonic core which may represent a bulge. This bulge is stable and persistent (in the microcanonical ensemble) and can be present at the centers of galaxies (see also the Remark at the end of Sec. VII E).

C. Very large DM halos with $M_h > (M_h)_{\rm MCP}$

We consider a very large DM halo with $M_h > (M_h)_{\rm MCP} \sim 2 \times 10^{12}\ M_\odot$. Since $\mu > \mu_{\rm MCP}$ the caloric curve has a Z-shape structure (see Fig. 48). We restrict ourselves to the microcanonical ensemble since the discussion in the canonical ensemble is the same as before. Again, we assume that the system evolves collisionally along the series of equilibria.

1. Gravothermal catastrophe and expulsion of an envelope

In the microcanonical ensemble, the system first evolves slowly from the gaseous phase (G) to the core-halo phase (CH) as before. Then, the series of equilibria becomes unstable at the turning point of energy E_c (see Fig. 48). At that point, the DM halo undergoes a gravothermal catastrophe [195] which is eventually halted by quantum mechanics (here, the repulsive self-interaction of the bosons). This takes the system from the core-halo (CH) phase to the condensed phase (C) in which only a fraction ($\sim 1/4$) of the mass of the DM halo forms a compact solitonic core while the rest of the mass forms a hot halo (see the analogous discussion for fermions in [33,186]). In the box model, the halo is held by the walls of the box. In more realistic models where the box is absent (see [40] in the case of fermionic DM), the halo is expelled at very large distances and forms a very extended atmosphere (see Fig 41 of [40]). The final outcome of this scenario is therefore a pure soliton of radius $R_c = 1$ kpc and mass $M_c \lesssim 10^{12}\ M_\odot$ with the ejection of a hot atmosphere of mass $M - M_c$. This core-halo structure is reminiscent of red-giant structure and supernovae in the context of compact stars (white dwarfs and neutron stars). However, this extreme core-halo structure is not observed in the case of DM halos (see the discussion in [40]) so this scenario should be rejected. A possible reason for the failure of this scenario is that the microcanonical evolution (gravothermal catastrophe) leads to another outcome as detailed below.

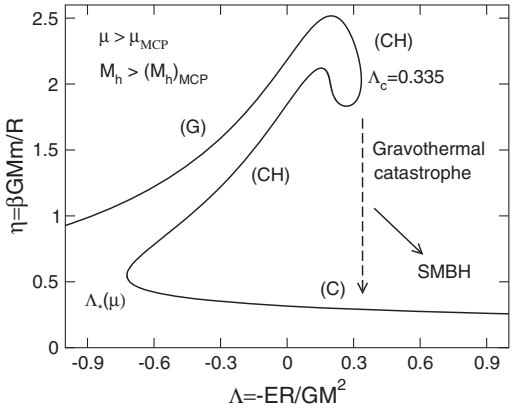

FIG. 48. For $M_h > (M_h)_{\rm MCP}$, the caloric curve has a Z-shape structure (dinosaur's neck) [33]. In the microcanonical ensemble, the gaseous phase (G) and the condensed phase (C) are stable. The core-halo phase (CH) before the first turning point of energy is also stable while the core-halo phase (CH) between the first and last turning points of energy is unstable. The system can evolve collisionally in the gaseous (G) and core-halo (CH) phases up to the turning point of energy E_c and collapse in the condensed phase (C). This corresponds to the gravothermal catastrophe (dotted arrow) [195]. As explained in the text, this scenario does not seem realistic. Another possibility is that the gravothermal catastophe triggers a dynamical instability of general relativistic origin leading to the formation of a SMBH [196].

Remark: This scenario (gravothermal catastrophe) could be valid in a different context in order to explain the formation of a supermassive boson star from the gravitational collapse of a dilute gaseous cloud of bosons (see Appendices J and K). The comments made at the end of Sec. IX B 3) also apply to the present situation.

2. Gravothermal catastrophe and black hole formation leaving the isothermal envelope undisturbed

As in the previous section we assume that the halo undergoes a gravothermal catastrophe at E_c but we consider another evolution in which the system is not affected by quantum mechanics (the validity of this hypothesis is considered in the following section). This scenario (already advocated in [39,40]) is based on the self-interacting DM model of Balberg *et al.* [196] who developed the idea of "avalanche-type contraction" towards a SMBH initially suggested by Zeldovich and Podurets [197], improved by Fackerell *et al.* [198], and confirmed numerically by Shapiro and Teukolsky [199–201]. The initial stage of the gravothermal catastrophe is well-known. The core collapses and reaches high densities and high temperatures while the halo is not sensibly affected by the collapse of the core and maintains its initial structure. Now, Balberg *et al.* [196] argue that during the gravothermal catastrophe, when the central density and the temperature increase above a critical value, the system undergoes a dynamical instability of general relativistic origin leading to the formation of a

SMBH on a dynamical time scale. Only the central region of the DM halo (not its outer part) is affected by this process so the final outcome of this scenario is an isothermal halo containing a central SMBH. The halo may have a critical King profile [39,40] as discussed in Appendix B.[52]

Remark: For large DM halos with $M_h > (M_h)_{\rm MCP} \sim 2 \times 10^{12}\ M_\odot$ the core-halo solutions with a large value of concentration χ (similar to those considered in Sec. VII F) are thermodynamically unstable so they cannot be reached by the system during a natural evolution (they lie well after the critical point of energy in the series of equilibria). On the other hand, the core-halo solutions with a small value of concentration χ (similar to those considered in Sec. VII E) lying before the critical point of energy in the series of equilibria are thermodynamically stable. Therefore, they can be reached by the system on a short timescale. However, on a long timescale, the system may evolve collisionally up to the critical point of energy E_c and collapse towards a SMBH. In conclusion, the core-halo phase (CH) is ultimately unstable in all statistical ensembles. Therefore, large DM halos with $M_h > (M_h)_{\rm MCP} \sim 2 \times 10^{12}\ M_\odot$ should not contain a solitonic core (bulge), or only temporarily. They should rather contain a SMBH resulting from the process of Balberg *et al.* [196] described previously.

[52]The gravothermal catastrophe has been studied in detail in the case of globular clusters evolving via two-body gravitational encounters. The dynamical evolution of the system is due to the gradient of temperature (velocity dispersion) between the core and the halo and the fact that the core has a negative specific heat. The core loses heat to the profit of the halo, becomes hotter, and contracts. If the temperature increases more rapidly in the core than in the halo there is no possible equilibrium and we get a runaway: this is the gravothermal catastrophe [195]. The collapse of the core is self-similar and leads to a singularity in which the central density and the temperature become infinite in a finite time (core collapse) [202,203]. However, the mass contained in the core tends to zero at the collapse time. The evolution may continue in a postcollapse regime with the formation of a binary star [204]. The energy released by the binary can stop the collapse and induce a reexpansion of the system. Then, a series of gravothermal oscillations should follow [205,206]. It has to be noted that, for globular clusters, this process is very long, taking place on a collisional relaxation timescale (of the order of the age of the Universe) since it is due to two-body gravitational encounters. In the model of Balberg *et al.* [196], the dynamical evolution of the system is due to the self-interaction of the DM particles. In that case, a typical halo has sufficient time to thermalize and acquire a gravothermal profile consisting of a flat core surrounded by an extended halo. The same idea may apply to our bosonic model (and also to the fermionic model of Refs. [39,40]) where the self-interaction of the bosons $a_s > 0$ could be responsible for the collisional evolution of the system. Using Eq. (104) and considering a cross section per unit of mass $\sigma/m = 1.25\ {\rm cm}^2/{\rm g}$ which corresponds to the constraint set by the Bullet Cluster [207] and which is consistent with the estimate of Davé *et al.* [208] used by Balberg *et al.* [196], we obtain a boson mass $m = 1.10 \times 10^{-3}\ {\rm eV/c^2}$ and a scattering length $a_s = 4.41 \times 10^{-6}$ fm. Balberg *et al.* [196] show that, during the gravothermal catastrophe, the core of the self-interacting DM halos passes from a long mean free path (LMFP) limit to a short mean free path (SMFP) limit. In the LMFP limit, the system displays a self-similar collapse analogous to that of globular clusters in which the core mass decreases rapidly. In the SMFP limit, the core mass decreases more slowly (and almost saturates) so that a relatively large mass can ultimately collapse into a SMBH.

D. Criterion for the possible existence of a black hole at the center of a galaxy

The scenario discussed in Sec. IX C 2 can lead to a black hole at the center of a galaxy only if the gravothermal catastrophe can take place and only if it is sufficiently efficient to allow the core of the system to develop high values of the density and of the temperature required to trigger a relativistic dynamical instability. However, quantum mechanics can prevent gravitational collapse and stop the gravothermal catastrophe. Therefore, the previous scenario can lead to a black hole only if the parameter μ is sufficiently larger than the microcanonical critical point $\mu_{\rm MCP} \sim 10^5$ at which the gravothermal catastrophe sets in. Using Eqs. (207) and (208), we conclude that only sufficiently large galaxies with $M_h > (M_h)_{\rm MCP} \sim 2 \times 10^{12}\ M_\odot$ can contain a SMBH resulting from the process of Sec. IX C 2. Smaller halos may not contain black holes (by this process) because they do not experience the gravothermal catastrophe. Indeed, the gravothermal catastrophe is inhibited by quantum mechanics. In that case, the halos can be either in the gaseous phase (G) or in the core-halo phase (CH) that are both thermodynamically stable in the microcanonical ensemble. This result—the fact that black holes can form only in sufficiently large galaxies—is consistent with the conclusion reached by Ferrarese [209] on the basis of observations. Furthermore, the order of magnitude of the critical mass that we find in Eq. (208) is consistent with her estimate of $\sim 5 \times 10^{11}\ M_\odot$. This qualitative agreement is encouraging in view of the crudeness of our theoretical model.

Remark: In the case of fermionic DM, the equivalent criterion $\mu > \mu_{\rm MCP}$ for the possible existence of a black hole at the centers of the galaxies (see Appendix H of [40]) is

$$(M_h)^{\rm F}_{\rm MCP} = 0.0106 \left(\frac{\mu^4_{\rm MCP} h^{12} \Sigma_0^3}{m^{16} G^6}\right)^{1/5}. \qquad (209)$$

If we take a fermion mass $m = 1.23\ {\rm keV/c^2}$ as in [40], we get $(M_h)^{\rm F}_{\rm MCP} = 1.74 \times 10^7\ M_\odot$. If we take the more relevant value $m = 170\ {\rm eV/c^2}$ obtained in Appendix D of [46], we obtain $(M_h)^{\rm F}_{\rm MCP} = 9.78 \times 10^9\ M_\odot$ in qualitative agreement with the estimate of Ferrarese [209].

E. Summary

The main results of our study are summarized in the phase diagram of Fig. 49.

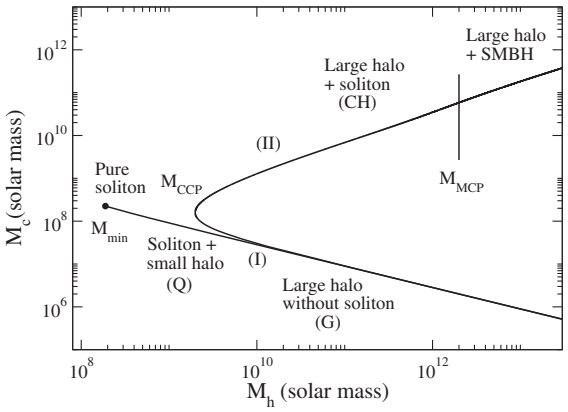

FIG. 49. Phase diagram summarizing our main results. It displays the ground state $(M_h)_{\rm min} = 1.86 \times 10^8\ M_\odot$ where the DM halo is a pure soliton without isothermal atmosphere. It also displays the canonical critical point $(M_h)_{\rm CCP} = 3.27 \times 10^9\ M_\odot$ at which a bifurcation occurs between the gaseous branch (G) where the DM halos are purely isothermal without central soliton and the core-halo branch (CH) where the DM halos are made of a solitonic core (bulge) surrounded by a large isothermal halo. Finally, it displays the microcanonical critical point $(M_h)_{\rm MCP} \sim 2 \times 10^{12}\ M_\odot$ above which the core-halo branch (CH) becomes unstable. In that case, the DM halos may undergo a gravothermal catastrophe leading to the formation of a central SMBH.

For $M_h = (M_h)_{\rm min} = 1.86 \times 10^8\ M_\odot$ (ground state), the DM halo is a pure soliton without atmosphere. This is a purely quantum object. Quantum mechanics (here, the repulsive self-interaction of the bosons) fixes the minimum mass and the minimum radius of BECDM halos. This situation may describe ultracompact dSphs like Fornax.

For $(M_h)_{\rm min} = 1.86 \times 10^8\ M_\odot < M_h < (M_h)_{\rm CCP} = 3.27 \times 10^9\ M_\odot$, the DM halo has a solitonic core surrounded by a tenuous isothermal atmosphere.[53] This is essentially a quantum (Q) object. The caloric curve is monotonic ($\mu < \mu_{\rm CCP}$; see Fig. 46). There is only one solution for any value of the temperature and of the energy. This equilibrium state is stable in the microcanonical and canonical ensembles. Even if the system evolves along the series of equilibria because of collisions, there is no collapse, hence no black hole formation. This situation may describe dSphs. Therefore, small halos like dSphs should not contain a SMBH.

For $(M_h)_{\rm CCP} = 3.27 \times 10^9\ M_\odot < M_h < (M_h)_{\rm MCP} \sim 2 \times 10^{12}\ M_\odot$, there are two solutions: a gaseous solution (G) corresponding to a purely isothermal halo without solitonic core and a core-halo (CH) solution with a solitonic core surrounded by a massive atmosphere. The soliton may mimic a bulge, not a black hole (see Sec. VII E). The caloric curve has an N-shape structure ($\mu_{\rm CCP} < \mu < \mu_{\rm MCP}$; see Fig. 47). The gaseous solution is stable in both ensembles. The core-halo solution is unstable in the canonical ensemble but is stable in the microcanonical ensemble. It has a negative specific heat. If the system evolves microcanonically along the series of equilibria because of collisions, it can pass from the gaseous phase to the core-halo phase without collapsing. There is no gravothermal catastrophe, hence no black hole formation. This situation may describe small spiral galaxies. In this sense, small spiral galaxies should not contain a SMBH (at least according to the scenario of Sec. IX C 2). Small spiral galaxies in the core-halo phase should rather contain a solitonic bulge. We note, however, that this bulge may itself induce the formation of a SMBH on a long timescale (see Sec. VII E).

For $M_h > (M_h)_{\rm MCP} \sim 2 \times 10^{12}\ M_\odot$, there are two solutions as before. However, the caloric curve now has a Z-shape structure ($\mu > \mu_{\rm MCP}$; see Fig. 48) and the core-halo solutions (CH) that lie after the turning point of energy are unstable in all ensembles. If the system evolves microcanonically along the series of equilibria because of collisions, it can undergo a gravothermal catastrophe leading to the formation of a SMBH by the mechanism described in Sec. IX C 2. This situation may apply to large spiral galaxies and elliptical galaxies. Therefore, large spiral galaxies and elliptical galaxies are expected to contain a SMBH, not a solitonic core.

The canonical critical point $(M_h)_{\rm CCP} = 3.27 \times 10^9\ M_\odot$ determines the bifurcation between gaseous (G) solutions (without soliton) having a positive specific heat and core-halo (CH) solutions (possessing a soliton) having a negative specific heat. The microcanonical critical point $(M_h)_{\rm MCP} \sim 2 \times 10^{12}\ M_\odot$ determines the transition between DM halos possessing a solitonic bulge and DM halos harboring a SMBH resulting from a gravothermal catastrophe followed by a general relativistic dynamical instability.

Remark: We note that quantum mechanics is very important for small halos on the (Q) branch ($\mu < \mu_{\rm CCP}$; dSphs). In particular, it determines the minimum mass $(M_h)_{\rm min}$ and the minimum radius $(r_h)_{\rm min}$ of BECDM halos ($\mu = \mu_{\rm min}$; ground state). Quantum mechanics is also important in the core of large halos on the (CH) branch (soliton). By contrast, quantum mechanics is negligible for large halos on the (G) branch (no soliton). However, if these halos evolve collisionally along the series of equilibria, quantum mechanics determines whether they pass smoothly from the gaseous (G) branch without soliton to the core-halo (CH) branch with a soliton ($\mu_{\rm CCP} < \mu < \mu_{\rm MCP}$; small spiral galaxies; quantum mechanics important) or if they undergo a gravothermal catastrophe and form a SMBH ($\mu > \mu_{\rm MCP}$; large spiral galaxies and elliptical galaxies; quantum mechanics unimportant).

[53]We note that the presence of an isothermal atmosphere, even tenuous, allows us to satisfy the observed mass-radius relation of DM halos corresponding to a constant surface density $\Sigma_0 = \rho_0 r_h = 141\ M_\odot/{\rm pc}^2$ [172–174]. This important point is developed in Appendix L.

X. CONCLUSION

In this paper, we have developed the model of BECDM halos with a solitonic core and an isothermal atmosphere introduced in Ref. [140]. Following previous works, we have assumed that the thermodynamical temperature $T_{\rm th}$ is equal to zero, or is much smaller than the condensation temperature T_c, so that the bosons form a pure BEC. Therefore, the system is basically described by the GPP equations (1) and (2). These equations develop a complicated process of gravitational cooling [132] and violent relaxation [136] leading to a quasiequilibrium state with a core-halo structure [96,97]. The core is a soliton, corresponding to a stationary solution of GPP equations (ground state), and the halo arises from quantum interferences of excited states. Numerical simulations [169,170] show that the halo is relatively close to an isothermal halo (or a more refined fermionic King model [39,40]) which is predicted from the theory of violent relaxation of collisionless self-gravitating systems [136,138]. In any case, an isothermal halo is a good working hypothesis to start with.

We have proposed to parametrize the complicated processes of gravitational cooling and violent relaxation on the coarse-grained scale by the generalized GPP equations (3) and (4). Through the Madelung transformation, these equations are equivalent to the fluid equations (8)–(15). They generalize the hydrodynamic equations of the CDM model by accounting for a quantum force arising from the Heisenberg uncertainty principle, a pressure force arising from the self-interaction of the bosons (scattering), a temperature, and a friction. These terms are due to quantum mechanics ($\hbar$ and a_s) and violent relaxation (T and ξ). The friction term accounts for the relaxation of the system towards an equilibrium state in which the gravitational attraction is balanced by the quantum pressure and by the thermal pressure.[54] This leads to the formation of virialized DM halos at small cosmological scales (i.e., at galactic scales) that do not suffer the problems of the CDM model. At large cosmological scales, quantum mechanics and violent relaxation are negligible (and coarse-graining is not necessary) so we recover the hydrodynamic equations of the CDM model that prove to be very relevant to explain the large-scale structure of the Universe. This amounts to taking $\hbar = a_s = T = \xi = 0$ in the generalized hydrodynamic equations (8)–(15). Therefore, quantum mechanics is potentially able to solve the problems of the CDM model at small scales without affecting the virtues of this model at large scales.

[54]The generalized GPP equations are able to account for the damped oscillations of a system of bosons experiencing gravitational cooling [132–134]. In particular, the damping term heuristically explains *how* a system of self-gravitating bosons rapidly reaches an equilibrium state by dissipating some free energy. This relaxation towards an equilibrium state is encapsulated in the H-theorem of Eq. (19).

If we neglect the quantum pressure (TF approximation), as we have done in this paper, the DM halos are described by an equation of state of the form

$$P = \frac{2\pi a_s \hbar^2 \rho^2}{m^3} + \rho \frac{k_B T}{m}. \tag{210}$$

This equation of state, which is at the basis of our study, is interesting in its own right and could have been introduced at the start without reference to the generalized GPP equations (8)–(15). It leads to DM halos presenting a core-halo structure with a solitonic core and an isothermal halo. The polytropic equation of state $P = 2\pi a_s \hbar^2 \rho^2/m^3$ dominates in the core where the density is high and the isothermal equation of state $P = \rho k_B T/m$ dominates in the halo where the density is low (the transition occurs at $\rho_i \sim k_B T m^2/2\pi a_s \hbar^2$). As a result, the equilibrium state is made of a compact core (BEC/soliton) with an equation of state $P = 2\pi a_s \hbar^2 \rho^2/m^3$, which is a stable stationary solution of the GPP equations (1) and (2) at $T = 0$ (ground state), surrounded by an isothermal atmosphere with an equation of state $P = \rho k_B T/m$ mimicking a halo of scalar radiation (quantum interferences) at an effective temperature T. The solitonic core is stabilized against gravitational collapse by quantum mechanics (here the repulsive self-interaction of the bosons) and has a smooth density profile replacing the r^{-1} cusp of CDM. On the other hand, the temperature term accounts for the almost isothermal atmosphere of DM halos, where the density approximately decreases as r^{-2}, leading to flat rotation curves. Therefore, the solitonic core solves the cusp problem and the isothermal halo leads to flat rotation curves.

We have constrained our model by imposing the universal value $\Sigma_0 = 141\ M_\odot/\mathrm{pc}^2$ of the surface density of DM halos. On the other hand, we have determined the ratio $a_s/m^3 = 3.28 \times 10^3\ \mathrm{fm}/(\mathrm{eV}/\mathrm{c}^2)^3$ of the DM particle by identifying the ground state of the GPP equations with the most compact halo that has been observed (we took the dSph Fornax as a reference but this choice could be improved if necessary). As a result, there is no free (arbitrary) parameter in our model.

We have first studied a model (model I) which is particularly well-adapted to small DM halos. This model predicts three types of DM halos depending on their mass:

(i) Dwarf DM halos with a mass $(M_h)_{\rm min} = 1.86 \times 10^8\ M_\odot$ are ultracompact objects that are completely condensed without atmosphere. They represent the ground state of the GPP equations (1) and (2) where the halo is a pure soliton. Therefore, their size $(r_h)_{\rm min} = 788$ pc is equal to the size of the BEC/soliton.

(ii) Larger, but still small, DM halos with a mass $(M_h)_{\rm min} = 1.86 \times 10^8\ M_\odot < M_h < (M_h)_* = 3.30 \times 10^9\ M_\odot$ are extended objects with a core-halo structure. They have a condensed core (BEC/soliton)

surrounded by a tenuous atmosphere made of scalar radiation (quantum interferences) with an approximately isothermal density profile decaying as r^{-2} at large distances (or, more realistically, with a NFW or Burkert profile decaying as r^{-3}). It is the atmosphere that determines their proper size while the soliton creates a central core that solves the cusp problem. There is no plateau between the core and the halo. The atmosphere can be much larger than the size of the soliton. The presence of the halo of scalar radiation explains why the size of the DM halos increases with their mass contrary to what is predicted from the ground state of the GPP equations according to which the size of DM halos has a constant value $R_c = 1$ kpc in the TF limit (see Appendix L).

(iii) Large DM halos with a mass $M_h > (M_h)_* = 3.30 \times 10^9\ M_\odot$ are purely isothermal without solitonic core. In that case, the central core is due to effective thermal effects, not to quantum mechanics. The size of the halos increases with their mass according to the law $M_h = 1.76\Sigma_0 r_h^2$.

In conclusion, model I predicts that DM halos are essentially classical isothermal spheres except close to the ground state where quantum effects become important. In other words, quantum mechanics is essential to provide a ground state corresponding to a minimum halo mass $(M_h)_{\rm min} = 1.86 \times 10^8\ M_\odot$ and a minimum halo radius $(r_h)_{\rm min} = 788$ pc. But as soon as $M_h > (M_h)_{\rm min} = 1.86 \times 10^8\ M_\odot$ quantum mechanics becomes negligible (the solitonic core disappears) and the halo is purely isothermal. This leads to the mass-radius relation reported in Fig. 16.

We have then studied another model (model II) which is particularly well adapted to large DM halos. By redefining the notion of "central density" we have found a new branch of solutions. A bifurcation from the branch of model I appears at a critical mass $(M_h)_b \sim (M_h)_* = 3.30 \times 10^9\ M_\odot$. Above that mass, the system may be purely isothermal without solitonic core (as in model I) or have a well-developed core-halo structure with a solitonic core and an isothermal envelope. The core mass scales with the halo as $M_c \propto M_h^{1/2}$ [see Eq. (181)]. The density profile presents a plateau between the core and the halo while the rotation curve presents a dip. This core-halo solution is similar to the one found by numerous authors [15,17,19–22,26,30,31,38,40,42,162–167] in the case of fermionic DM. However, we have found that the solitonic core cannot mimic a SMBH at the centers of the galaxies because it is too big. It may rather represent a bulge that may be present now (see the Remark at the end of Sec. VII E) or that, in the past, may have triggered the collapse of the surrounding gas, leading to a SMBH and a quasar.

Finally, we have been able to recover the bifurcation at $(M_h)_b$ from a box model of self-gravitating bosons, establishing an interesting connection between the statistical mechanics of self-gravitating bosons in a box and real DM halos. In this connection, the bifurcation point $(M_h)_b \sim (M_h)_* = 3.30 \times 10^9\ M_\odot$ corresponds to a canonical critical point $(M_h)_{\rm CCP} = 3.27 \times 10^9\ M_\odot$ where the caloric curve takes an N-shape structure leading to a region of negative specific heats associated with a canonical phase transition and a situation of ensembles inequivalence. We have shown that the core-halo solution is unstable in the canonical ensemble while it is stable in the microcanonical ensemble. In that last case (microcanonical ensemble), if the DM halos evolve collisionally, they can slowly pass from the gaseous phase (without soliton) to the core-halo phase (with a soliton). The core-halo phase may also be directly formed by a process of violent collisionless relaxation. We have identified another critical mass $(M_h)_{\rm MCP} = 2 \times 10^{12}\ M_\odot$ corresponding to a microcanonical critical point where the caloric curve takes a Z-shape structure leading to a microcanonical phase transition. In that case, the core-halo phase becomes unstable. If the DM halos evolve collisionally, they can undergo a slow gravothermal catastrophe ultimately leading to the formation of a SMBH on a dynamical timescale [196]. Our model therefore predicts that black holes can form (by this process) only in sufficiently large halos with a mass $M_h > (M_h)_{\rm MCP} = 2 \times 10^{12}\ M_\odot$. Interestingly, this typical mass is qualitatively consistent with the results of Ferrarese [209] obtained from observations and leading to a critical mass $\sim 5 \times 10^{11}\ M_\odot$.

In our model, the atmosphere is assumed to be isothermal in agreement with very general thermodynamical arguments. This is the "most probable" or "most natural" profile. However, the isothermal density profile decreases as r^{-2}. Therefore, a purely isothermal atmosphere is clearly an idealization since it has an infinite mass. Furthermore, the isothermal profile ($\rho \propto r^{-2}$) is apparently different from the observational Burkert profile ($\rho \propto r^{-3}$). We have shown that for large halos $M_h > (M_h)_c = 6.86 \times 10^{10}\ M_\odot$, the two profiles are indistinguishable on the scale of observations ($r_h < 100$ kpc). For smaller halos, $(M_h)_* = 3.30 \times 10^9\ M_\odot < M_h < (M_h)_c = 6.86 \times 10^{10}\ M_\odot$, the two profiles show differences in slope. We have suggested, following our previous works [39,40], that the deviation from the (most probable) isothermal law may be explained by incomplete violent relaxation, tidal effects, or stochastic forcing (see Appendix B). More precisely, we have argued that large halos, instead of being described by the isothermal profile, should be described by the King profile at the point of marginal microcanonical stability. At criticality, the King profile almost coincides with the modified Hubble profile which decreases as $\rho \propto r^{-3}$ like the Burkert profile. For $r_h \sim 100$ kpc the modified Hubble profile is much closer to the Burkert profile than the isothermal profile. This may explain the confinement of DM halos and the observed logarithmic slope -3 of their density profile instead of the ideal slope -2.

In a forthcoming paper [142], we shall adapt our model to the case of bosons without self-interaction, to the case of bosons with an attractive self-interaction, and to fermions. Preliminary results, which are in good agreement with the results of Schive *et al.* [96,97] for noninteracting bosons and to the results of Ruffini *et al.* [38] for fermions, are presented at the end of Appendix I. They provide a thermodynamical justification of their core mass/halo mass relations.

APPENDIX A: EFFECTIVE THERMAL EFFECTS VERSUS QUANTUM MECHANICS

In model I of our paper (see Sec. VI), there is an important distinction to make between small DM halos and large DM halos:

(i) Small DM halos have a core-halo structure with a solitonic core and an envelope. The core is due to quantum mechanics. The envelope is expected to be identical to that of a classical (nonquantum) collisionless self-gravitating system described by the Vlasov equation.[55] It may be described by an isothermal or (fermionic) King profile. Such profiles are consistent with the Burkert and NFW profiles at large distances (see Sec. VI F and Appendix B).

(ii) Large DM halos have no solitonic core. There are not quantum objects. Still they have a core with a finite density (instead of a cusp) that is due to effective thermal effects. They are well described by an isothermal or King profile. Such profiles are consistent with the Burkert profile at all distances (including the core) or with the NFW profile at large distances (the cusp being regularized by thermal effects).

Therefore, the small DM halos of model I are similar to those found by Schive *et al.* [96,97] but the large DM halos, being purely classical without a solitonic core, are different. In the case of small DM halos, the core is due to quantum mechanics, not to thermal effects. In the case of large DM halos, the core is due to effective thermal pressure, not to quantum mechanics. Quantum mechanics is negligible at large scales while it provides a ground state at small scales (see Sec. VI B).

In model II of our paper (see Sec. VII), both small and large DM halos have a core-halo structure with a solitonic core due to quantum mechanics and an essentially classical isothermal atmosphere. In that case, quantum mechanics (leading to the soliton) is important in the core of all types of DM halos (small and large). The DM halos of model II are similar to those found by Schive *et al.* [96,97].

[55]In the context of the GPP equations the envelope arises from quantum interferences of interaction-free excited states. It is expected to match the classical envelope arising from a process of collisionless violent relaxation based on the Vlasov-Poisson equations [169,170]. The interesting correspondence between the Schrödinger-Poisson and Vlasov-Poisson equations is discussed in [170].

APPENDIX B: SOME REASONS FOR THE DIFFERENCE BETWEEN THE ISOTHERMAL PROFILE AND THE OBSERVATIONAL BURKERT PROFILE

We have seen in Sec. VI F that the isothermal DM halos of our model with a mass $(M_h)_* = 3.30 \times 10^9\ M_\odot < M_h < (M_h)_c = 6.86 \times 10^{10}\ M_\odot$ exhibit a pronounced difference with the observational Burkert profile in the sense that their density profiles decrease at large distances as r^{-2} (isothermal) instead of r^{-3} (Burkert). Our point of view is that the isothermal profile is the "ideal" profile that a self-gravitating BEC is expected to reach through violent relaxation, gravitational cooling, or through successive mergings with other halos (in a process of hierarchical clustering). Indeed, the isothermal distribution is predicted from general thermodynamical considerations, whatever the origin of the relaxation (collisional, collisionless, stochastic, etc.) [33,154]. It corresponds to the "most probable state," i.e., to the maximum entropy state. In this sense, our isothermal model is ideal. However, in practice, there are many "nonideal" effects that prevent the system from reaching the isothermal distribution.[56] Let us briefly discuss some of these effects.

1. Incomplete violent relaxation

In the Introduction, we have developed a parallel between the process of gravitational cooling [132] for self-gravitating bosons and the process of violent relaxation [136] for collisionless stellar systems (or collisionless DM halos). Indeed, it is reasonable to consider that the formation of the atmosphere that results from gravitational cooling or hierarchical clustering is similar to the process of violent relaxation in stellar dynamics. Far from the core, quantum mechanics effects are negligible and the system behaves as a classical collisionless gas. Complete violent relaxation leads to the Lynden-Bell distribution that is similar to the Fermi-Dirac distribution (for a reason different from quantum mechanics). It leads to configurations with a core-halo structure made of a fermionic core (fermion ball) surrounded by an isothermal halo. At large distances, the density should decrease as r^{-2} [136].

[56]This is actually obvious for self-gravitating systems since the isothermal profile, decreasing at large distances as r^{-2}, has an infinite mass [135]. In other words, there is no maximum entropy state for self-gravitating systems in an unbounded domain [33,154]. In reality, the density of the halos is steeper than what is predicted by statistical mechanics. We note in this respect that the exponent $\alpha = 3$ (NFW/Burkert) of the density profile $\rho \sim r^{-\alpha}$ of observed DM halos is the closest exponent to the ideal exponent $\alpha = 2$ (isothermal) that yields a halo with a (marginal) finite mass. This rough argument may explain why the exponent $\alpha = 3$ is selected.

However, in practice, this isothermal profile (that would have an infinite mass) is not reached because of incomplete relaxation. Direct numerical simulations of collisionless stellar systems [210–213] and theoretical models of incomplete relaxation [214–216] lead to a density profile that decreases as r^{-4} at large distances. These configurations are relatively close to Hénon's isochrone profile [217]. This r^{-4} profile is steeper than the Burkert profile. Therefore, other reasons must be advocated to explain the observed r^{-3} profile.

2. Stochastic forcing

In practice, a DM halo is never completely isolated from the surrounding but is permanently subjected to perturbations caused by its environment (infall, accretion, merger, bars, tidal fields, resonances, etc.). These perturbations can be modeled by a stochastic forcing that can alter the density profiles of the halos. We suggest that the observational Burkert profile may be (partly) justified by this stochastic forcing resulting from the interaction of the system with its environment.

3. Tidal effects: King and Hubble profiles

DM halos may experience tidal interactions from other halos and galaxies. Tidal effects have been extensively studied in astrophysics in the context of globular clusters [135]. It was shown that, because of tidal interactions, the isothermal distribution is replaced by the King distribution [218]. The same ideas can be exported to the case of DM halos.[57] In Refs. [39,40], we have given arguments according to which large DM halos should be described by the King profile at the point of marginal stability in the microcanonical ensemble.[58] We call it below the "critical King profile." We have shown that the critical King profile is well fitted by the modified Hubble profile (see Appendix D 6) on the range $0 \leq r \leq 30r_h$. The modified Hubble profile decreases at large distances as r^{-3} like the Burkert profile. Therefore, tidal interactions can produce a r^{-3} density profile. The isothermal profile, the critical King profile, the modified Hubble profile and the Burkert profile are plotted in Fig. 50. For $r/r_h \leq 6$, they are very close to each other. By contrast, in the range $6 \leq r/r_h \leq 30$, the critical King profile and the modified Hubble profile are closer to the Burkert profile than the isothermal profile because they display a slope -3 instead of a slope -2. We argue that large DM halos are described by the King profile at the point of marginal microcanonical stability. The critical King profile turns out to be relatively close to the empirical modified Hubble profile and to the observational Burket profile. Therefore, tidal effects may explain why the DM halos are more confined than the isothermal profile and, consequently, why they are well fitted by the Burkert profile. As argued in [39,40], the critical King profile may provide a justification of the observed logarithmic slope $\alpha = 3$ of the density profile of DM halos from physical, instead of empirical (fit), arguments. This is confirmed by the recent paper of Argüelles *et al.* [42] who consider the fermionic King model [39,40] and show that tidal effects are important to match observational data.

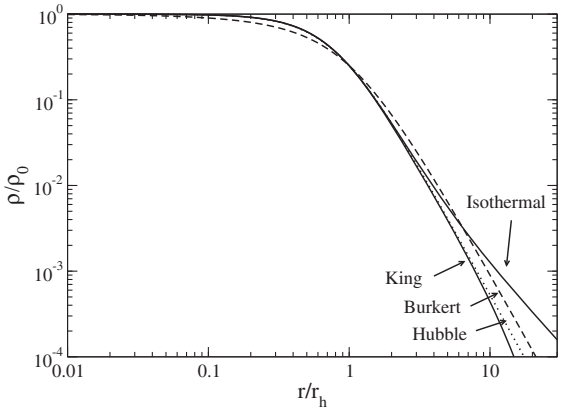

FIG. 50. Normalized density profiles up to $30r_h$. We have plotted the isothermal profile (upper solid line), the critical King profile (lower solid line), the modified Hubble profile (dotted line), and the Burkert profile (dashed line). At large distances, the critical King profile, the modified Hubble profile and the Burkert profile decrease as r^{-3} while the isothermal profile decreases as r^{-2}. Among these profiles, only the King profile is physical and relies on a rigorous theoretical modeling taking tidal effects into account (it improves upon the ideal isothermal profile that has an infinite mass). The modified Hubble profile and the Burkert profile are empirical profiles that provide a good fit of DM halos but do not have a physical justification.

APPENDIX C: COMPLEX HYDRODYNAMIC REPRESENTATION OF THE GENERALIZED SCHRÖDINGER EQUATION

In this appendix, we show that the generalized Schrödinger equation

$$i\hbar\frac{\partial\psi}{\partial t} = -\frac{\hbar^2}{2m}\Delta\psi + m\Phi\psi + 2k_BT\ln|\psi|\psi - i\frac{\hbar}{2}\xi\left[\ln\left(\frac{\psi}{\psi^*}\right) - \left\langle\ln\left(\frac{\psi}{\psi^*}\right)\right\rangle\right]\psi \quad \text{(C1)}$$

[57]Globular clusters evolve through collisional relaxation driven by two-body gravitational encounters. By contrast, DM halos are essentially collisionless for what concerns gravitational encounters (the Chandrasekhar time exceeds the age of the Universe by several orders of magnitudes). However, there can be other sources of evolution (e.g., strong collisions due to the self-interaction of the particles in the core of the system [196] or collisions between quasiparticles [122,193]) that can justify a King—or close to King—distribution for DM halos [39,40].

[58]In the present model they correspond to DM halos of mass $M_h > (M_h)_{\rm MCP} \sim 2\times 10^{12}\ M_\odot$. The point of marginal microcanonical stability in the King model is analogous to the point Λ_c in Fig. 48.

can be written as an hydrodynamic equation involving a complex velocity field and an imaginary viscosity. We then briefly mention the connection between this equation and the theory of scale relativity developed by Nottale [148] and with the stochastic interpretation of quantum mechanics developed by Nelson [219]. A more detailed discussion is given in a separate paper [220] where we adopt the opposite presentation, i.e., we derive the generalized Schrödinger equation from a complex hydrodynamic equation.

1. Complex Burgers equation

It is easy to check that the generalized Schrödinger equation (C1) can be rewritten as

$$i\hbar\frac{\partial\psi}{\partial t}=-\frac{\hbar^2}{2m}\Delta\psi+m\Phi\psi+V\psi+\hbar\mathrm{Im}(\gamma\ln\psi)\psi, \tag{C2}$$

where

$$V(t)=i\frac{\hbar}{2}\mathrm{Re}(\gamma)\left\langle\ln\left(\frac{\psi}{\psi^*}\right)\right\rangle \tag{C3}$$

is a real function of time and

$$\gamma=\xi+i\frac{2k_BT}{\hbar} \tag{C4}$$

is a complex friction coefficient. If we make the WKB transformation

$$\psi=e^{i\mathcal{S}/\hbar}, \tag{C5}$$

where $\mathcal{S}$ is a complex action, we obtain the complex Hamilton-Jacobi equation

$$\frac{\partial\mathcal{S}}{\partial t}+\frac{1}{2m}(\nabla\mathcal{S})^2-i\frac{\hbar}{2m}\Delta\mathcal{S}+m\Phi+V(t)+\mathrm{Re}(\gamma\mathcal{S})=0. \tag{C6}$$

When $\hbar=\gamma=0$ we recover the classical Hamilton-Jacobi equation (in that case $\mathcal{S}$ is real). If we introduce the complex velocity

$$\mathbf{U}=\frac{\nabla\mathcal{S}}{m}, \tag{C7}$$

and take the gradient of Eq. (C6), we obtain

$$\frac{\partial\mathbf{U}}{\partial t}+(\mathbf{U}\cdot\nabla)\mathbf{U}=i\frac{\hbar}{2m}\Delta\mathbf{U}-\nabla\Phi-\mathrm{Re}(\gamma\mathbf{U}). \tag{C8}$$

This equation can be interpreted as a damped viscous Burgers equation (no pressure term) involving a complex velocity field and an imaginary viscosity

$$\nu=\frac{i\hbar}{2m} \tag{C9}$$

proportional to the Planck constant and inversely proportional to the mass of the particle.

2. Relation to the work of Nottale

The complex hydrodynamic equation (C8) can be written as

$$\frac{D\mathbf{U}}{Dt}=-\nabla\Phi-\mathrm{Re}(\gamma\mathbf{U}), \tag{C10}$$

where

$$\frac{D\mathbf{U}}{Dt}=\frac{\partial\mathbf{U}}{\partial t}+(\mathbf{U}\cdot\nabla)\mathbf{U}-i\mathcal{D}\Delta\mathbf{U} \tag{C11}$$

is a scale covariant derivative and

$$\mathcal{D}=\frac{\hbar}{2m} \tag{C12}$$

is a quantum diffusion coefficient. When $\gamma=0$, Eq. (C10) can be interpreted as a scale covariant equation of dynamics (Newton's law). Nottale [148] has shown that a particle that has a nondifferentiable trajectory is described by an equation of that form. He considered the conservative case $\gamma=0$ where Eq. (C10) leads to the ordinary Schrödinger equation. If we take into account dissipative effects ($\gamma\neq 0$) in Eq. (C10), we obtain the generalized Schrödinger equation (C1) involving an effective temperature term (T) and a friction term (ξ).[59] In this formulation, the temperature and the dissipation are two manifestations of the same phenomenon, i.e., they represent the real and the imaginary parts of the complex friction coefficient γ [see Eq. (C4)].

Remark: We note that, in Nottale's theory, $\mathcal{D}$ may be different from $\hbar/2m$. In other words, the (generalized) Schrödinger Eq. (C1) may be valid in a more general context than quantum mechanics. Indeed, it may apply to particles that have nondifferentiable trajectories due to their chaotic motion or due to the fractal structure of spacetime itself at large (cosmological) scales. This opens new perspectives for the interpretation of the Schrödinger-Poisson and GPP equations for DM as discussed in [141].

3. Relation to the work of Nelson

If we write $\mathbf{U}=\mathbf{u}-i\mathbf{u}_Q$ where [see Eqs. (7), (C5), and (C7)]

[59]The fact that T and ξ in Eq. (C1) can be interpreted as a temperature and a friction coefficient is explained in Sec. II using the Madelung transformation (see also [140,220]).

$$\mathbf{u}=\frac{\nabla S}{m} \quad \text{and} \quad \mathbf{u}_Q=\frac{\hbar}{2m}\nabla \ln\rho \tag{C13}$$

are the classical and quantum velocities, and take the real and imaginary parts of the generalized complex viscous Burgers equation (C8), we obtain the two real coupled equations

$$\frac{\partial \mathbf{u}}{\partial t}+(\mathbf{u}\cdot\nabla)\mathbf{u}-(\mathbf{u}_Q\cdot\nabla)\mathbf{u}_Q=\frac{\hbar}{2m}\Delta\mathbf{u}_Q-\nabla\Phi - \mathrm{Re}(\gamma)\mathbf{u}-\mathrm{Im}(\gamma)\mathbf{u}_Q, \tag{C14}$$

$$\frac{\partial \mathbf{u}_Q}{\partial t}+(\mathbf{u}_Q\cdot\nabla)\mathbf{u}+(\mathbf{u}\cdot\nabla)\mathbf{u}_Q=-\frac{\hbar}{2m}\Delta\mathbf{u}. \tag{C15}$$

When $\gamma=0$ these equations coincide with those introduced by Nelson [219] in his stochastic interpretation of quantum mechanics.[60] In that case, $\mathbf{u}_Q$ is called the osmotic velocity (see footnote 41 in [220]). Nelson derived these equations from Newton's law and showed their equivalence with the ordinary Schrödinger equation. Equations (C14) and (C15) can therefore be viewed as a generalization of Nelson's equations taking dissipative effects into account.

4. Generalized Einstein relation

It is interesting to note that the complex nature of the friction coefficient $\gamma=\gamma_{\mathrm{R}}+\gamma_{\mathrm{I}}$ [see Eq. (C4)] leads to a generalized Schrödinger equation (C1) exhibiting *simultaneously* a friction term and an effective temperature term. They correspond to the real and imaginary parts of γ. This may be viewed as a new form of fluctuation-dissipation theorem. In this respect, we note that the relation

$$\mathcal{D}=\frac{k_BT}{m\gamma_I} \tag{C16}$$

resulting from Eqs. (C4) and (C12) is similar to the Einstein relation of Brownian motion [221].

On the other hand, if we assume that $\gamma_{\mathrm{R}}=\gamma_{\mathrm{I}}$ (see the argument given in Appendix D of [141]), we obtain the relation

$$\mathcal{D}=\frac{k_BT}{m\xi}. \tag{C17}$$

Explicitly,

$$\frac{\hbar}{2m}=\frac{k_BT}{m\xi} \quad \text{or} \quad \frac{\hbar}{2}=\frac{k_BT}{\xi}. \tag{C18}$$

Again, this can be viewed as a sort of generalized Einstein relation expressing a form of fluctuation-dissipation theorem. Here, the diffusion coefficient has a quantum origin.

[60]We note that Eqs. (C14) and (C15) are equivalent to the Madelung hydrodynamic equations (8) and (9); see [220] for more details.

APPENDIX D: PARTICULAR PROFILES OF SELF-GRAVITATION SYSTEMS

In this appendix, we consider particular profiles of self-gravitating systems that are useful in our study to interpret the structure of DM halos.

1. Basic equations and definitions

The condition of hydrostatic equilibrium of a self-gravitating system described by a barotropic equation of state $P(\rho)$ is

$$\nabla P+\rho\nabla\Phi=\mathbf{0}. \tag{D1}$$

Dividing this equation by ρ, taking its divergence and using the Poisson equation (10), we obtain the fundamental differential equation [158]:

$$\nabla\cdot\left(\frac{1}{\rho}\nabla P\right)=-4\pi G\rho. \tag{D2}$$

Depending on the equation of state this equation can be solved analytically or numerically to obtain the density profile $\rho(r)$.

The halo radius r_h is defined as the distance at which the central density ρ_0 is divided by 4,

$$\frac{\rho(r_h)}{\rho_0}=\frac{1}{4}. \tag{D3}$$

The mass $M(r)$ contained within a sphere of radius r is given by

$$M(r)=\int_0^r \rho(r')4\pi r'^2dr'. \tag{D4}$$

The halo mass is

$$M_h=M(r_h). \tag{D5}$$

The circular velocity is defined by

$$v^2(r)=\frac{GM(r)}{r}. \tag{D6}$$

The circular velocity at the halo radius is

$$v_h^2=v^2(r_h)=\frac{GM_h}{r_h}. \tag{D7}$$

We note the identity

$$\frac{v_h^2}{G\rho_0r_h^2}=\frac{M_h}{\rho_0r_h^3}. \tag{D8}$$

2. Isothermal profile

We consider the isothermal equation of state [158]:

$$P = \rho \frac{k_B T}{m}, \tag{D9}$$

where T is the temperature. The fundamental equation of hydrostatic equilibrium (D2) can be rewritten as

$$\frac{k_B T}{m} \Delta \ln \rho = -4\pi G \rho. \tag{D10}$$

Writing

$$\rho = \rho_0 e^{-\psi}, \tag{D11}$$

where ρ_0 is the central density, introducing the normalized radial distance

$$\xi = r/r_0, \qquad r_0 = \left(\frac{k_B T}{4\pi G \rho_0 m}\right)^{1/2}, \tag{D12}$$

where r_0 is the thermal core radius, and assuming spherical symmetry, we obtain the Emden equation [158]:

$$\frac{1}{\xi^2}\frac{d}{d\xi}\left(\xi^2 \frac{d\psi}{d\xi}\right) = e^{-\psi}, \tag{D13}$$

$$\psi(0) = \psi'(0) = 0. \tag{D14}$$

Using Eqs. (D4), (D11), (D12), and (D13), the mass contained within the sphere of radius r is given by

$$M(r) = 4\pi \rho_0 r_0^3 \xi^2 \psi'(\xi). \tag{D15}$$

According to Eqs. (D6), (D12) and (D15), the circular velocity is

$$v^2(r) = 4\pi G \rho_0 r_0^2 \xi \psi'(\xi). \tag{D16}$$

Using Eq. (D12), we find that the temperature satisfies the relation

$$\frac{k_B T}{m} = 4\pi G \rho_0 r_0^2. \tag{D17}$$

Therefore, we can rewrite Eq. (D16) as

$$\frac{m v^2(r)}{k_B T} = \xi \psi'(\xi). \tag{D18}$$

The halo radius defined by Eq. (D3) is given by $r_h = \xi_h r_0$, where ξ_h is determined by the equation

$$e^{-\psi(\xi_h)} = \frac{1}{4}. \tag{D19}$$

Solving the Emden equation (D13) numerically, we find

$$\xi_h = 3.63, \qquad \psi'(\xi_h) = 0.507. \tag{D20}$$

The normalized halo mass is

$$\frac{M_h}{\rho_0 r_h^3} = 4\pi \frac{\psi'(\xi_h)}{\xi_h} = 1.76. \tag{D21}$$

The normalized circular velocity at the halo radius is

$$\frac{v_h^2}{4\pi G \rho_0 r_h^2} = \frac{\psi'(\xi_h)}{\xi_h} = 0.140. \tag{D22}$$

The normalized temperature is

$$\frac{k_B T}{G m \rho_0 r_h^2} = \frac{4\pi}{\xi_h^2} = 0.954. \tag{D23}$$

3. Polytropic profiles

We consider the polytropic equation of state [158]:

$$P = K\rho^\gamma, \qquad \gamma = 1 + \frac{1}{n}, \tag{D24}$$

where K is the polytropic constant and γ (or n) is the polytropic index. The fundamental equation of hydrostatic equilibrium (D2) can be rewritten as

$$K(n+1)\Delta \rho^{1/n} = -4\pi G \rho. \tag{D25}$$

Writing

$$\rho = \rho_0 \theta^n, \tag{D26}$$

where ρ_0 is the central density, introducing the normalized radial distance

$$\xi = r/r_0, \qquad r_0 = \left[\frac{K(n+1)}{4\pi G \rho_0^{1-1/n}}\right]^{1/2}, \tag{D27}$$

where r_0 is the polytropic core radius, and assuming spherical symmetry, we obtain the Lane-Emden equation [158]:

$$\frac{1}{\xi^2}\frac{d}{d\xi}\left(\xi^2 \frac{d\theta}{d\xi}\right) = -\theta^n, \tag{D28}$$

$$\theta(0) = 1, \qquad \theta'(0) = 0. \tag{D29}$$

Using Eqs. (D4), (D26), (D27), and (D28), the mass contained within the sphere of radius r is given by

$$M(r) = -4\pi\rho_0 r_0^3 \xi^2 \theta'(\xi). \tag{D30}$$

According to Eqs. (D6), (D27) and (D30), the circular velocity is

$$v^2(r) = -4\pi G\rho_0 r_0^2 \xi\theta'(\xi). \tag{D31}$$

The halo radius defined by Eq. (D3) is given by $r_h = \xi_h r_0$, where ξ_h is determined by the equation

$$\theta(\xi_h)^n = \frac{1}{4}. \tag{D32}$$

The value of ξ_h can be obtained by solving the Lane-Emden equation (D28) for a given value of n. The normalized halo mass is

$$\frac{M_h}{\rho_0 r_h^3} = -4\pi\frac{\theta'(\xi_h)}{\xi_h}. \tag{D33}$$

The normalized circular velocity at the halo radius is

$$\frac{v_h^2}{4\pi G\rho_0 r_h^2} = -\frac{\theta'(\xi_h)}{\xi_h}. \tag{D34}$$

When $n < 5$, the polytropes are self-confined (their density has a compact support). We denote by ξ_1 the normalized radius at which the density vanishes: $\theta_1 = 0$. Their total mass M and their radius R are given by

$$M = -4\pi\rho_0 r_0^3 \xi_1^2 \theta_1', \qquad R = \xi_1 r_0. \tag{D35}$$

Eliminating the central density between these two equations, we obtain the mass-radius relation [158]:

$$M^{(n-1)/n} R^{(3-n)/n} = \frac{K(n+1)}{G(4\pi)^{1/n}} \omega_n^{(n-1)/n}, \tag{D36}$$

where $\omega_n = -\xi_1^{(n+1)/(n-1)}\theta_1'$.

For the polytrope $n = 1$ the Lane-Emden equation (D28) can be solved analytically. The solution is [158]

$$\frac{\rho(r)}{\rho_0} = \theta = \frac{\sin(\xi)}{\xi}. \tag{D37}$$

The normalized radial distance is $\xi = r/r_0$ where $r_0 = (K/2\pi G)^{1/2}$ is independent of the central density. The density vanishes at $\xi_1 = \pi$. This corresponds to a radius

$$R = \pi\left(\frac{K}{2\pi G}\right)^{1/2}. \tag{D38}$$

We can then write $\xi = \pi r/R$. The central density is related to the total mass by

$$\rho_0 = \frac{\pi M}{4R^3} = \frac{M}{4\pi^2}\left(\frac{2\pi G}{K}\right)^{3/2}. \tag{D39}$$

The halo radius is $r_h = \xi_h R/\pi$ where ξ_h is the smallest root of $\sin(\xi_h)/\xi_h = 1/4$. We find

$$\xi_h = 2.4746, \ \theta'(\xi_h) = -0.41853. \tag{D40}$$

The mass profile and the circular velocity profile can be written as

$$M(r) = \frac{4\pi\rho_0 r_h^3}{\xi_h^3}[\sin(\xi) - \xi\cos(\xi)], \tag{D41}$$

$$v^2(r) = \frac{4\pi G\rho_0 r_h^2}{\xi_h^2}\left[\frac{\sin(\xi)}{\xi} - \cos(\xi)\right]. \tag{D42}$$

The normalized halo mass and the normalized circular velocity at the halo radius are

$$\frac{M_h}{\rho_0 r_h^3} = 2.12534, \qquad \frac{v_h^2}{4\pi G\rho_0 r_h^2} = 0.169129. \tag{D43}$$

4. Burkert profile

The Burkert profile [6] is given by the empirical law

$$\frac{\rho(r)}{\rho_0} = \frac{1}{(1+x)(1+x^2)}, \qquad x = \frac{r}{r_h}. \tag{D44}$$

The corresponding rotation curve is

$$v^2(r) = 2\pi G\frac{\rho_0 r_h^2}{x}\left[\ln(1+x) - \arctan x + \frac{1}{2}\ln(1+x^2)\right]. \tag{D45}$$

The normalized halo mass and the normalized circular velocity at the halo radius are

$$\frac{M_h}{\rho_0 r_h^3} = 1.60, \qquad \frac{v_h^2}{4\pi G\rho_0 r_h^2} = 0.127. \tag{D46}$$

5. Pseudo-isothermal profile

The pseudo-isothermal profile is given by

$$\frac{\rho(r)}{\rho_0} = \frac{1}{1+3x^2}, \qquad x = \frac{r}{r_h}. \tag{D47}$$

The corresponding rotation curve is

$$v^2(r) = \frac{4\pi G\rho_0 r_h^2}{3}\left[1 - \frac{\arctan(\sqrt{3}x)}{\sqrt{3}x}\right]. \tag{D48}$$

The normalized halo mass and the normalized circular velocity at the halo radius are

$$\frac{M_h}{\rho_0 r_h^3}=1.66, \qquad \frac{v_h^2}{4\pi G\rho_0 r_h^2}=0.132. \tag{D49}$$

6. Modified Hubble profile

The modified Hubble model [135] is given by

$$\frac{\rho(r)}{\rho_0}=\frac{1}{(1+ax^2)^{3/2}}, \qquad x=\frac{r}{r_h}, \tag{D50}$$

where $a=4^{2/3}-1=1.52$. The corresponding rotation curve is

$$v^2(r)=4\pi G\frac{\rho_0 r_h^2}{x}\left[\frac{\sinh^{-1}(\sqrt{a}x)}{a^{3/2}}-\frac{x}{a\sqrt{1+ax^2}}\right]. \tag{D51}$$

The normalized halo mass and the normalized circular velocity at the halo radius are

$$\frac{M_h}{\rho_0 r_h^3}=1.75, \qquad \frac{v_h^2}{4\pi G\rho_0 r_h^2}=0.139. \tag{D52}$$

7. Natarajan and Lynden-Bell profile

The Natarajan and Lynden-Bell profile [161] is given by

$$\frac{\rho}{\rho_0}=\frac{A}{a^2+\xi^2}-\frac{B}{b^2+\xi^2}, \tag{D53}$$

where ξ is defined by Eq. (D12). The corresponding rotation curve is

$$v^2(r)=\frac{4\pi G\rho_0 r_0^2}{\xi}\left\{Aa\left[\frac{\xi}{a}-\tanh^{-1}\left(\frac{\xi}{a}\right)\right]-Bb\left[\frac{\xi}{b}-\tanh^{-1}\left(\frac{\xi}{b}\right)\right]\right\}. \tag{D54}$$

The halo radius defined by Eq. (D3) is given by $r_h=\xi_h r_0$, where ξ_h is determined by the second degree equation (for ξ_h^2):

$$\xi_h^4+(a^2+b^2+4B-4A)\xi_h^2+a^2b^2-4Ab^2+4Ba^2=0. \tag{D55}$$

A good approximation of the isothermal profile is obtained by taking $A=50$, $a^2=10$, $B=48$, and $b^2=12$ [161]. This gives $\xi_h=3.64$. The normalized halo mass and the normalized circular velocity at the halo radius are then given by

$$\frac{M_h}{\rho_0 r_h^3}=1.75, \qquad \frac{v_h^2}{4\pi G\rho_0 r_h^2}=0.139, \tag{D56}$$

in very good agreement with the exact results from Appendix D 2.

APPENDIX E: FUNDAMENTAL DIFFERENTIAL EQUATION OF OUR MODEL

In our model [140,141], the density of the DM halos is determined by the fundamental differential equation

$$\frac{\hbar^2}{2m^2}\Delta\left(\frac{\Delta\sqrt{\rho}}{\sqrt{\rho}}\right)-\frac{K\gamma}{\gamma-1}\Delta\rho^{\gamma-1}-\frac{k_BT}{m}\Delta\ln\rho=4\pi G\rho+3\omega_0^2. \tag{E1}$$

If we define

$$\rho=\rho_0 e^{-\psi}, \qquad \xi=\left(\frac{4\pi G\rho_0 m}{k_BT}\right)^{1/2}r, \tag{E2}$$

$$\chi=\frac{K\gamma m\rho_0^{\gamma-1}}{k_BT}, \quad \epsilon=\frac{2\pi G\rho_0\hbar^2}{(k_BT)^2}, \quad \Omega^2=\frac{3\omega_0^2}{4\pi G\rho_0}, \tag{E3}$$

we find that Eq. (E1) takes the form of a generalized Emden equation

$$\epsilon\Delta(e^{\psi/2}\Delta e^{-\psi/2})+\Delta\psi+\chi\nabla\cdot[e^{-(\gamma-1)\psi}\nabla\psi]=e^{-\psi}+\Omega^2. \tag{E4}$$

The ordinary Emden equation (D13) is recovered for $\epsilon=\chi=\Omega=0$. Alternatively, if we define

$$\rho=\rho_0\theta^n, \qquad \xi=\left[\frac{4\pi G}{K(n+1)\rho_0^{1/n-1}}\right]^{1/2}r, \tag{E5}$$

we find that Eq. (E1) takes the form of a generalized Lane-Emden equation

$$-\frac{\epsilon}{n^2\chi^2}\Delta\left(\frac{\Delta\theta^{n/2}}{\theta^{n/2}}\right)+\frac{1}{\chi}\Delta\ln\theta+\Delta\theta=-\theta^n-\Omega^2. \tag{E6}$$

The ordinary Lane-Emden equation (D28) is recovered for $\epsilon=1/\chi=\Omega=0$.

APPENDIX F: COMPARISON WITH THE MODEL OF SLEPIAN AND GOODMAN

Our model of BECDM halos shows analogies with the model of Slepian and Goodman [168] but is fundamentally different, thereby escaping the problems mentioned by these authors to construct BECDM halos consistent with the observations.

Slepian and Goodman [168] consider a self-gravitating boson gas at finite temperature, corresponding to a true statistical equilibrium state of bosons resulting from a collisional relaxation. They take into account the repulsive self-interaction of the bosons and the possibility that the bosons form a BEC above a critical density ρ_c. They derive the equation of state of this system and show that it behaves as $P \sim \rho k_B T_{\rm th}/m$ (isothermal) at low densities and as $P \sim 2\pi a_s \hbar^2 \rho^2/m^3$ (condensate) at high densities. The normalized equation of state depends on a dimensionless parameter $\theta \sim a_s/\Lambda_{\rm dB}$ where $\Lambda_{\rm dB} = h/\sqrt{2\pi m k_B T_{\rm th}}$ is the thermal de Broglie wavelength. Importantly, it displays a plateau after ρ_c when $\theta \ll 1$. Slepian and Goodman [168] numerically determine the density and circular velocity profiles corresponding to this equation of state. They find that the circular velocity profile presents a dip which increases as θ decreases and argue that, in order to match the observations (which do not exhibit a strong dip), we must have $\theta \geq 10^{-4}$.[61] This implies that $m \geq 10\ {\rm eV/c^2}$ (assuming $v_\infty = 100$ km/s and $R_c = 1$ kpc). However, this constraint is not consistent with the constraint $m < 10^{-3}\ {\rm eV/c^2}$ implied by the Bullet Cluster (see Appendix D of [46]). They conclude therefore that the thermal BECDM model is ruled out.

Their model is physically different from ours because it describes the true statistical equilibrium state of self-gravitating bosons at finite temperature while our model is an heuristic parametrization of the GPP equations at $T_{\rm th} = 0$ (or $T_{\rm th} \ll T_c$) taking into account violent relaxation and gravitational cooling. In their model, $T_{\rm th}$ represents the true thermodynamic temperature while in our model T is an effective out-of-equilibrium temperature (like in Lynden-Bell's theory of violent relaxation). In the same way, their equation of state aims at representing the true equation of state of a self-interacting boson gas at statistical equilibrium while our equation of state (14) is a heuristic equation of state of an out-of-equilibrium self-interacting boson gas (again like in Lynden-Bell's theory of violent relaxation). Therefore, their equation of state is different, and more complex, than ours (although they both have the same asymptotic behaviors). In particular, it display a plateau between the condensed phase and the uncondensed phase which is responsible for the problems that they encounter to constuct a DM halo satisfying all the observational constraints. In our out-of-equilibrium equation of state there is no such plateau so there is no problem to obtain solutions satisfying the observational constraints.

Slepian and Goodman [168] were careful to mention that their conclusions only apply to self-gravitating bosons at statistical equilibrium. Since we consider out-of-equilibrium (but still virialized) self-gravitating bosons described by a different equation of state their critics do not apply to our model.

[61] We note that Slepian and Goodman [168] impose $\theta\hat{\nu}(0) = 1$ which corresponds to $\chi \sim 1$ in our notations. According to Eq. (111) this is equivalent to the equality between the soliton radius and the thermal core radius: $r_0 \sim R_c$.

APPENDIX G: CONDENSATION TEMPERATURE

We have seen that large DM halos have an isothermal, or almost isothermal, atmosphere which is responsible for the flat, or almost flat, rotation curves of the galaxies. The temperature T is related to the circular velocity at infinity v_∞ by the relation

$$\frac{k_B T}{m} = \frac{v_\infty^2}{2}. \tag{G1}$$

For the medium spiral, $v_\infty = 153$ km/s (see Sec. VI C). For bosons with a repulsive self-interaction, the boson mass must be in the range $2.92 \times 10^{-22}\ {\rm eV}/c^2 < m < 1.10 \times 10^{-3}\ {\rm eV}/c^2$ in order to account for the mass and size of ultracompact dwarf halos at $T = 0$ such as Fornax as well as the constraint set by the bullet cluster (see Appendix D of Ref. [46]). In that case, we find from Eq. (G1) that the temperature of large halos such as the medium spiral is $4.41 \times 10^{-25}\ {\rm K} < T < 1.66 \times 10^{-6}\ {\rm K}$. Such a small temperature may not be physical. This strongly suggests that T is not the true thermodynamic temperature. It may rather represent an effective temperature as we have suggested in the present paper. In that case, T has not a real physical meaning. Only the quantity $k_B T/m$ has a physical meaning.

The condensation temperature of a boson gas is given by

$$T_c = \frac{2\pi\hbar^2 \rho^{2/3}}{m^{5/3} k_B \zeta(3/2)^{2/3}}, \tag{G2}$$

where $\zeta(3/2) = 2.6124\ldots$. The bosons are uncondensed for $T_{\rm th} > T_c$ while they form a BEC for $T_{\rm th} < T_c$. Evaluated at the center of large DM halos such as the medium spiral where $\rho_0 = 7.02 \times 10^{-3}\ M_\odot/{\rm pc}^3$ (see Sec. VI C), we get $5.29 \times 10^5\ {\rm K} < T_c < 4.82 \times 10^{36}\ {\rm K}$. This value of the condensation temperature is considerably larger than the thermodynamic temperature of radiation $T_{\rm th} \sim 3$ K, than the effective temperature of the DM halos $4.41 \times 10^{-25}\ {\rm K} < T < 1.66 \times 10^{-6}\ {\rm K}$ and than any reasonable temperature. This indicates that the bosons are completely condensed and that we can consider that $T_{\rm th} = 0$. This justifies our starting hypothesis.

Of course, in a given halo, the condensation temperature decreases as the density decreases. For a given temperature, we can define a critical density

$$\rho_c = \frac{\zeta(3/2)}{(2\pi)^{3/2}} \frac{(k_B T_{\rm th})^{3/2} m^{5/2}}{\hbar^3} \tag{G3}$$

above which the bosons form a BEC. Taking $T_{\rm th} \sim 3$ K (thermodynamic temperature of radiation), we get

$3.44 \times 10^{-57}\ M_\odot/\mathrm{pc}^3 < \rho_c < 9.48 \times 10^{-11}\ M_\odot/\mathrm{pc}^3$. This is much smaller than the typical densities represented in Fig. 23 indicating that the bosons are always completely condensed. Therefore, in all relevant cases, we can assume that $T_{\rm th} = 0$.

Remark: If we assume that DM halos are made of fermions, like sterile neutrinos, then the fermion mass must be $m \sim 170\ \mathrm{eV}/c^2$ in order to account for the mass and size of ultracompact dwarf halos at $T = 0$ such as Fornax (see Appendix D of [46]). In that case, we find from Eq. (G1) that the temperature of large halos such as the medium spiral is $T \sim 0.257$ K. This temperature is more physical suggesting that, if DM is made of fermions, T may represent the true thermodynamic temperature. There remains, however, the timescale problem to reach a statistical equilibrium state, as discussed in the Introduction.

APPENDIX H: PROOF THAT THE SOLITONIC CORE IN OUR MODEL IS ALWAYS NONRELATIVISTIC

The soliton of mass M_c and radius R_c studied in Sec. VII F would be strongly relativistic, and could mimic a SMBH, if its radius were of the order of the Schwarzschild radius:

$$R_c \sim R_S = \frac{2GM_c}{c^2}. \tag{H1}$$

Using Eq. (181), we find that

$$\frac{R_c}{R_S} = \frac{R_c c^2}{2GM_c} = 0.695 \frac{c^2}{G\sqrt{\Sigma_0 M_h}} \frac{1}{\ln(\frac{M_h}{\Sigma_0 R_c^2})}. \tag{H2}$$

Interestingly, in our model, the compactness R_c/R_S of the soliton is independent of the properties of the DM particle (a_s and m), except for a logarithmic correction (the logarithmic factor depends on R_c, hence on a_s/m^3). For a halo of mass $M_h = 10^{11}\ M_\odot$, similar to the one that surrounds our Galaxy, we get $R_c/R_S = 5.89 \times 10^5 \gg 1$. Therefore, the soliton is not a black hole, not even a relativistic object. We find that R_c/R_S becomes of order unity for a halo mass

$$(M_h)_{\rm crit} = 0.121 \frac{c^4}{\Sigma_0 G^2} \frac{1}{\ln^2(\frac{c^2}{G\Sigma_0 R_c})}. \tag{H3}$$

When $M_h \ll (M_h)_{\rm crit}$ the soliton is nonrelativistic. When M_h approaches $(M_h)_{\rm crit}$ the soliton becomes strongly relativistic and may mimic a black hole (in that case, a general relativistic treatment becomes mandatory). Using Eqs. (94) and (101), we obtain

$$(M_h)_{\rm crit} \sim 10^{21}\ M_\odot. \tag{H4}$$

This value is independent of the properties of the DM particle. This critical mass is much larger than any relevant mass of DM halos in the Universe. We therefore conclude that the solitonic core in our model is always nonrelativistic and cannot mimic a black hole. This justifies *a posteriori* our Newtonian approach.

Another, sensibly equivalent, argument can be given as follows. When general relativity is taken into account, we know that a self-interacting boson star in the TF regime is stable only below a maximum mass [159,222,223]:

$$(M_c)_{\rm max} = 0.307 \frac{\hbar c^2 \sqrt{a_s}}{(Gm)^{3/2}} = 9.78 \times 10^{-2} \frac{c^2 R_c}{G}. \tag{H5}$$

Using Eq. (101), we get

$$(M_c)_{\rm max} = 2.04 \times 10^{15}\ M_\odot. \tag{H6}$$

When $M_c \sim (M_c)_{\rm max}$, the boson star is strongly relativistic and when $M_c > (M_c)_{\rm max}$ it collapses into a black hole. Inversely, when $M_c \ll (M_c)_{\rm max}$, the boson star is nonrelativistic. For a halo of mass $M_h = 10^{11}\ M_\odot$, the mass of the soliton is $M_c = 1.77 \times 10^{10}\ M_\odot$ (see Sec. VII F). Since $M_c \ll (M_c)_{\rm max}$, the soliton is nonrelativistic. The soliton would collapse into a black hole if its mass satisfied $M_c > (M_c)_{\rm max}$. From Eqs. (181) and (H5) we find that

$$\frac{M_c}{(M_c)_{\rm max}} = 7.35 \frac{G\sqrt{\Sigma_0 M_h}}{c^2} \ln\left(\frac{M_h}{\Sigma_0 R_c^2}\right). \tag{H7}$$

Therefore, M_c would be larger that $(M_c)_{\rm max}$ in a halo of mass $M_h > (M_h)'_{\rm crit}$ where $(M_h)'_{\rm crit}$ [obtained from Eq. (H7)] is essentially the same mass as in Eqs. (H3) and (H4). Therefore, we conclude that the soliton is always nonrelativistic (for all the halos in the Universe) and that it cannot collapse into a black hole. This does not prevent, however, the possibility that the solitonic bulge attracts the gas around it and creates a situation favorable to the formation of a SMBH and a quasar as discussed in Sec. VII E.

Remark: We can similarly compute the maximum soliton mass in the case of noninteracting bosons. Using $(M_c)_{\rm max} = 0.633\hbar c/Gm$ [156,224] and $m = 2.92 \times 10^{-22}\ \mathrm{eV/c^2}$ (see Sec. VI B), we obtain $(M_c)_{\rm max} = 2.90 \times 10^{11}\ M_\odot$. On the other hand, the maximum mass of the fermion ball $(M_c)_{\rm max} = 0.384(\hbar c/G)^{3/2}/m^2$ [225] in the case of fermions of mass $m = 170\ \mathrm{eV/c^2}$ (see Sec. VI B) is $(M_c)_{\rm max} = 2.16 \times 10^{13}\ M_\odot$. These maximum masses are much larger than the core masses of DM halos [$M_c \ll (M_c)_{\rm max}$] so the cores of DM halos are generally nonrelativistic. We note that Ruffini *et al.* [38] reach a different conclusion because they take a much larger mass of the fermionic particle, $m = 48\ \mathrm{keV/c^2}$, which is not consistent with the arguments given in Sec. VI B.

APPENDIX I: ANALYTICAL MODEL OF A SELF-GRAVITATING BEC WITH AN ISOTHERMAL ATMOSPHERE IN A BOX

In this appendix, we develop an analytical model of a self-gravitating BEC with an isothermal atmosphere enclosed within a box of radius R.[62] This model returns the gaseous (G), core-halo (CH), and condensed (C) phases obtained in Sec. VIII. It allows us to analytically obtain the relation $M_c(M_h)$ between the core mass and the halo mass by extremizing the free energy $F(M_c)$ with respect to M_c. Furthermore, it shows that the gaseous and condensed solutions are thermodynamically stable (minima of free energy) while the core-halo solution is thermodynamically unstable in the canonical ensemble (maximum of free energy).[63]

We modelize the core by a pure soliton of mass M_c and radius R_c as in Sec. III B 2. For a self-interacting BEC in the TF approximation, we recall that the soliton radius R_c has a unique value given by Eq. (71). On the other hand, the internal energy and the gravitational energy of the soliton are given by [78]

$$U_c = \frac{GM_c^2}{4R_c}, \qquad W_c = -\frac{3GM_c^2}{4R_c}. \tag{I1}$$

We modelize the halo by an isothermal atmosphere of uniform density and mass $M - M_c$ contained between the spheres of radius R_c and R. The internal energy of the atmosphere is given by

$$U_h = \frac{k_B T}{m}(M - M_c)[\ln(M - M_c) - \ln V - 1], \tag{I2}$$

and its gravitational energy (in the presence of the solitonic core) by

$$W_h = -\frac{3GM_c(M - M_c)}{2R} - \frac{3G(M - M_c)^2}{5R}. \tag{I3}$$

To obtain these results, we have assumed that $R_c \ll R$ [28].

The free energy of the system is therefore

$$F = -\frac{GM_c^2}{2R_c} + \frac{k_B T}{m}(M - M_c)[\ln(M - M_c) - \ln V - 1] - \frac{3GM_c(M - M_c)}{2R} - \frac{3G(M - M_c)^2}{5R}. \tag{I4}$$

This is a function $F(M_c)$ of the core mass for a given value of M, R, and T. The extrema of this function determine the possible equilibrium states of the system. More precisely, they determine the possible equilibrium core masses $M_c^{(i)}$ as a function of M, R, and T. This is valid both in the canonical and microcanonical ensembles [28] (see Sec. VIII D 5). In the canonical ensemble, a minimum of $F(M_c)$ corresponds to a stable equilibrium state (most probable state) while a maximum of $F(M_c)$ corresponds to an unstable equilibrium state (less probable state).

It is convenient to introduce the dimensionless quantities

$$x = \frac{M_c}{M}, \qquad \eta = \frac{\beta GMm}{R}, \tag{I5}$$

$$\mu = \pi^2\left(\frac{R}{R_c}\right)^2, \qquad f(x) = \frac{F(M_c)R}{GM^2}, \tag{I6}$$

so that Eq. (I4) can be rewritten as

$$f(x) = -\frac{\sqrt{\mu}}{2\pi}x^2 + \frac{1}{\eta}(1 - x)\left[\ln\left(\frac{M}{V}\right) + \ln(1 - x) - 1\right] - \frac{3}{2}x(1 - x) - \frac{3}{5}(1 - x)^2, \tag{I7}$$

with $0 \leq x \leq 1$.

The equilibrium states, corresponding to $f'(x) = 0$, are the solutions of the equation

$$\ln(1 - x) + \left(\frac{\sqrt{\mu}}{\pi} - \frac{9}{5}\right)x\eta + \frac{3}{10}\eta + \ln\left(\frac{M}{V}\right) = 0. \tag{I8}$$

This equation determines the core mass $x = M_c/M$ as a function of η, μ and M/V. For $x = 0$ (purely gaseous phase) we find $\eta(0) = -(10/3)\ln(M/V)$ and, for reasons that will become clear below, we shall identify this value with $\eta_c = 2.52$, the minimum temperature of a classical self-gravitating isothermal gas [194]. Therefore, we set

$$\ln\left(\frac{M}{V}\right) = -\frac{3}{10}\eta_c. \tag{I9}$$

We can then rewrite Eq. (I8) as

$$\ln(1 - x) + \left(\frac{\sqrt{\mu}}{\pi} - \frac{9}{5}\right)x\eta + \frac{3}{10}(\eta - \eta_c) = 0. \tag{I10}$$

The solutions of this equation can be easily found by studying the inverse function

$$\eta(x) = \frac{\eta_c - \frac{10}{3}\ln(1 - x)}{1 + \frac{10}{3}(\frac{\sqrt{\mu}}{\pi} - \frac{9}{5})x} \tag{I11}$$

for a given value of μ (see Fig 51). For $x \to 0$, we get

[62] This model is directly inspired by the analytical model developed in Refs. [26,28,186] for self-gravitating fermions.

[63] It is possible to generalize this model in the microcanonical ensemble [157]. In that case, it can be shown that the core-halo phase may be microcanonically stable in agreement with the discussion of Sec. VIII D 5.

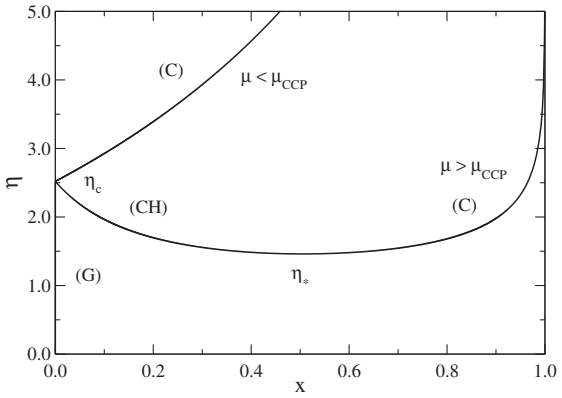

FIG. 51. The function $\eta(x)$ for $\mu < \mu_{\rm CCP}^{\rm app} = 47.6$ (specifically $\mu = 30$) and for $\mu > \mu_{\rm CCP}^{\rm app}$ (specifically $\mu = 100$). We have represented the gaseous phase (G), the condensed phase (C), and the core-halo phase (CH).

$$\eta(x) = \eta_c + \frac{10}{3}\left[1 - \left(\frac{\sqrt{\mu}}{\pi} - \frac{9}{5}\right)\eta_c\right]x + \ldots. \tag{I12}$$

Close to $x = 0$, the curve $\eta(x)$ is increasing when $\mu < \mu_{\rm CCP}^{\rm app.}$ and decreasing when $\mu > \mu_{\rm CCP}^{\rm app.}$, where

$$\mu_{\rm CCP}^{\rm app.} = \pi^2\left(\frac{1}{\eta_c} + \frac{9}{5}\right)^2 = 47.6. \tag{I13}$$

This value can be identified with the canonical critical point. For $x \to 1$, we get

$$\eta \sim \frac{-\ln(1-x)}{\frac{\sqrt{\mu}}{\pi} - \frac{3}{2}} \to +\infty, \tag{I14}$$

where we have assumed $\mu > (3\pi/2)^2 = 22.2$ to avoid unphysical results due to the invalidity of our model for small values of μ.

For $\mu > \mu_{\rm CCP}^{\rm app.}$, the minimum of the curve $\eta(x)$, denoted (x_*, η_*), is determined by the equations

$$\ln(1-x_*) + \frac{x_*}{1-x_*} + \frac{3}{10(\frac{\sqrt{\mu}}{\pi} - \frac{9}{5})(1-x_*)} - \frac{3}{10}\eta_c = 0 \tag{I15}$$

and

$$\eta_* = \frac{1}{(\frac{\sqrt{\mu}}{\pi} - \frac{9}{5})(1-x_*)}. \tag{I16}$$

Instead of solving Eq. (I15) for x_* as a function of μ, it is simpler to study the inverse function

$$\mu(x_*) = \left[\frac{9\pi}{5} + \frac{\frac{3\pi}{10(1-x_*)}}{\frac{3}{10}\eta_c - \ln(1-x_*) - \frac{x_*}{1-x_*}}\right]^2. \tag{I17}$$

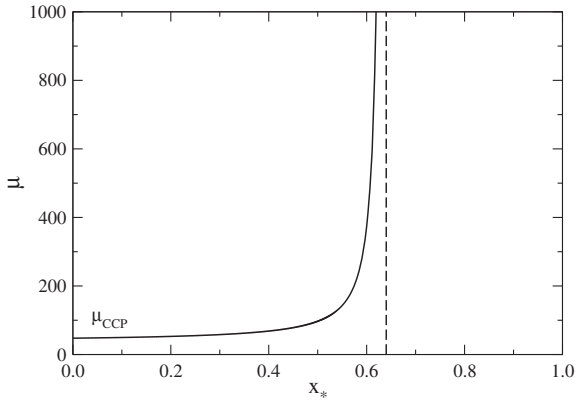

FIG. 52. The function $\mu(x_*)$. By inversion, it gives the value of x_* as a function of μ.

The values of x_* and η_* characterizing the minimum of the curve $\eta(x)$ as a function of μ are plotted in Figs. 52 and 53. For $\mu \to \mu_{\rm CCP}^{\rm app.} = 47.6$, we find that $x_* \to 0$ and $\eta_* \to \eta_c$. For $\mu \to +\infty$, we find that $x_* \to x_*^c$, where x_*^c is the solution of the equation

$$\ln(1-x_*) + \frac{x_*}{1-x_*} - \frac{3}{10}\eta_c = 0. \tag{I18}$$

We numerically obtain $x_*^c \simeq 0.640$. We then find that

$$\eta_* \sim \frac{\pi}{\sqrt{\mu}(1-x_*)} \sim \frac{8.73}{\sqrt{\mu}} \to 0. \tag{I19}$$

Let us now consider more specifically the function $f(x)$ giving the free energy as a function of the core mass x for a given value of μ and η (see Fig. 54). Using Eq. (I9), we can rewrite Eq. (I7) as

$$f(x) = -\frac{\sqrt{\mu}}{2\pi}x^2 + \frac{1}{\eta}(1-x)\left[-\frac{3}{10}\eta_c + \ln(1-x) - 1\right] - \frac{3}{2}x(1-x) - \frac{3}{5}(1-x)^2. \tag{I20}$$

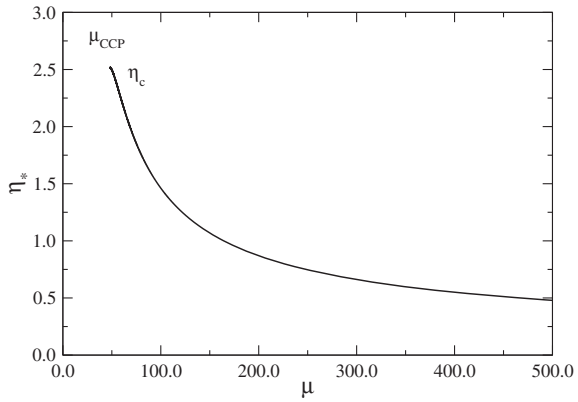

FIG. 53. The value of η_* as a function of μ.

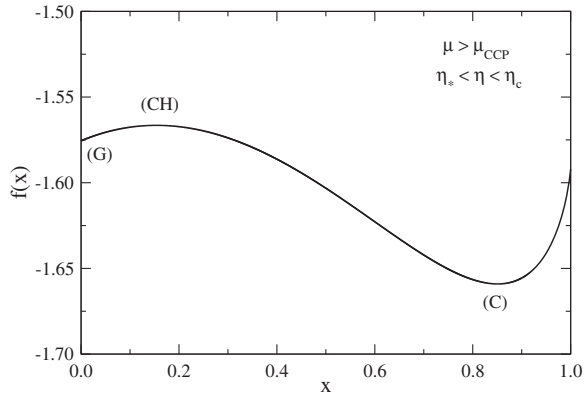

FIG. 54. The function $f(x)$ for $\mu > \mu_{\rm CCP}^{\rm app}$ and $\eta_* < \eta < \eta_c$ (specifically $\mu = 100$ and $\eta = 1.8$) where three equilibrium states exist.

Its first derivative is

$$f'(x) = -\frac{\sqrt{\mu}}{\pi}x + \frac{3}{10}\frac{\eta_c}{\eta} - \frac{1}{\eta}\ln(1-x) - \frac{3}{10} + \frac{9}{5}x. \quad \text{(I21)}$$

The condition $f'(x) = 0$ determines the equilibrium states as we have just seen. The stability of these equilibrium states in the canonical ensemble is then determined by the sign of the second derivative of the free energy:

$$f''(x) = -\frac{\sqrt{\mu}}{\pi} + \frac{1}{\eta(1-x)} + \frac{9}{5}. \quad \text{(I22)}$$

An equilibrium state is stable when $f''(x) > 0$, corresponding to a minimum of free energy, and unstable when $f''(x) < 0$, corresponding to a maximum of free energy. Coming back to the function $f(x)$, its values at $x = 0$ and $x = 1$ are

$$f(0) = -\frac{1}{\eta}\left(\frac{3}{10}\eta_c + 1\right) - \frac{3}{5} \quad \text{(I23)}$$

and

$$f(1) = -\frac{\sqrt{\mu}}{2\pi}. \quad \text{(I24)}$$

For $x \to 0$, we find that

$$f(x) = f(0) + \frac{3}{10}\left(\frac{\eta_c}{\eta} - 1\right)x + \ldots. \quad \text{(I25)}$$

The term in parentheses is positive when $\eta < \eta_c$ and negative when $\eta > \eta_c$. Since the function $f(x)$ is defined for $x \geq 0$, the solution $x = 0$ (purely gaseous phase) is a local minimum of $f(x)$ for $\eta < \eta_c$ even though $f'(0) \neq 0$. We shall therefore consider that this solution is a stable equilibrium state.

We are now ready to perform the complete analysis of the equilibrium states of our simple analytical model. We note that the function $\eta(x)$ defined by Eq. (I11) is the counterpart of the function $\eta(\chi)$ defined in Sec. VIII.

For $\mu < \mu_{\rm CCP}^{\rm app}$, the curve $\eta(x)$ is made of a vertical branch at $x = 0$ up to $\eta = \eta_c$, then it increases monotonically up to infinity (see Fig. 51). This is similar to Figs. 41 and 46. For $\eta < \eta_c$ there is a unique equilibrium state with $x = 0$ corresponding to the gaseous phase (G). For $\eta > \eta_c$ there is a unique equilibrium state with $x > 0$ corresponding to the condensed phase (C). They are both stable (minima of free energy). There is no phase transition in the present situation. Here, η_c just separates the gaseous configurations from the condensed configurations.

For $\mu > \mu_{\rm CCP}^{\rm app}$, the curve $\eta(x)$ is made of a vertical branch at $x = 0$ up to $\eta = \eta_c$, then it decreases up to η_* and finally it increases up to infinity (see Fig. 51). This is similar to Figs. 42 and 47. When $\eta < \eta_*$, there is a unique equilibrium state with $x = 0$. It corresponds to the gaseous phase (G). When $\eta > \eta_c$, there is a unique equilibrium state with $x \simeq 1$. It corresponds to the condensed phase (C). They are both stable (minima of free energy). When $\eta_* < \eta < \eta_c$ there are three equilibrium states (see Fig. 54): (i) a gaseous phase (G) with $x = 0$, (ii) a core-halo phase (CH) with $x \ll 1$, (iii) a condensed phase (C) with $x \simeq 1$. Let us analyze these solutions in more detail in the limit $\mu \to +\infty$:

(i) The gaseous solution (G) corresponds to a purely isothermal halo without soliton. The core mass is equal to zero: $x_1 = 0$. This solution is stable, being a minimum of free energy, although the derivative of $f(x)$ is not defined at $x = 0$ (as explained above).

(ii) The core-halo solution (CH) corresponds to an isothermal halo harboring a central soliton with a small mass. From Eq. (I10), we find that the core mass scales as

$$x_2 \propto \frac{1}{\sqrt{\mu}}, \quad \text{(I26)}$$

leading to the results of Sec. VIII D 4. Substituting Eq. (I26) into Eq. (I22) we find that $f''(x_2) = -\sqrt{\mu}/\pi < 0$. Therefore, the core-halo solution is unstable in the canonical ensemble. It may, however, be stable in the microcanonical ensemble (see Sec. VIII D 5).

(iii) The condensed solution (C) corresponds to a solitonic core surrounded by a tenuous atmosphere. From Eq. (I10), we find that the core mass scales as

$$1 - x_3 \propto e^{-\sqrt{\mu}\eta/\pi}, \quad \text{(I27)}$$

showing that the soliton contains almost all the mass. Substituting Eq. (I27) into Eq. (I22) we find that $f''(x_3) \sim (1/\eta)e^{\eta\sqrt{\mu}/\pi} \to +\infty$. Therefore, the condensed solution is stable.

We now show that the result (I26) can be obtained from the "velocity dispersion tracing" relation

$$v_c^2 \sim v_h^2 \tag{I28}$$

stating that the velocity dispersion in the core $v_c^2 \sim GM_c/R_c$ is of the same order as the velocity dispersion in the halo $v_h^2 \sim GM_h/r_h$. This condition gives

$$M_c \propto \frac{R_c}{r_h} M_h. \tag{I29}$$

Using $\mu \propto (r_h/R_c)^2$ it can be rewritten as Eq. (I26). Therefore, Eq. (I26) is fully consistent with the velocity dispersion tracing relation (I28) which, in the noninteracting case ($a_s = 0$), leads to the core mass/halo mass relation found by Schive *et al.* [97] (see the discussion in Mocz *et al.* [226]). In the present case (self-interacting bosons), since R_c is independent of M_c and since $M_h \propto \Sigma_0 r_h^2$, we get

$$M_c \propto R_c\sqrt{\Sigma_0 M_h} \propto \left(\frac{a_s\hbar^2\Sigma_0 M_h}{Gm^3}\right)^{1/2} \propto M_h^{1/2} \tag{I30}$$

in agreement with Eqs. (183) and (201) obtained by two different methods (in total, we have presented four independent arguments leading to this relation).

We conclude this appendix by presenting preliminary results obtained for noninteracting bosons and fermions (they will be developed in a specific paper [157]).

As we have seen previously for self-interacting bosons, the relation $M_c(M_h)$ can be obtained either by extremizing the free energy with respect to M_c [157] or, more directly, by assuming the velocity dispersion tracing relation (I28) or (I29).[64] In the case of noninteracting bosons, using the mass-radius relation $M_c R_c = 9.95\hbar^2/Gm^2$ [50,78,79], we obtain

$$M_c \propto \left(\frac{\hbar^2 M_h}{Gm^2 r_h}\right)^{1/2} \propto \left(\frac{\hbar^4\Sigma_0 M_h}{G^2 m^4}\right)^{1/4} \propto M_h^{1/4}. \tag{I31}$$

In the case of fermions, using the mass-radius relation $M_c R_c^3 = 1.49\times 10^{-3} h^6/G^3 m^8$ [158], we get

$$M_c \propto \frac{\hbar^{3/2}}{m^2}\left(\frac{M_h}{Gr_h}\right)^{3/4} \propto \left(\frac{\hbar^3}{m^4}\right)^{1/2}\left(\frac{M_h\Sigma_0}{G^2}\right)^{3/8} \propto M_h^{3/8}. \tag{I32}$$

We now note that the mass-radius relation $M_h \propto r_h^2$ used in the present paper (based on the observation that the surface density of DM halos is constant [172–174]) is different from the mass-radius relation $M_v \propto r_v^3$ used by Schive *et al.* [97]. This suggests that the halo mass M_v considered by these authors is different from the halo mass M_h considered here. Using the relation $GM_h/r_h \sim GM_v/r_v$ (consistent with the velocity dispersion tracing relation), we get $M_h \propto M_v^{4/3}$. Using this relation[65] together with the $M_c(M_h)$ relations obtained previously, we obtain for self-interacting bosons

$$M_c \propto M_v^{2/3}, \tag{I33}$$

for noninteracting bosons

$$M_c \propto M_v^{1/3}, \tag{I34}$$

and for fermions

$$M_c \propto M_v^{1/2}. \tag{I35}$$

The scaling of Eq. (I34) is consistent with the numerical results of Schive *et al.* [97]. The scaling of Eq. (I35), previously given in the form of Eq. (I32) in Appendix H of [40], is consistent with the scaling of Ruffini *et al.* [38] who find 0.52 instead of 1/2. We have shown in [157] that our procedure of extremizing the free energy is always equivalent to the velocity dispersion tracing relation (I28). Therefore, our approach provides a justification of the results of Schive *et al.* [97] and Ruffini *et al.* [38] from thermodynamical arguments. The prefactor in Eqs. (I33)–(I35) can be obtained from our approach [like in Eq. (183) for self-interacting bosons] but this requires additional calculations that will be presented in future works [142,157].

Remark: It is interesting to study how the mass M_c, the radius R_c, the velocity dispersion GM_c/R_c and the energy GM_c^2/R_c in the core behave in the classical limit $\hbar \to 0$. For self-interacting bosons, using Eq. (I30), we find $M_c \sim R_c \sim GM_c^2/R_c \sim \hbar \to 0$ and $GM_c/R_c \sim 1$. For noninteracting bosons, using Eq. (I31), we find $M_c \sim R_c \sim GM_c^2/R_c \sim \hbar \to 0$ and $GM_c/R_c \sim 1$. For fermions, using Eq. (I32), we find $M_c \sim R_c \sim GM_c^2/R_c \sim \hbar^{3/2} \to 0$ and $GM_c/R_c \sim 1$.

APPENDIX J: PHASE TRANSITIONS LEADING TO A BOSON OR FERMION BALL MIMICKING A SMBH AT THE CENTERS OF ELLIPTICAL GALAXIES

In this Appendix, we consider the possibility that the SMBHs of mass $M \sim 10^9\ M_\odot$ that reside at the centers of elliptical galaxies are actually boson or fermion balls corresponding to a purely condensed phase (C) without halo.

Let us consider a dilute gas of bosons or fermions with a mass $M \sim 10^9\ M_\odot$ and a sufficiently large radius R so

[64] We note that this relation is not obvious *a priori* and that other relations are possible such as the "energy tracing" relation [226]. The fact that relation (I28) can be justified from a free energy extremization principle [157] provides a physical basis for it.

[65] From $M_h \propto r_h^2$ and $v_h^2 = GM_h/r_h \propto r_h$, we get $v_h \propto M_h^{1/4}$ which is the Tully-Fisher relation [227,228]. Using $M_h \propto M_v^{4/3}$ we get $v_h \propto M_v^{1/3}$ which is consistent with the scaling reported in [209,229]. This gives some confidence to the relation $M_h \propto M_v^{4/3}$.

that a canonical phase transition can take place (this requires that $\mu > \mu_{\rm CCP}$ so that the caloric curve has the shape of Figs. 47 and 48). In that case, below the critical temperature T_c (corresponding to $\eta_c \simeq 2.52$), the gas undergoes a gravitational collapse (isothermal collapse) and forms a compact object (completely condensed boson or fermion star) of about the same mass $M \sim 10^9\ M_\odot$ but with a much smaller radius $R_* \ll R$. This corresponds to a zeroth order phase transition from a gaseous phase (G) to a condensed phase (C). The condensed solution (C) represents a pure boson or fermion star without DM halo.

The boson or fermion star (compact object) may mimic a SMBH of mass $M \sim 10^9\ M_\odot$ at the center of an elliptical galaxy if its maximum mass $M_{\rm max}$ is close to $M \sim 10^9\ M_\odot$. In that case, the boson or fermion star is very relativistic and general relativity must be taken into account.

Using the results of Appendix F of [119] we can estimate the characteristics of the corresponding DM particle.[66] For noninteracting bosons, using $M_{\rm max} = 0.633\hbar c/Gm$ and $R_* = 9.53GM_{\rm max}/c^2$ [156,224] we find that $M_{\rm max} = 10^9\ M_\odot$ (with $R_* = 4.56 \times 10^{-4}$ pc) provided that $m = 8.46 \times 10^{-20}\ {\rm eV/c^2}$. For self-interacting bosons in the TF limit, using $M_{\rm max} = 0.307\hbar c^2\sqrt{a_s}/(Gm)^{3/2}$ and $R_* = 6.25GM_{\rm max}/c^2$ [222,223] we find that $M_{\rm max} = 10^9\ M_\odot$ (with $R_* = 2.99 \times 10^{-4}$ pc) provided that $a_s/m^3 = 7.86 \times 10^{-10}\ {\rm fm/(eV/c^2)^3}$. For fermions, using $M_{\rm max} = 0.384(\hbar c/G)^{3/2}/m^2$ and $R_* = 8.73GM_{\rm max}/c^2$ [225], we find that $M_{\rm max} = 10^9\ M_\odot$ (with $R_* = 4.18 \times 10^{-4}$ pc) provided that $m = 25.0\ {\rm keV/c^2}$.

The results are essentially the same in the microcanonical ensemble but the existence of a microcanonical phase transition requires an initially larger system size ($\mu > \mu_{\rm MCP}$) so that the caloric curve has the shape of Fig. 48. On the other hand, the compact object resulting from the gravitational collapse (gravothermal catastrophe) at E_c (corresponding to $\Lambda_c \simeq 0.335$) contains a fraction ($\sim 1/4$) of the initial mass [33,186]. The formation of the compact object (implosion) is accompanied by the expulsion of a hot envelope (explosion). This core-halo structure is reminiscent to the onset of red-giant structure and to the supernova phenomenon in the context of compact stars (white dwarfs and neutron stars).

To study these phase transitions in detail we have to use general relativity. This has been done in the case of fermions in Refs. [27,186]. Numerical applications have been made for fermionic particles of mass $m = 17.2\ {\rm keV/c^2}$. It is shown that they can form fermion balls of mass $M \sim 10^9\ M_\odot$ similar to the mass of the presumed black holes that reside at the centers of elliptical galaxies.

[66]Similar numerical applications have been made in Appendix F of [119] to model the compact object Sgr A^* of mass $M = 4.2 \times 10^6\ M_\odot$ at the center of our Galaxy (purported to be a SMBH) by a general relativistic boson or fermion star.

Remark: It is important to note that, in the present appendix, we are considering the purely condensed solution (C), not the core-halo solution (CH). Since we are not trying to construct a self-consistent "core + halo" solution we do not face the difficulties encountered in Sec. VII F. Furthermore, the solution (C) is canonically stable while the solution (CH) is canonically unstable. Therefore, the results of this appendix suggest that large galaxies may contain a DM compact object (boson or fermion star) mimicking a SMBH but that this object is *not* surrounded by a DM halo. If this scenario is correct, large galaxies should not contain a DM halo, just a DM compact object. Note that other scenarios are possible such as those considered in Sec. IX in which large galaxies contain a bulge (soliton), or a central black hole, surrounded by a DM halo.

APPENDIX K: PROBLEMS WITH THE BOSON OR FERMION BALL SCENARIO TO MIMIC A SMBH

In this appendix, we show the impossibility for a noninteracting boson or fermion ball to simultaneously mimic a SMBH of mass $M \sim 10^9\ M_\odot$ at the centers of elliptical galaxies (see Appendix J) and a compact object (Sgr A^*) of mass $M = 4.2 \times 10^6\ M_\odot$ and sufficiently small radius $R < R_{\rm P} = 6 \times 10^{-4}$ pc at the center of our Galaxy (see Sec. VII F).[67] Our discussion confirms and extends the arguments given in Ref. [183].

In Appendix J, we have determined the characteristics that the DM particle must have so that the maximum mass of the associated boson or fermion ball is $M_{\rm max} = 10^9\ M_\odot$. Below, we show that the associated boson or fermion ball of mass $M = 4.2 \times 10^6\ M_\odot$ has a radius $R > R_{\rm P} = 6 \times 10^{-4}$ pc so that it cannot account for the compact object (Sgr A^*) at the center of our Galaxy.

For noninteracting bosons, using the mass-radius relation $MR = 9.95\hbar^2/Gm^2$ [50,78,79] and taking $m = 8.46 \times 10^{-20}\ {\rm eV/c^2}$ (see Appendix J) we find $R = 0.283\ {\rm pc} > R_{\rm P}$. Inversely, the constraint $R < R_{\rm P}$ implies $m > 1.84 \times 10^{-18}\ {\rm eV/c^2}$. However, in this case, the boson star cannot mimic a SMBH of mass $M_{\rm max} \sim 10^9\ M_\odot$ at the centers of elliptical galaxies since this requires $m = 8.46 \times 10^{-20}\ {\rm eV/c^2}$. Indeed, if we take $m > 1.84 \times 10^{-18}\ {\rm eV/c^2}$ we find $M_{\rm max} = 4.60 \times 10^7\ M_\odot < 10^9\ M_\odot$.

[67]If a boson or fermion ball can mimic a BH of mass $M \sim 10^9\ M_\odot$ this means that $M_{\rm max} \sim 10^9\ M_\odot$. In that case, it cannot mimic a BH of smaller mass, $M \sim 10^6$–10^9, because it would be nonrelativistic ($M \ll M_{\rm max}$) and it cannot mimic a BH of larger mass because it would be unstable ($M > M_{\rm max}$). However, the compact object of mass $M = 4.2 \times 10^6\ M_\odot \ll M_{\rm max} \sim 10^9\ M_\odot$ that resides at the center of our Galaxy is not necessarily a black hole, not even a relativistic object. We just require that it has a radius $R < R_{\rm P} = 6 \times 10^{-4}\ {\rm pc} = 1492R_S$ in order to be consistent with the observations. Therefore, we can use the nonrelativistic mass-radius relation of a boson or fermion ball to describe this object.

For fermions, using the mass-radius relation $MR^3 = 1.49 \times 10^{-3} h^6/G^3 m^8$ [158] and taking $m = 25.0\ \mathrm{keV/c^2}$ (see Appendix J) we find $R = 4.81 \times 10^{-3}\ \mathrm{pc} > R_{\mathrm{P}}$. Inversely, the constraint $R < R_{\mathrm{P}}$ implies $m > 54.5\ \mathrm{keV/c^2}$. However, in this case, the fermion star cannot mimic a SMBH of mass $M_{\max} \sim 10^9\ M_\odot$ at the centers of elliptical galaxies since this requires $m = 25.0\ \mathrm{keV/c^2}$. Indeed, if we take $m > 54.5\ \mathrm{keV/c^2}$ we find $M_{\max} = 2.11 \times 10^8\ M_\odot < 10^9\ M_\odot$.[68]

Interestingly, it turns out that self-interacting boson stars can simultaneously mimic a SMBH of mass $M \sim 10^9\ M_\odot$ and a compact object like Sgr A^*. To our knowledge, this result has not been pointed out previously. For self-interacting bosons in the TF limit, using the fact that their radius is $R = \pi(a_s\hbar^2/Gm^3)^{1/2}$ [53,60,67,69,78,159,160] and taking $a_s/m^3 = 7.86 \times 10^{-10}\ \mathrm{fm/(eV/c^2)^3}$ (see Appendix J) we find $R = 4.90 \times 10^{-4}\ \mathrm{pc} < R_{\mathrm{P}}$. Inversely, the constraint $R < R_{\mathrm{P}}$ implies $a_s/m^3 < 1.18 \times 10^{-9}\ \mathrm{fm/(eV/c^2)^3}$. In that case, the bosonic particle can mimic a SMBH of mass $M_{\max} \sim 10^9\ M_\odot$ at the centers of elliptical galaxies since this requires $a_s/m^3 = 7.86 \times 10^{-10}\ \mathrm{fm/(eV/c^2)^3}$. Indeed, if we take $a_s/m^3 \lesssim 1.18 \times 10^{-9}\ \mathrm{fm/(eV/c^2)^3}$ we find $M_{\max} = 1.22 \times 10^9\ M_\odot \gtrsim 10^9\ M_\odot$.

However, there are important problems with the boson or fermion ball model that also concern the case of self-interacting bosons. In particular, the characteristics of the DM particle that we find in Appendix J and in this appendix are not consistent with the characteristics of the DM particle obtained from the minimum halo model of Sec. VI B. Indeed, we have argued that the most compact halos (dSphs like Fornax) should correspond to the ground state of the self-gravitating boson or fermion gas. This immediately fixes the characteristics of the DM particle. Comparing the results found in Sec. VI B with the results found above, we see that they are not consistent. As a result, if we determine the characteristics of the DM particle from the minimum halo model (see Sec. VI B), then the boson or fermion ball corresponding to the self-consistent core-halo (CH) solution that we obtain for a DM halo similar to the Milky Way has the form of a large bulge (see Sec. VII E), not the form of a small compact object like a BH (see Sec. VII F). In addition, even if we relax the constraint from the minimum halo model we cannot get a self-consistent core-halo solution mimicking a BH as shown in Sec. VII F.

Remark: It is not excluded (actually it is even very likely) that DM is made of different types of particles (bosons and fermions) with different characteristics. Some of these particles (like bosons) could form a solitonic bulge and other particles (like fermions) could form a fermion ball mimicking SMBHs. However, accounting for several species obviously introduces arbitrariness in the models and limits therefore their predictive power. This is why, in this paper, we have just considered one type of DM particle.

APPENDIX L: SOLUTION OF AN APPARENT PARADOX RELATED TO THE MASS-RADIUS RELATION OF DM HALOS

We have seen that the ground state of the GPP equations (1) and (2) corresponds to a soliton. For noninteracting bosons, the mass-radius relation of the soliton is given by [50,78,79]

$$R = 9.95\frac{\hbar^2}{GMm^2}, \tag{L1}$$

implying that the radius decreases as the mass increases. For self-interacting bosons, in the TF approximation, the soliton has a unique radius

$$R = \pi\left(\frac{a_s\hbar^2}{Gm^3}\right)^{1/2} \tag{L2}$$

which is independent of its mass [53,60,67,69,78,159,160]. Clearly, these results are in contradiction with the universality of the surface density of DM halos [see Eq. (94)] implying that the radius increases with the mass as $r_h \propto M_h^{1/2}$.

This apparent paradox was pointed out in Appendix F of Ref. [40] and in the Introduction of Ref. [140]. This difficulty was rediscussed later by Deng *et al.* [231] who concluded that ultralight DM may not be able to solve the cusp problem. Alternatively, we had suggested in our previous works [40,140] that the above-mentioned apparent paradox could be solved by accounting for the presence of an (isothermal) atmosphere surrounding the solitonic core of large DM halos.

More precisely, we argued that a pure soliton describes only the ground state of the GPP equations (1) and (2) corresponding to ultracompact halos such as Fornax (see Sec. VI B). The mass-radius relations (L1) and (L2) apply only to these ultracompact halos. Larger halos contain a solitonic core plus an atmosphere resulting from quantum interferences related to the complicated processes of gravitational cooling [132–134] and violent relaxation [136]. The atmosphere is approximately isothermal. It is the atmosphere that determines the size of large DM halos. As a result, we cannot apply the mass-radius relations (L1) and (L2) to large DM halos, but just to their solitonic core. It is the atmosphere that fixes the size of large DM halos and yields the relation $r_h \propto M_h^{1/2}$. In this sense, there is no

[68] In relation to this fundamental incompatibility, we note that Argüelles and Ruffini [230] consider a fermion of mass $10\ \mathrm{keV/c^2}$ to mimic a SMBH of mass $10^9\ M_\odot$ at the centers of elliptical galaxies while Argüelles *et al.* [42] consider another fermion of larger mass, $48\ \mathrm{keV/c^2}$, to mimic the compact object at the center of our Galaxy.

paradox anymore and ultralight DM may be able to solve the cusp problem.

The ideas sketched in Refs. [40,140] have been confirmed in the present paper. As soon as there is an (isothermal) atmosphere surrounding the solitonic core it is possible to satisfy the constraint from Eq. (94). The BECDM halos that we have constructed in this paper all satisfy this contraint. We thus find that the mass-radius relation of large DM halos is given by Eq. (105) in agreement with the observations [172–174].

In the present paper, the universality of Σ_0 is imposed to our model as an observational constraint (see Sec. VI A). This implies that the temperature T of the atmosphere of our DM halos must change precisely in order to satisfy this constraint (see Fig. 19). This leads to the relations of Sec. VI D 6.

However, in Ref. [232] we have shown that it is possible to predict the universal value of Σ_0 from a cosmological model based on a logotropic equation of state. This model can be derived from a generalized GP equation similar to Eq. (3) but involving a nonlinearity of the form $-Am/|\psi|^2$ instead of $2k_BT\ln|\psi|$ (see Eq. (C.56) of [232]). In that case, we can theoretically predict that [175,232]

$$\Sigma_0^{\rm th}=\left(\frac{B}{32}\right)^{1/2}\frac{\xi_h}{\pi}\frac{\sqrt{\Lambda}c}{G}\simeq 133\ M_\odot/{\rm pc}^2, \qquad \text{(L3)}$$

where $\Lambda=1.00\times10^{-35}\ {\rm s}^{-2}$ is the effective cosmological constant of the model while $\xi_h=5.8458\ldots$ and $B=3.53\times10^{-3}$ are coefficients derived from the theory (the consequences of this relation are further discussed in [175]). The theoretical value (L3) is in good agreement with the observational value (94) up to error bars. This suggests replacing the isothermal atmosphere of the present paper by a logotropic atmosphere. In that case, our model will be characterized by a universal constant Λ instead of being characterized by a temperature T changing from halo to halo. This logotropic model will be considered in a future contribution [142]. For the present, we think that it is better to develop our model with a more conventional isothermal atmosphere as done in this paper.

Remark: The same arguments apply to the fermionic DM model. The mass-radius relation of a self-gravitating Fermi gas at $T=0$ (ground state) [158]

$$R=0.114\frac{h^2}{Gm^{8/3}M^{1/3}} \qquad \text{(L4)}$$

implies that the radius decreases as the mass increases in contradiction with the observational DM halo mass-radius relation $r_h\propto M_h^{1/2}$. This paradox is solved by assuming that the fermionic DM halos have a core-halo structure with a fermion ball (core) and an isothermal atmosphere (halo) [40,140]. The mass-radius relation (L4) is only valid for ultracompact DM halos and in the core of large DM halos. It is the atmosphere that fixes the size of the DM halos and yields the relation $r_h\propto M_h^{1/2}$. Again, the T-changing isothermal atmosphere could be replaced by a logotropic atmosphere characterized by a universal constant Λ.

[1] G. Jungman, M. Kamionkowski, and K. Griest, Phys. Rep. **267**, 195 (1996).
[2] P. J. E. Peebles, *The Large-Scale Structure of the Universe* (Princeton University Press, Princeton, NJ, 1980).
[3] Planck Collaboration, Astron. Astrophys. **571**, A66 (2014).
[4] Planck Collaboration, Astron. Astrophys. **594**, A13 (2016).
[5] J. F. Navarro, C. S. Frenk, and S. D. M. White, Astrophys. J. **462**, 563 (1996).
[6] A. Burkert, Astrophys. J. **447**, L25 (1995).
[7] G. Kauffmann, S. D. M. White, and B. Guiderdoni, Mon. Not. R. Astron. Soc. **264**, 201 (1993); A. Klypin, A. V. Kravtsov, and O. Valenzuela, Astrophys. J. **522**, 82 (1999); M. Kamionkowski and A. R. Liddle, Phys. Rev. Lett. **84**, 4525 (2000).
[8] D. N. Spergel and P. J. Steinhardt, Phys. Rev. Lett. **84**, 3760 (2000).
[9] P. Bode, J. P. Ostriker, and N. Turok, Astrophys. J. **556**, 93 (2001).
[10] E. Romano-Díaz, I. Shlosman, Y. Hoffman, and C. Heller, Astrophys. J. **685**, L105 (2008); A. Pontzen and F. Governato, Nature (London) **506**, 171 (2014); J. Oñorbe, M. Boylan-Kolchin, J. S. Bullock, P. F. Hopkins, D. Kereš, C.-A. Faucher-Giguère, Eliot Quataert, and Norman Murray, Mon. Not. R. Astron. Soc. **454**, 2092 (2015).
[11] M. A. Markov, Phys. Lett. **10**, 122 (1964).
[12] R. Cowsik and J. McClelland, Phys. Rev. Lett. **29**, 669 (1972).
[13] R. Cowsik and J. McClelland, Astrophys. J. **180**, 7 (1973).
[14] J. G. Gao and R. Ruffini, Phys. Lett. **97B**, 388 (1980).
[15] R. Ruffini and L. Stella, Astron. Astrophys. **119**, 35 (1983).
[16] J. L. Zhang, W. Y. Chau, K. Lake, and J. Stone, Astrophys. Space Sci. **96**, 417 (1983).
[17] W. Y. Chau, K. Lake, and J. Stone, Astrophys. J. **281**, 560 (1984).
[18] W. Y. Chau and K. Lake, Phys. Lett. **134B**, 409 (1984).
[19] G. Ingrosso and R. Ruffini, Nuovo Cimento **101**, 369 (1988).

[20] J. G. Gao, M. Merafina, and R. Ruffini, Astron. Astrophys. **235**, 1 (1990).
[21] M. Merafina, Nuovo Cimento **105**, 985 (1990).
[22] G. Ingrosso, M. Merafina, R. Ruffini, and F. Strafella, Astron. Astrophys. **258**, 223 (1992).
[23] R. D. Viollier, D. Trautmann, and G. B. Tupper, Phys. Lett. B **306**, 79 (1993).
[24] N. Bilic and R. D. Viollier, Phys. Lett. B **408**, 75 (1997).
[25] N. Bilic, F. Munyaneza, and R. D. Viollier, Phys. Rev. D **59**, 024003 (1998).
[26] P. H. Chavanis and J. Sommeria, Mon. Not. R. Astron. Soc. **296**, 569 (1998).
[27] N. Bilic and R. D. Viollier, Eur. Phys. J. C **11**, 173 (1999).
[28] P. H. Chavanis, Phys. Rev. E **65**, 056123 (2002).
[29] P. H. Chavanis, The self-gravitating Fermi gas, in *Dark Matter in Astro- and Particle Physics*, edited by H. V. Klapdor-Kleingrothaus and R. D. Viollier (Springer, New York, 2002).
[30] N. Bilic, F. Munyaneza, G. B. Tupper, and R. D. Viollier, Prog. Part. Nucl. Phys. **48**, 291 (2002).
[31] N. Bilic, G. B. Tupper, and R. D. Viollier, Lect. Notes Phys. **616**, 24 (2003).
[32] P. H. Chavanis and M. Rieutord, Astron. Astrophys. **412**, 1 (2003).
[33] P. H. Chavanis, Int. J. Mod. Phys. B **20**, 3113 (2006).
[34] C. Destri, H. J. de Vega, and N. G. Sanchez, New Astron. **22**, 39 (2013).
[35] C. Destri, H. J. de Vega, and N. G. Sanchez, Astropart. Phys. **46**, 14 (2013).
[36] H. J. de Vega, P. Salucci, and N. G. Sanchez, Mon. Not. R. Astron. Soc. **442**, 2717 (2014).
[37] V. Domcke and A. Urbano, J. Cosmol. Astropart. Phys. 01 (2015) 002.
[38] R. Ruffini, C. R. Argüelles, and J. A. Rueda, Mon. Not. R. Astron. Soc. **451**, 622 (2015).
[39] P. H. Chavanis, M. Lemou, and F. Méhats, Phys. Rev. D **91**, 063531 (2015).
[40] P. H. Chavanis, M. Lemou, and F. Méhats, Phys. Rev. D **92**, 123527 (2015).
[41] H. J. de Vega and N. G. Sanchez, Int. J. Mod. Phys. A **31**, 1650073 (2016).
[42] C. R. Argüelles, A. Krut, J. A. Rueda, and R. Ruffini, Phys. Dark Universe **21**, 82 (2018).
[43] H. J. de Vega and N. G. Sanchez, Eur. Phys. J. C **77**, 81 (2017).
[44] L. Randall, J. Scholtz, and J. Unwin, Mon. Not. R. Astron. Soc. **467**, 1515 (2017).
[45] V. C. Rubin and W. K. Ford, Astrophys. J. **159**, 379 (1970); V. C. Rubin, W. K. Ford, and N. Thonnard, Astrophys. J. **238**, 471 (1980); A. Bosma, Astron. J. **86**, 1791 (1981); M. Persic, P. Salucci, and F. Stel, Mon. Not. R. Astron. Soc. **281**, 27 (1996).
[46] A. Suárez and P. H. Chavanis, Phys. Rev. D **95**, 063515 (2017).
[47] D. Marsh, Phys. Rep. **643**, 1 (2016).
[48] M. R. Baldeschi, G. B. Gelmini, and R. Ruffini, Phys. Lett. B **122**, 221 (1983).
[49] M. Yu. Khlopov, B. A. Malomed, and Ya. B. Zeldovich, Mon. Not. R. Astron. Soc. **215**, 575 (1985).
[50] M. Membrado, A. F. Pacheco, and J. Sanudo, Phys. Rev. A **39**, 4207 (1989).
[51] S. J. Sin, Phys. Rev. D **50**, 3650 (1994).
[52] S. U. Ji and S. J. Sin, Phys. Rev. D **50**, 3655 (1994).
[53] J. W. Lee and I. Koh, Phys. Rev. D **53**, 2236 (1996).
[54] F. E. Schunck, arXiv:astro-ph/9802258.
[55] F. S. Guzmán, T. Matos, and H. B. Villegas, Astron. Nachr. **320**, 97 (1999).
[56] V. Sahni and L. Wang, Phys. Rev. D **62**, 103517 (2000).
[57] F. S. Guzmán and T. Matos, Classical Quantum Gravity **17**, L9 (2000).
[58] W. Hu, R. Barkana, and A. Gruzinov, Phys. Rev. Lett. **85**, 1158 (2000).
[59] P. J. E. Peebles, Astrophys. J. **534**, L127 (2000).
[60] J. Goodman, New Astron. **5**, 103 (2000).
[61] T. Matos and L. A. Ureña-López, Phys. Rev. D **63**, 063506 (2001).
[62] A. Arbey, J. Lesgourgues, and P. Salati, Phys. Rev. D **64**, 123528 (2001).
[63] M. P. Silverman and R. L. Mallett, Classical Quantum Gravity **18**, L103 (2001).
[64] M. Alcubierre, F. S. Guzmán, T. Matos, D. Núñez, L. A. Ureña-López, and P. Wiederhold, Classical Quantum Gravity **19**, 5017 (2002).
[65] M. P. Silverman and R. L. Mallett, Gen. Relativ. Gravit. **34**, 633 (2002).
[66] J. Lesgourgues, A. Arbey, and P. Salati, New Astron. Rev. **46**, 791 (2002).
[67] A. Arbey, J. Lesgourgues, and P. Salati, Phys. Rev. D **68**, 023511 (2003).
[68] T. Fukuyama and M. Morikawa, Prog. Theor. Phys. **115**, 1047 (2006).
[69] C. G. Böhmer and T. Harko, J. Cosmol. Astropart. Phys. 06 (2007) 025.
[70] T. Fukuyama, M. Morikawa, and T. Tatekawa, J. Cosmol. Astropart. Phys. 06 (2008) 033.
[71] A. Bernal, T. Matos, and D. Núñez, Rev. Mex. Astron. Astrofis. **44**, 149 (2008).
[72] T. Fukuyama and M. Morikawa, Phys. Rev. D **80**, 063520 (2009).
[73] P. Sikivie and Q. Yang, Phys. Rev. Lett. **103**, 111301 (2009).
[74] T. Matos, A. Vázquez-González, and J. Magaña, Mon. Not. R. Astron. Soc. **393**, 1359 (2009).
[75] J. W. Lee, Phys. Lett. B **681**, 118 (2009).
[76] T. P. Woo and T. Chiueh, Astrophys. J. **697**, 850 (2009).
[77] J. W. Lee and S. Lim, J. Cosmol. Astropart. Phys. 01 (2010) 007.
[78] P. H. Chavanis, Phys. Rev. D **84**, 043531 (2011).
[79] P. H. Chavanis and L. Delfini, Phys. Rev. D **84**, 043532 (2011).
[80] P. H. Chavanis, Phys. Rev. D **84**, 063518 (2011).
[81] F. Briscese, Phys. Lett. B **696**, 315 (2011).
[82] T. Harko, Mon. Not. R. Astron. Soc. **413**, 3095 (2011).
[83] T. Harko, J. Cosmol. Astropart. Phys. 05 (2011) 022.
[84] A. Suárez and T. Matos, Mon. Not. R. Astron. Soc. **416**, 87 (2011).
[85] P. H. Chavanis, Astron. Astrophys. **537**, A127 (2012).
[86] H. Velten and E. Wamba, Phys. Lett. B **709**, 1 (2012).

[87] M. O. C. Pires and J. C. C. de Souza, J. Cosmol. Astropart. Phys. 11 (2012) 024.
[88] C.-G. Park, J.-C. Hwang, and H. Noh, Phys. Rev. D **86**, 083535 (2012).
[89] V. H. Robles and T. Matos, Mon. Not. R. Astron. Soc. **422**, 282 (2012).
[90] T. Rindler-Daller and P. R. Shapiro, Mon. Not. R. Astron. Soc. **422**, 135 (2012).
[91] V. Lora, J. Magaña, A. Bernal, F. J. Sánchez-Salcedo, and E. K. Grebel, J. Cosmol. Astropart. Phys. 02 (2012) 011.
[92] J. Magaña, T. Matos, A. Suárez, and F. J. Sánchez-Salcedo, J. Cosmol. Astropart. Phys. 10 (2012) 003.
[93] G. Manfredi, P. A. Hervieux, and F. Haas, Classical Quantum Gravity **30**, 075006 (2013).
[94] A. X. González-Morales, A. Diez-Tejedor, L. A. Ureña-López, and O. Valenzuela, Phys. Rev. D **87**, 021301(R) (2013).
[95] F. S. Guzmán, F. D. Lora-Clavijo, J. J. González-Avilés, and F. J. Rivera-Paleo, J. Cosmol. Astropart. Phys. 09 (2013) 034.
[96] H. Y. Schive, T. Chiueh, and T. Broadhurst, Nat. Phys. **10**, 496 (2014).
[97] H. Y. Schive, M.-H. Liao, T.-P. Woo, S.-K. Wong, T. Chiueh, T. Broadhurst, and W.-Y. Pauchy Hwang, Phys. Rev. Lett. **113**, 261302 (2014).
[98] B. Li, T. Rindler-Daller, and P. R. Shapiro, Phys. Rev. D **89**, 083536 (2014).
[99] D. Bettoni, M. Colombo, and S. Liberati, J. Cosmol. Astropart. Phys. 02 (2014) 004.
[100] V. Lora and J. Magaña, J. Cosmol. Astropart. Phys. 09 (2014) 011.
[101] P. H. Chavanis, Eur. Phys. J. Plus **130**, 180 (2015).
[102] E. J. M. Madarassy and V. T. Toth, Phys. Rev. D **91**, 044041 (2015).
[103] A. Suárez and P. H. Chavanis, Phys. Rev. D **92**, 023510 (2015).
[104] A. Suárez and P. H. Chavanis, J. Phys. Conf. Ser. **654**, 012008 (2015).
[105] P. H. Chavanis, Phys. Rev. D **92**, 103004 (2015).
[106] A. H. Guth, M. P. Hertzberg, and C. Prescod-Weinstein, Phys. Rev. D **92**, 103513 (2015).
[107] J. C. C. de Souza and M. Ujevic, Gen. Relativ. Gravit. **47**, 100 (2015).
[108] R. C. de Freitas and H. Velten, Eur. Phys. J. C **75**, 597 (2015).
[109] J. Alexandre, Phys. Rev. D **92**, 123524 (2015).
[110] K. Schroven, M. List, and C. Lämmerzahl, Phys. Rev. D **92**, 124008 (2015).
[111] D. Marsh and A. R. Pop, Mon. Not. R. Astron. Soc. **451**, 2479 (2015).
[112] J. Eby, C. Kouvaris, N. G. Nielsen, and L. C. R. Wijewardhana, J. High Energy Phys. 02 (2016) 028.
[113] J. A. R. Cembranos, A. L. Maroto, and S. J. Núñez Jareño, J. High Energy Phys. 03 (2016) 013.
[114] E. Braaten, A. Mohapatra, and H. Zhang, Phys. Rev. Lett. **117**, 121801 (2016).
[115] S. Davidson and T. Schwetz, Phys. Rev. D **93**, 123509 (2016).
[116] B. Schwabe, J. Niemeyer, and J. Engels, Phys. Rev. D **94**, 043513 (2016).
[117] J. Fan, Phys. Dark Universe **14**, 84 (2016).
[118] E. Calabrese and D. N. Spergel, Mon. Not. R. Astron. Soc. **460**, 4397 (2016).
[119] P. H. Chavanis, Phys. Rev. D **94**, 083007 (2016).
[120] E. Cotner, Phys. Rev. D **94**, 063503 (2016).
[121] P. H. Chavanis and T. Matos, Eur. Phys. J. Plus **132**, 30 (2017).
[122] L. Hui, J. Ostriker, S. Tremaine, and E. Witten, Phys. Rev. D **95**, 043541 (2017).
[123] J. Zhang, Y. L. Sming Tsai, J. L. Kuo, K. Cheung, and M. C. Chu, Astrophys. J. **853**, 51 (2018).
[124] D. G. Levkov, A. G. Panin, and I. I. Tkachev, Phys. Rev. Lett. **118**, 011301 (2017).
[125] B. Li, T. Rindler-Daller, and P. R. Shapiro, Phys. Rev. D **96**, 063505 (2017).
[126] P. H. Chavanis, Phys. Rev. D **98**, 023009 (2018).
[127] A. Suárez and P. H. Chavanis, Phys. Rev. D **98**, 083529 (2018).
[128] V. Desjacques, A. Kehagias, and A. Riotto, Phys. Rev. D **97**, 023529 (2018).
[129] N. Bar, D. Blas, K. Blum, and S. Sibiryakov, Phys. Rev. D **98**, 083027 (2018).
[130] J. E. Kim and G. Carosi, Rev. Mod. Phys. **82**, 557 (2010).
[131] R. D. Peccei and H. R. Quinn, Phys. Rev. Lett. **38**, 1440 (1977).
[132] E. Seidel and W. M. Suen, Phys. Rev. Lett. **72**, 2516 (1994).
[133] F. S. Guzmán and L. A. Ureña-López, Phys. Rev. D **69**, 124033 (2004).
[134] F. S. Guzmán and L. A. Ureña-López, Astrophys. J. **645**, 814 (2006).
[135] J. Binney and S. Tremaine, *Galactic Dynamics* (Princeton University Press, Princeton, NJ, 1987).
[136] D. Lynden-Bell, Mon. Not. R. Astron. Soc. **136**, 101 (1967).
[137] P. H. Chavanis, J. Sommeria, and R. Robert, Astrophys. J. **471**, 385 (1996).
[138] P. H. Chavanis, Mon. Not. R. Astron. Soc. **300**, 981 (1998).
[139] P. H. Chavanis, Statistical mechanics of violent relaxation in stellar systems, in *Multiscale Problems in Science and Technology*, edited by N. Antonić, C. J. van Duijn, W. Jäger, and A. Mikelić (Springer, New York, 2002).
[140] P. H. Chavanis, Eur. Phys. J. Plus **132**, 248 (2017).
[141] P. H. Chavanis, Phys. Dark Universe **22**, 80 (2018).
[142] P. H. Chavanis (to be published).
[143] P. H. Chavanis, Eur. Phys. J. Plus **134**, 352 (2019).
[144] E. P. Gross, Ann. Phys. (N.Y.) **4**, 57 (1958).
[145] E. P. Gross, Nuovo Cimento **20**, 454 (1961).
[146] E. P. Gross, J. Math. Phys. (N.Y.) **4**, 195 (1963).
[147] L. P. Pitaevskii, Sov. Phys. JETP **13**, 451 (1961).
[148] L. Nottale, *Scale Relativity and Fractal Space-Time* (Imperial College Press, London, 2011).
[149] E. Madelung, Z. Phys. **40**, 322 (1927).
[150] P. H. Chavanis, Phys. Rev. E **84**, 031101 (2011).
[151] P. H. Chavanis, Eur. Phys. J. B **62**, 179 (2008).
[152] P. H. Chavanis, Entropy **17**, 3205 (2015).
[153] P. H. Chavanis, C. Rosier, and C. Sire, Phys. Rev. E **66**, 036105 (2002); C. Sire and P. H. Chavanis, Phys. Rev. E **66**, 046133 (2002); P. H. Chavanis and C. Sire, Phys. Rev.

E **69**, 016116 (2004); C. Sire and P. H. Chavanis, Phys. Rev. E **69**, 066109 (2004).
[154] T. Padmanabhan, Phys. Rep. **188**, 285 (1990).
[155] P. Ledoux and C. L. Pekeris, Astrophys. J. **94**, 124 (1941).
[156] R. Ruffini and S. Bonazzola, Phys. Rev. **187**, 1767 (1969).
[157] P. H. Chavanis, arXiv:1905.08137.
[158] S. Chandrasekhar, *An Introduction to the Study of Stellar Structure* (Dover, New York, 1958).
[159] I. I. Tkachev, Sov. Astron. Lett. **12**, 305 (1986).
[160] M. Membrado, J. Abad, A. F. Pacheco, and J. Sañudo, Phys. Rev. D **40**, 2736 (1989).
[161] P. Natarajan and D. Lynden-Bell, Mon. Not. R. Astron. Soc. **286**, 268 (1997).
[162] G. W. Wares, Astrophys. J. **100**, 158 (1944).
[163] T. Margrave, Astrophys. Space Sci. **2**, 504 (1968).
[164] P. Hertel and W. Thirring, in *Quanten und Felder*, edited by H. P. Dürr (Vieweg, Braunschweig, 1971).
[165] S. A. Bludman and K. A. Van Riper, Astrophys. J. **212**, 859 (1977).
[166] T. W. Edwards and M. P. Merilan, Astrophys. J. **244**, 600 (1981).
[167] T. W. Edwards, Astrophys. J. **288**, 630 (1985).
[168] Z. Slepian and J. Goodman, Mon. Not. R. Astron. Soc. **427**, 839 (2012).
[169] S. C. Lin, H. Y. Schive, S. K. Wong, and T. Chiueh, Phys. Rev. D **97**, 103523 (2018).
[170] P. Mocz, L. Lancaster, A. Fialkov, F. Becerra, and P. H. Chavanis, Phys. Rev. D **97**, 083519 (2018).
[171] P. H. Chavanis, Astron. Astrophys. **381**, 340 (2002).
[172] J. Kormendy and K. C. Freeman, in *Proceedings of the IAU Symposium 220, Dark Matter in Galaxies. Astronomical Society of the Pacific, San Francisco*, edited by S. D. Ryder, D. J. Pisano, M. A. Walker, and K. C. Freeman (2004), p. 377.
[173] M. Spano, M. Marcelin, P. Amram, C. Carignan, B. Epinat, and O. Hernandez, Mon. Not. R. Astron. Soc. **383**, 297 (2008).
[174] F. Donato, G. Gentile, P. Salucci, C. Frigerio Martins, M. I. Wilkinson, G. Gilmore, E. K. Grebel, A. Koch, and R. Wyse, Mon. Not. R. Astron. Soc. **397**, 1169 (2009).
[175] P. H. Chavanis, Phys. Dark Universe **24**, 100271 (2019).
[176] L. E. Strigari, J. S. Bullock, M. Kaplinghat, J. D. Simon, M. Geha, B. Willman, and M. G. Walker, Nature (London) **454**, 1096 (2008).
[177] I. De Martino *et al.*, arXiv:1807.08153.
[178] M. Zoccali *et al.*, Astron. Astrophys. **562**, A66 (2014).
[179] M. Portail, O. Gerhard, C. Wegg, and M. Ness, Mon. Not. R. Astron. Soc. **465**, 1621 (2017).
[180] S. Gillessen, F. Eisenhauer, T. K. Fritz, H. Bartko, K. Dodds-Eden, O. Pfuhl, T. Ott, and R. Genzel, Astrophys. J. **707**, L114 (2009).
[181] R. Schödel *et al.*, Nature (London) **419**, 694 (2002).
[182] M. J. Reid, Int. J. Mod. Phys. D **18**, 889 (2009).
[183] R. Genzel, F. Eisenhauer, and S. Gillessen, Rev. Mod. Phys. **82**, 3121 (2010).
[184] D. F. Torres, S. Capozziello, and G. Lambiase, Phys. Rev. D **62**, 104012 (2000).
[185] F. S. Guzmán, Phys. Rev. D **73**, 021501 (2006).
[186] G. Alberti and P. H. Chavanis, arXiv:1808.01007.
[187] A. Campa, T. Dauxois, D. Fanelli, and S. Ruffo, *Physics of Long-Range Interacting Systems* (Oxford University Press, Oxford, 2014).
[188] H. Poincaré, Acta Math. **7**, 259 (1885).
[189] J. Katz, Mon. Not. R. Astron. Soc. **183**, 765 (1978).
[190] P. H. Chavanis, Astron. Astrophys. **432**, 117 (2005).
[191] A. Campa and P. H. Chavanis, J. Stat. Mech. (2010) 06001.
[192] A. Naso, P. H. Chavanis, and B. Dubrulle, Eur. Phys. J. B **77**, 187 (2010).
[193] B. Bar-Or, J. B. Fouvry, and S. Tremaine, Astrophys. J. **871**, 28 (2019).
[194] P. H. Chavanis, Astron. Astrophys. **381**, 340 (2002).
[195] D. Lynden-Bell and R. Wood, Mon. Not. R. Astron. Soc. **138**, 495 (1968).
[196] S. Balberg, S. L. Shapiro, and S. Inagaki, Astrophys. J. **568**, 475 (2002).
[197] Ya. B. Zel'dovich and M. A. Podurets, Sov. Astron. **9**, 742 (1966).
[198] D. Fackerell, J. Ipser, and K. Thorne, Comments Astrophys. Space Phys. **1**, 134 (1969).
[199] S. L. Shapiro and S. A. Teukolsky, Astrophys. J. **298**, 58 (1985).
[200] S. L. Shapiro and S. A. Teukolsky, Astrophys. J. **292**, L41 (1985).
[201] S. L. Shapiro and S. A. Teukolsky, Astrophys. J. **307**, 575 (1986).
[202] D. Lynden-Bell and P. P. Eggleton, Mon. Not. R. Astron. Soc. **191**, 483 (1980).
[203] H. Cohn, Astrophys. J. **242**, 765 (1980).
[204] S. Inagaki and D. Lynden-Bell, Mon. Not. R. Astron. Soc. **205**, 913 (1983).
[205] D. Sugimoto and E. Bettwieser, Mon. Not. R. Astron. Soc. **204**, 19 (1983).
[206] D. Heggie and N. Ramamani, Mon. Not. R. Astron. Soc. **237**, 757 (1989).
[207] S. W. Randall, M. Markevitch, D. Clowe, A. H. Gonzalez, and M. Bradac, Astrophys. J. **679**, 1173 (2008).
[208] R. Davé, D. N. Spergel, P. J. Steinhardt, and B. J. Wandelt, Astrophys. J. **547**, 574 (2001).
[209] L. Ferrarese, Astrophys. J. **578**, 90 (2002).
[210] M. Hénon, Ann. Astrophys. **27**, 83 (1964).
[211] T. S. van Albada, Mon. Not. R. Astron. Soc. **201**, 939 (1982).
[212] F. Roy and J. Perez, Mon. Not. R. Astron. Soc. **348**, 62 (2004).
[213] M. Joyce, B. Marcos, and F. Sylos Labini, Mon. Not. R. Astron. Soc. **397**, 775 (2009).
[214] G. Bertin and M. Stiavelli, Astron. Astrophys. **137**, 26 (1984).
[215] M. Stiavelli and G. Bertin, Mon. Not. R. Astron. Soc. **229**, 61 (1987).
[216] J. Hjorth and J. Madsen, Mon. Not. R. Astron. Soc. **253**, 703 (1991).
[217] M. Hénon, Ann. Astrophys. **22**, 126 (1959).
[218] I. R. King, Astron. J. **70**, 376 (1965).
[219] E. Nelson, Phys. Rev. **150**, 1079 (1966).
[220] P. H. Chavanis, Eur. Phys. J. Plus **132**, 286 (2017).
[221] A. Einstein, Ann. Phys. (Berlin) **322**, 549 (1905).

[222] M. Colpi, S. L. Shapiro, and I. Wasserman, Phys. Rev. Lett. **57**, 2485 (1986).
[223] P. H. Chavanis and T. Harko, Phys. Rev. D **86**, 064011 (2012).
[224] D. J. Kaup, Phys. Rev. **172**, 1331 (1968).
[225] J. R. Oppenheimer and G. M. Volkoff, Phys. Rev. **55**, 374 (1939).
[226] P. Mocz, M. Vogelsberger, V. H. Robles, J. Zavala, M. Boylan-Kolchin, A. Fialkov, and L. Hernquist, Mon. Not. R. Astron. Soc. **471**, 4559 (2017).
[227] R. B. Tully and J. R. Fisher, Astron. Astrophys. **54**, 661 (1977).
[228] S. S. McGaugh, Astron. J. **143**, 40 (2012).
[229] V. H. Robles, J. S. Bullock, and M. Boylan-Kolchin, Mon. Not. R. Astron. Soc. **483**, 289 (2019).
[230] C. R. Argüelles and R. Ruffini, Int. J. Mod. Phys. D **23**, 1442020 (2014).
[231] H. Deng, M. P. Hertzberg, M. H. Namjoo, and A. Masoumi, Phys. Rev. D **98**, 023513 (2018).
[232] P. H. Chavanis, Eur. Phys. J. Plus **130**, 130 (2015).